Studies on the Structure and Function of Protein Kinase G, a Virulence Factor of *Mycobacterium tuberculosis*

Inauguraldissertation

zur

Erlangung der Würde eines Doktors der Philosophie
vorgelegt der
Philosophisch-Naturwissenschaftlichen Fakultät
der Universität Basel

von

Nicole Scherr
aus Landau/Pfalz, Deutschland

Basel, 2008

Genehmigt von der Philosophisch-Naturwissenschaftlichen Fakultät auf Antrag von
Prof. Jean Pieters, Prof. Peter Philippsen und Dr. Michel Steinmetz.

Basel, den 24. Juni 2008

Prof. Hans-Peter Hauri

The work described in this thesis has been performed from August 2004 to April 2008 at the Biozentrum, Department of Biochemistry, University of Basel, Switzerland, in the laboratory of Prof. Jean Pieters.

Table of contents

- CHAPTER 1 -

The Eukaryotic-like Serine/Threonine Protein Kinase Family in Mycobacteria

Based on

Book Chapter „Mycobacterium: Genomics and Molecular Biology“

Nicole Scherr und Jean Pieters

(Caister Academic Press, January 2009)

Mycobacteria have a complex life style comprising different environments and developmental stages. Signal sensing and transduction leading to cellular responses must be tightly regulated to allow survival under variable conditions. Prokaryotes normally regulate their signal transduction processes through two-component systems, however, the genome sequence of *Mycobacterium tuberculosis* revealed a large number of eukaryotic-like serine/threonine kinases. It is becoming clear that in *M. tuberculosis*, many of these kinases are involved in the regulation of metabolic processes, transport of metabolites, cell division and virulence. This chapter summarizes the current knowledge on eukaryotic-like serine/threonine protein kinases in mycobacteria. Investigating the biochemistry and the physiological role of these enzymes may lead to a better understanding of the signalling networks in mycobacteria.

1.1 Signal transduction systems

Cellular responses such as differentiation and adaptation are carried out by signal transduction systems, many of which are based on protein phosphorylation. Prokaryotes utilize two different principles to respond to their environment: The so-called two-component systems with kinases phosphorylating asparagine residues upon autophosphorylation of histidine residues, and, less frequently, eukaryotic-like kinases phosphorylating serine or threonine residues (Parkinson, 1993; Stock et al., 2000).

Two-component systems consist of a membrane-bound sensor histidine kinase and a cytosolic response regulator (figure 1.1). The histidine kinase contains an extracellular domain responsible for binding of small molecular weight ligands. Binding of ligands leads to activation of the kinase domain resulting in autophosphorylation of a specific histidine residue. The activated phosphate group is then transferred to a conserved aspartate residue in the receiver domain of the response regulator, thereby activating the output domain. The activated output domain finally initiates the adequate cellular response (Dutta et al., 1999; Stock et al., 2000).

Eukaryotic-like serine/threonine protein kinases employ the γ-phosphate of adenosine triphosphate (ATP) to form phosphate monoesters using the hydroxyl groups of serine or threonine as phosphate acceptors (figure 1.1). These enzymes share several conserved motifs within the two-lobed catalytic domain which consists of 250-300 amino acid residues. The

kinase domain contains 11 conserved subdomains (I-XI) folding into a complex catalytic core structure which carries out the following functions (Hanks and Hunter, 1995):

a) binding and orientation of ATP complexed with a divalent cation such as Mg^{2+} or Mn^{2+}
b) binding and orientation of the protein substrate
c) transfer of the γ-phosphate from ATP to the acceptor hydroxyl group of serine or threonine

Serine/threonine kinases can be either membrane-bound acting as signal receptors, or be located as a soluble molecule in the cytosol.

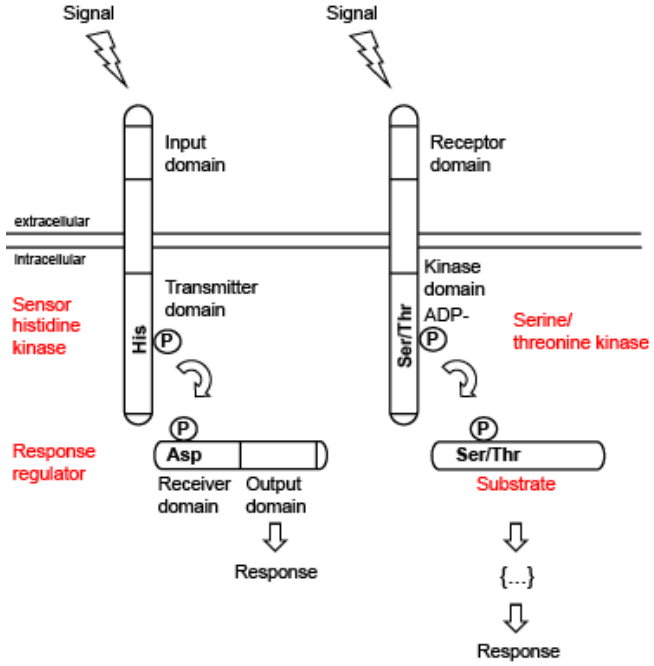

Figure 1.1. Schemes showing a two-component signal transduction system and a receptor-type serine/threonine kinase. Left side: Two-component system. The input domain of the histidine kinase detects a signal resulting in autophosphorylation of a conserved histidine residue. The phosphate is transferred to an aspartate residue in the receiver domain of the response regulator leading to activation of the output domain which then carries out the cellular response. Right side: Serine/threonine kinase: The receptor domain at the C-terminus of the protein senses the signal leading to a conformational change/activation of the kinase. The kinase domain located at the N-terminus binds ATP, whose γ-phosphate is transferred to the acceptor serine or threonine residue of the bound substrate.

1.2 Appearance of Eukaryotic-like Serine/Threonine Kinases in Bacteria

Two-component systems have long been considered as the only signal transduction systems existing in prokaryotes. The expression of serine/threonine protein kinases was believed to be restricted to eukaryotes. However, due to the recent availability of hundreds of microbial genome sequences it is becoming apparent that serine/threonine protein kinases may also be widely expressed in the prokaryotic kingdom (CMR/TIGR database). While some species,

such as *E. coli,* possess only very few genes encoding serine/threonine kinases, other bacterial genomes, such as the ones from Anabaena and Myxococcus, display a high prevalence of these genes.

The first serine/threonine protein kinase described in a prokaryote was protein kinase N1 (Pkn1), expressed in *Myxococcus xanthus*. This soil bacterium is characterized by a complex social behavior; it grows vegetatively in the presence of nutrients but forms fruiting bodies upon starvation. Pkn1 was shown to play an important role in this differentiation process (Munoz-Dorado et al., 1991; Zhang et al., 1992). Another kinase also expressed by *M. xanthus*, protein kinase N2 (Pkn2), was the first receptor-type serine/threonine protein kinase identified in prokaryotes and found to function as a negative regulator of fruiting body formation (Udo et al., 1996; Udo et al., 1997).

Regarding the origin of eukaryotic-like serine/threonine kinases in bacteria, two hypotheses have evolved: the first hypothesis states that genes encoding serine/threonine kinases were already present in the common ancestor of the phyla bacteria, archea and eukaryotes. Consequently, the kinase genes evolved and adapted to their genetic background or even disappeared in some prokaryotes (Han and Zhang, 2001; Ogawara et al., 1999; Ponting et al., 1999). The second hypothesis postulates that genes encoding serine/threonine protein kinases were acquired by prokaryotes through horizontal gene transfer from eukaryotic organisms (Leonard et al., 1998; Ochman et al., 2000). In order to clarify the origin of prokaryotic genes encoding serine/threonine kinases, the G+C-content and codon usage of open reading frames has been analyzed. In *Synechocystis* sp. PCC 6803 and several other prokaryotic species including *Mycobacterium tuberculosis* (Han and Zhang, 2001; Ogawara et al., 1999) it was shown that G+C content and codon usage of individual open reading frames of serine/threonine kinases are similar to the average of all genes from this particular genome. These findings therefore suggest that the so-called eukaryotic-like kinases were already present before eukaryotes and prokaryotes diverged. Phylogenetic analysis of kinases within a certain species showed that they are only distantly related, supporting the theory that they have diverged early in evolution and evolved independently of each other (Han and Zhang, 2001; Ogawara et al., 1999; Ponting et al., 1999).

On the other hand, the horizontal transfer hypothesis is supported by the presence of certain eukaryotic domains (such as β-propeller domains) in prokaryotic serine/threonine kinases,

which implies that these domains were acquired from eukaryotic donors, possibly due to a parasitic life-style. Domains with universal distribution such as tetratricopeptide repeats and PDZ domains are likely to have been present already in the common ancestor of eukaryota, archea and bacteria (Ponting et al., 1999).

1.3 Mycobacterial Kinases

In mycobacteria, signal transduction processes occur through both two-component systems as well as serine/threonine protein kinases. Sequence analysis of the *M. tuberculosis* genome revealed the presence of genes encoding 11 two-component systems as well as 11 eukaryotic-like serine/threonine protein kinases (Av-Gay and Everett, 2000; Cole et al., 1998; Ponting et al., 1999). Thus, as opposed to other bacterial species having comparable genome sizes, mycobacterial genomes contain a relatively low number of two-component systems and an unusual high number of serine/threonine protein kinases. However, it should be noted that the number of serine/threonine kinases varies from four in *Mycobacterium leprae* to 24 in *Mycobacterium marinum* (Wehenkel et al., 2008). Interestingly, *M. leprae* is characterized by a lower G+C content and a 26% reduced genome size compared to *M. tuberculosis* (Cole et al., 2001). In addition, only about half of the genome codes for proteins, while the remaining sequences are regulatory or cover pseudogenes, which is in marked contrast to *M. tuberculosis* possessing over 90% protein coding genes. The extensive gene decay in *M. leprae* suggests that this mycobacterial species retained a minimal set of genes required for pathogenicity. Consequently, the four genes encoding serine/threonine kinases still present in its genome are regarded as essential and probably carry out crucial physiological functions (Cole et al., 2001) (figure 1.2).

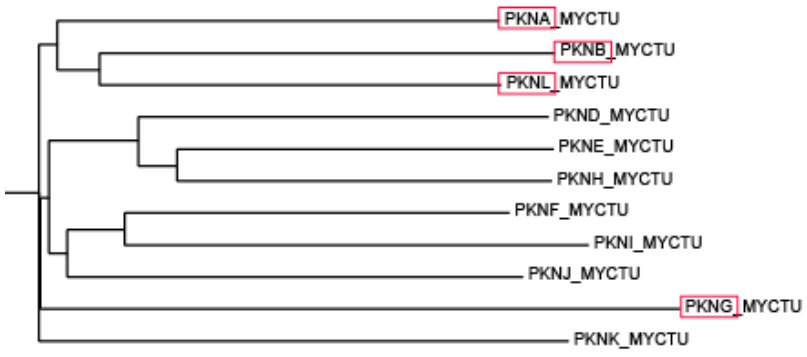

Figure 1.2. Members of the serine/threonine protein kinase family of *M. tuberculosis*. Based on their amino acid sequence, the receptor-like kinases can be clustered in three distinct groups: group I: PknA, PknB, PknL, group II: PknD, PknE, PknH and group III: PknF, PknI, PknJ. PknG and PknK, the soluble kinases, are only distantly related to the other kinases. In red boxes are the four kinases present in M. leprae. The phylogenetic tree was created using ClustalW and Phylodendron software.

Of the 11 kinases identified in the genome of *M. tuberculosis*, nine are typical receptor-like kinases containing a transmembrane domain, whereas two of these kinases are predicted to be cytosolic, namely protein kinase G (PknG) and protein kinase K (PknK) (Cole et al., 1998). Based on their amino acid sequence similarity, the receptor kinases can be clustered in the following three distinct groups: PknA/PknB/PknL, PknD/PknE/PknH, and PknF/PknI/PknJ (Av-Gay and Everett, 2000; Gopalaswamy et al., 2004; Narayan et al., 2007) (Figure 1.2 and 1.3). All mycobacterial serine/threonine kinases possess eleven conserved motifs characteristic of Hanks-type kinases (Wehenkel et al., 2008) and are thus members of the Protein Kinase N2 family which is most closely related to eukaryotic serine/threonine kinases (Boitel et al., 2003, Cole et al., 1998).

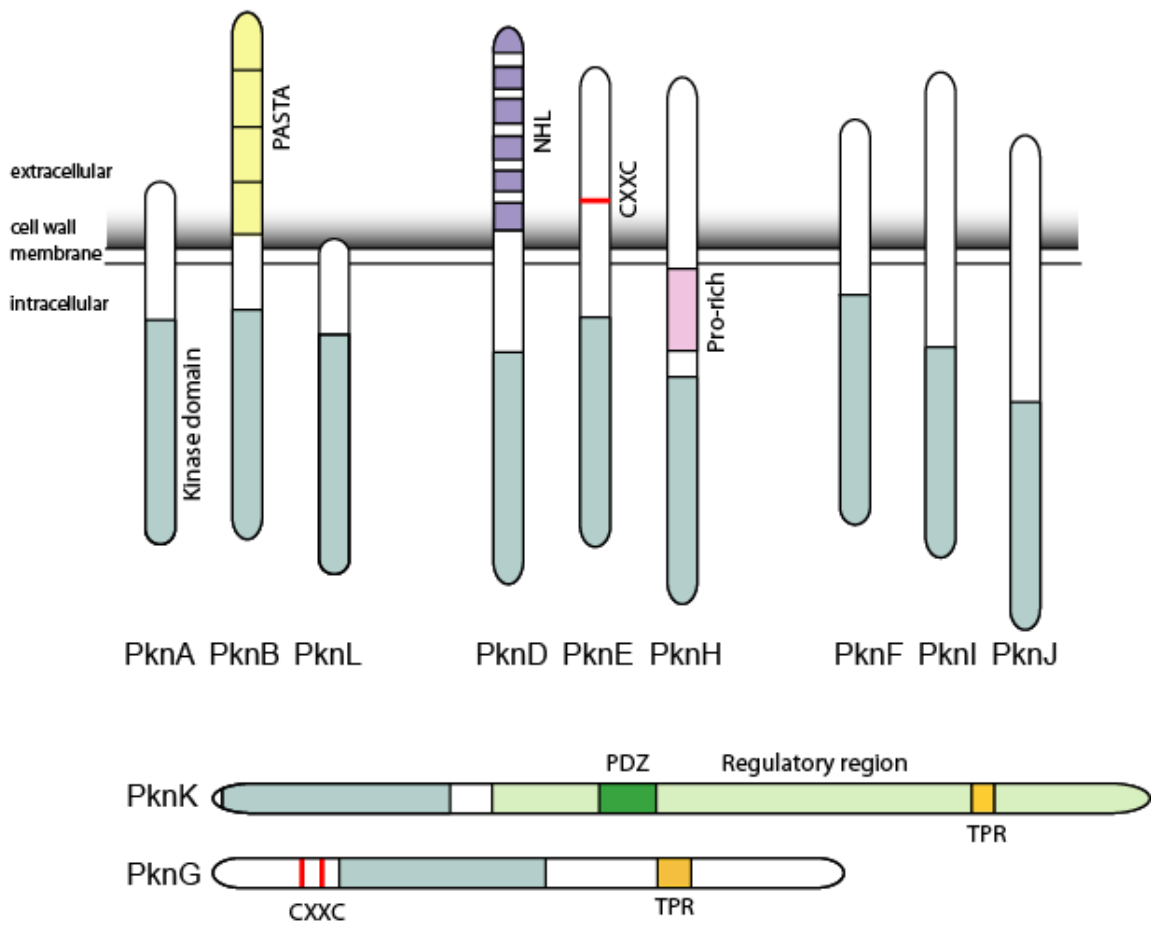

Figure 1.3. Overview of the eleven eukaryotic-like serine/threonine protein kinases of *M. tuberculosis* grouped according to their sequence similarity. The N-terminally located kinase domains are labelled in light blue, characteristic features are indicated (CXXC: Thioredoxin motif, TPR: Tetratricopeptide repeat domain, PDZ domain: **P**ost synaptic density protein (PSD95), Drosophila **d**isc large tumor suppressor A (DlgA), and **Z**onula occludens-1 protein (zo-1), PASTA: Penicillin A binding and Ser/Thr kinase attached, NHL-β-propeller: Ncl-1, HT2A and Lin-41 proteins, Pro-rich: Prolin-rich region).

1.3.1 Group I Serine/Threonine Kinases: Protein Kinases A, B and L

Protein kinase A (PknA)

In *M. tuberculosis*, the genes coding for protein kinase A and protein kinase B (*pkn*A and *pkn*B) are located within a gene cluster encompassing two genes implicated in the synthesis of cell wall components (*php*A and *rod*A) as well as *mst*P, which encodes the single mycobacterial serine/threonine phosphatase belonging to the protein phosphatase 2A (PP2A) family of protein phosphatases (Cole et al., 1998). MstP, a manganese-dependant phosphatase with a transmembrane domain, was shown to efficiently dephosphorylate PknA and PknB suggesting that MstP regulates the activity of these kinases (Chopra et al., 2003). The genes forming this operon are present across pathogenic and non-pathogenic mycobacterial species supporting the idea that their function is essential for survival of the bacteria (Narayan et al., 2007; Sassetti et al., 2003). Indeed, mycobacteria with PknA and PknB null mutations are not viable (Kang et al., 2005).

Initial experiments involving PknA overexpression both in *E. coli* as well as in mycobacteria demonstrated that the cells became elongated, pointing to a possible role in DNA replication and segregation or, alternatively, in septum formation (Chaba et al., 2002; Kang et al., 2005). Interestingly, PknA overexpression resulted in mono-and bi-nucleoidal cells suggesting that PknA interacts with proteins implicated in septum formation (Chaba et al., 2002). The mutant cells displayed an irregular shape which included broad, long and branched mycobacteria. Protein kinase A was found to phosphorylate a conserved hypothetical protein of unknown function (Rv1422), and the Rv2145c gene product Wag31, also known as Ag84 or DivIVA. Wag31, which contains a sequence motif identified by a peptide library screen, is an essential protein in *M. tuberculosis* involved in regulation of the cell shape and septum formation (Kang et al., 2005). Overexpression of Wag31 causes a phenotype which includes aberrant cell shapes and unbalanced septum formation (Nguyen et al., 2007). The specific interaction between PknA and Wag31 was confirmed *in vitro* by kinase assays and *in vivo* by Western Blot analysis including Wag31 overexpressing strains. It was shown that the phosphorylation state of Wag31 is crucial for its capacity to control cell shape formation (Kang et al., 2005).

Another substrate for PknA is bacterial FtsZ, a GTPase representing the homologue of eukaryotic tubulin which acts in septum formation. Phosphorylation on threonines abolishes the capability of mFtsZ to hydrolyze GTP as well as its property to polymerize (Dubnau et al., 2000; Thakur and Chakraborti, 2006).

Additional substrates for PknA have been reported recently. PknA is able to phosphorylate enzymes involved in the biosynthesis of mycolic acids which are considered as major virulence factors of mycobacteria (Dubnau et al., 2000). These substrates, KasA and KasB, are part of a fatty acid elongation system, the so-called FAS-II cycle, in which they control the synthesis of α-branched β-hydroxy fatty acids by catalyzing condensation steps. Another component of this pathway, *mt*FabD, which is encoded by the same operon, carries out the first condensation step and was also shown to be efficiently phosphorylated by PknA. It should be mentioned that these substrates which actually do not possess a FHA-domain, are phosphorylated by PknB, PknE, PknF, and PknH as well (Molle et al., 2006).

Overall, these findings strongly support a role for PknA in the regulation of mycobacterial cell division and cell shape control.

Protein kinase B (PknB)

M. tuberculosis protein kinase B, whose genomic locus is conserved throughout *Mycobacterium* spp, was found to be essential in *M. tuberculosis* and *M. smegmatis*. Gene disruption was only possible by performing allelic gene replacements using a merodiploid *M. tuberculosis* strain; bacteria depleted of *pkn*B were not viable (Wehenkel et al., 2006). Full length PknB as well as the catalytic domain alone display autophosphorylation activity (Av-Gay et al., 1999) suggesting that regions external to the kinase domain are not required to stabilize an active conformation (Boitel et al., 2003). The extracellular domain of PknB contains four sequence repeats of 66-68 amino acids classified as so-called “Penicillin A binding and Ser/Thr kinase attached” (PASTA) domains (Yeats et al., 2002), which often occur in prokaryotic penicillin binding proteins and play a role in cell wall synthesis (Young et al., 2003).

PknB, like PknA, is dephosphorylated by MstP, the only known serine/threonine phosphatase present in *M. tuberculosis*. Since the corresponding genes are located within the same operon,

a functional relationship is suggested (Boitel et al., 2003; Chopra et al., 2003). Dephosphorylation of PknB at Thr171 and Thr173 results in decreased kinase activity, demonstrating that the phosphorylation state of the activation loop regulates PknB activity (Boitel et al., 2003).

PknB expression increases about 10-fold when the cells enter the stationary phase. Studies involving PknB overexpression and partial depletion of *pkn*B resulted in severe morphological defects and reduced viability of the cells pointing to a role of PknB in controlling cell shape (Kang et al., 2005).

A search for PknB substrates resulted in the identification of GarA (Rv1827), a 17.3 kDa protein, as the only soluble mycobacterial substrate (Villarino et al., 2005). At its C-terminus, GarA contains a forkhead-associated (FHA) domain (Durocher and Jackson, 2002). These domains are phosphoprotein recognition units (Durocher and Jackson, 2002; Pallen et al., 2002) which form 11-stranded β-sandwiches mediating phosphorylation-dependent protein-protein interactions. Notably, in GarA, the FHA-domain spans one third of the full protein length. Potential phospho-acceptor sites are located in the N-terminal region of GarA. Kinase assays with a truncated version of GarA as well as mass spectrometry analysis allowed the identification of a single phosphorylated residue in the GarA molecule. PstP treatment of PknB or mutating both autophosphorylation sites of the PknB catalytic loop led to a significant decrease of GarA phosphorylation implicating that recruitment of GarA is dependent on autophosphorylated and thus activated PknB. Interestingly, the interaction between PknB-GarA is not dependent on GarA phosphorylation, suggesting that the PknB catalytic domain is not involved in the interaction (Villarino et al., 2005). It should also be realized that various FHA-containing proteins can be phosphorylated by other mycobacterial kinases, including PknA, PknB, PknD, PknE, PknF, PknG and PknH (Grundner et al., 2005; Molle et al., 2003; Molle et al., 2004; Sharma et al., 2006). Therefore, GarA might be a generic substrate for this class of serine/threonine kinases, rather than a physiological substrate within living bacteria (Sharma et al., 2006).

Besides GarA, Penicillin binding protein A (PBPA), which belongs to a group of serine acyl transferases involved in peptidoglycan synthesis (Popham and Young, 2003), has been shown to localize to the septa and to be phosphorylated by PknB (Dasgupta et al., 2006). Mutagenesis of Thr437, a potential phosphorylation site of PBPA, results in a reduced

growth rate and mis-localization suggesting that PknB phosphorylates PBPA, thereby targeting it to the septum (Dasgupta et al., 2006).

Elucidation of the atomic structure of PknB revealed that the intracellular kinase domain of 268 amino acids is connected through a short linker region to the transmembrane helix and the extracellular domain (Young et al., 2003). The overall fold of the kinase domain displayed the characteristic two-lobed structure consisting of an N-terminal subdomain with a curled β-sheet and a long αC-helix and a C-terminal lobe containing α-helices (Ortiz-Lombardia et al., 2003). The closest structural relative of PknB was found to be the cAMP-dependent protein kinase (cAPK) in its activated state (Young et al., 2003). Most conformational signatures within the catalytic domain pointed to an universally active state (meaning closed conformation) when compared to eukaryotic kinases; however, the disorder of the activation loop and the position of αC-helix were considered as striking, but could be explained by the fact that hyperphosphorylation of the activation loop might be responsible for the observed disorders. A high degree of conservation was found in the area of the ATP binding pocket as well as on the "backside" of the N-terminal lobe (Young et al., 2003).

Recently, the catalytic domain of PknB was crystallized in complex with mitoxantrone, an ATP competitive drug used in cancer treatments (Shenkenberg and Von Hoff, 1986; Wehenkel et al., 2006). The inhibitor is bound in a hydrophobic cleft that is usually occupied by ATP. Mitoxantrone does not fully exploit the shape of the ATP binding pocket suggesting a potential to optimize the drug. Based on the fact that the PknB-mitoxantrone complex crystallized as a back-to-back homodimer consisting of similar monomers having a different space group as observed previously, it was assumed that this conformation has physiological relevance. Comparisons with dimerized PKR, the human RNA-dependent antiviral protein kinase (Dar et al., 2005), as well as with the PknB-like protein kinase PrkC from *B. subtilis* (Madec et al., 2002) led to the assumption that the extracellular domain of PknB could trigger back-to-back homodimerization. Oligomerization in turn allows regulation of PknB activity, presumably by autophosphorylation of threonine residues within the activation loop.

The fact that PknB, like PknA, is an essential kinase has made these molecules potential targets for the development of anti-tuberculosis compounds. Together with results discussed later in this chapter, such a strategy may ultimately result in the successful targeting of PknA and B in order to block growth of *M. tuberculosis.*

Protein kinase L (PknL)

PknL is composed of 399 amino acids corresponding to a calculated molecular weight of 42.8 kDa. PknL differs from the other receptor-like kinases in that its transmembrane domain is located at the extreme C-terminus. Together with PknA, PknB and PknG, PknL belongs to those mycobacterial kinases with homologues in the pathogen *M. leprae* and is therefore considered as essential for virulence. Bioinformatic analysis has revealed that PknL homologues in other species of actinobacteria possess a PASTA domain (Yeats et al., 2002), an extracellular sensor domain, which in mycobacteria is also found in PknB, pointing to the possibility that these two kinases might have a common origin (Narayan et al., 2007). This assumption is further supported by the analysis of the *pkn*L gene locus in *M. tuberculosis*. As observed for *pkn*B, the *pkn*L gene is part of a 30 kb cluster which encompasses several genes involved in cell wall synthesis and cell division, suggesting that the two kinases might act in the same signal transduction cascade controlling cell division (Narayan et al., 2007). Recent work identified Rv2175c, whose genomic locus is adjacent to *pknL*, as a substrate of PknL (Canova et al., 2008). The protein shares similarity with transcriptional regulatory proteins by containing a helix-turn-helix motif characteristic of DNA-binding proteins. Phosphorylation of Rv2175 was found to be dependent on a specific phosphorylated threonine residue, located within the activation loop of PknL (Canova et al., 2008).

1.3.2 Group II Serine/Threonine Kinases: Protein Kinases D, E and H

Protein kinase D (PknD)

M. tuberculosis protein kinase D is a 69.5 kDa transmembrane protein which has an C-terminal extracellular domain containing six tandem repeats of a module size of 40 amino acids. The gene encoding PknD is located between *pst*S-2 and *pst*A-1, two genes encoding a phosphate-binding protein and a membrane-bound phosphate permease protein subunit. Due to this chromosomal arrangement, a role for PknD in regulating phosphate transport has been proposed, although no experimental evidence exists at present (Peirs et al., 2005). PknD from *M. tuberculosis* localizes to the cell envelope, whereas PknD from *M. bovis* BCG is a truncated protein of 31 kDa, lacking the transmembrane and the C-terminal regulatory domain, and is therefore likely to act as a cytoplasmic kinase (Peirs et al., 2000).

As with many other serine/threonine kinases, PknD possesses autophosphorylation activity and shows a rather complex phosphorylation pattern. The phosphorylation sites are located within the kinase domain including the activation loop (Thr169, Thr171, Thr173) as well as in a segment close to the kinase domain (Duran et al., 2005; Virginie Molle, 2006). Purified PknD is able to phosphorylate the forkhead-associated domain A (FHA-A) of Rv1747, which provides evidence that an interacting partner does not always originate from the same operon (Grundner et al., 2005). A multiply phosphorylated potential substrate of 83 kDa was found by 2D-gel analysis and subsequently identified as MmpL7, a membrane protein with 12 transmembrane regions (Perez et al., 2006). In total, 13 MmpL genes exist in *M. tuberculosis*; many of these are located close to genes coding for proteins involved in fatty acid or polyketide synthesis. MmpL7 is believed to be involved in virulence, since it is responsible for the transport of phtiocerol dimycoceroserate (PDIM) and sulfolipid-N that are important mycobacterial cell wall components. However, a direct interaction between PknD and MmpL7 is unlikely, since the MmpL7 phospho-acceptor sites are extracellular whereas the kinase domain of PknD is located within the cytosol (Perez et al., 2006).

To elucidate the role of PknD in signalling, PknD was expressed under control of an acetamide-inducible promoter (Greenstein et al., 2007). A gene homologous to anti-anti-sigma factors, Rv0516c, was observed to be significantly induced upon PknD overexpression. It was found that PknD specifically phosphorylates Rv0516c on one single threonine residue; the reaction was inhibited by SP600125, a c-Jun N-terminal kinase inhibitor, in a dose-dependent manner (Greenstein et al., 2007). The fact that an anti-anti-sigma factor is regulated by an eukaryotic-like serine/threonine kinase is an unexpected finding, since these proteins are usually regulated by anti-sigma factors.

Not much is known about the sensor domains of the mycobacterial kinases that react to external signals. Based on structure predictions, the PknD sensor domain has been proposed to contain a ß-propeller, a motif found in diverse eukaryotic proteins. The structure of the 261 amino acid PknD sensor domain (figure 1.4) has been solved at a resolution of 1.8 Å, revealing that the sensor domain forms a ß-propeller consisting of six blades which are arranged in a circle around a central pore (Good et al., 2004). The blades are characterized by high internal sequence conservation, as opposed to the loops, which show considerable variability. Loops connecting the blades form a cup-like structure which often comprises the active site or a functional binding surface. Due to the remarkable sequence identity of the

blades, it has been speculated that PknD might in fact bind six homologous ligands (figure 1.4). Alternatively, PknD may interact via its variable residues with a single asymmetric ligand (Good et al., 2004).

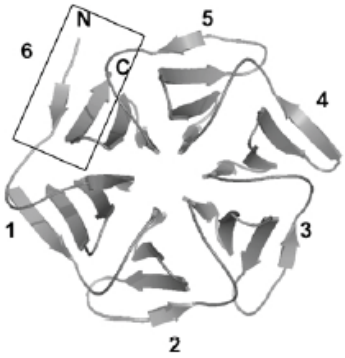

Figure 1.4. Sensor domain of PknD. Structure of the β-propeller of PknD consisting of 6 identical blades (numbered 1-6) arranged around a central pore. Each blade is composed of four antiparallel β-strands. Loops connecting the blades form a cup-like structure which often comprises the active site or a functional binding surface. Indicated by a box is the topological overlap which holds the structure together (taken from Good et al., JMB, 2004)

Dimerization of PknD leads to allosteric activation of the kinase (Greenstein et al., 2007), a mechanism that has also been proposed for PknB, PknE, PknG, and PknK, since these kinases contain N-terminally located potential interaction domains. It is unlikely to occur in PknA, PknF, PknH, PknI and PknJ because of the different predicted N-terminal structures of these kinases (Greenstein et al., 2007).

Protein kinase E (PknE)

Biochemical characterization of PknE revealed that this kinase becomes autophosphorylated on multiple serine and threonine residues within the catalytic domain and especially in the activation loop (Duran et al., 2005; Molle et al., 2003a; Virginie Molle, 2006). Interestingly, phosphorylation of the juxtamembrane region was not only shown for PknE, but also for PknB, PknD and PknF, indicating that these sites could be relevant for stability, activity or alternatively, for binding of interacting partners (Duran et al., 2005). PknE was found to phosphorylate Rv1747, a putative ABC transporter which is also a substrate for PknB, PknD and PknF (Grundner et al., 2005). Moreover, PknE phosphorylates GarA *in vitro*, which, as mentioned, is also phosphorylated by several other protein kinases (Villarino et al., 2005).

The PknE kinase domain is a homodimer in analogy to PknB with which it shares 37% sequence similarity (Gay et al., 2006). However, some interactions across the dimer interface clearly differ in PknE as compared to PknB. The PknE subunits adopt an open conformation characteristic of inactive serine/threonine kinases although the soluble protein was

phosphorylated and active (but as well monomeric). The conformation of critical catalytic residues within the kinase domain indicates that PknE is unable to bind ATP (Gay et al., 2006).

The promoter of *pkn*E responds to nitric stress. Exposure to nitric oxide donors such as sodium nitroprusside (SNP) or S-nitrosoglutathione (GSNO) leads to up-regulation of promoter activity. In contrast, transcription is downregulated by hydrogen peroxide thus supporting the idea that *pkn*E expression is not required during oxidative stress (Jayakumar et al., 2007).

To elucidate a role for PknE, the *pkn*E gene was deleted by specialized transduction. Mycobacteria lacking PknE showed no growth defect or differential sensitivity towards nitric stress (Jayakumar et al., 2007). However, the mutant strain was more sensitive to reducing agents, such as dithiotreitol (DTT) and reduced glutathione (Otter et al., 1992), and to certain metal ions, such as Zn and Cd. Based on these findings, a role for PknE in scavenging nitric-oxide free radicals is proposed, which would increase the resistance to this innate defence mechanism during macrophage infection.

The observed sensitivity to reducing agents can be explained by the presence of a protein disulfide isomerase DSBA-like thioredoxin domain at the C-terminus of PknE. Proteins harbouring such CXXC-motifs are thought to be involved in redox signalling or -homeostasis. Pathogenic species, such as *Neisseria meningitides*, express disulfide oxidoreductases, members of the thioredoxin family which contain CXXC motifs at their active site. These enzymes act as chaperones and reduce their substrates, mostly membrane-bound or exported proteins, to ensure stability or proper folding (Tinsley et al., 2004). Mycobacteria encounter different redox environments, ranging from aerobic conditions of free-living bacteria to an oxygen-depleted situation in granulomas; a lifestyle which requires a tight adaptation and regulation of protein function, and the presence of CXXC motifs in mycobacterial serine/threonine kinases may help to regulate protein function appropriately.

Since the presence of nitric oxide can be linked to host cell apoptosis, the *M. tuberculosis* Δ*pkn*E mutant was used in a macrophage infection model and the possible contribution of PknE to apoptosis was studied. Apoptosis was found to be significantly increased in the case of the mutant strain and the apoptotic effect was even more pronounced upon treatment of

macrophages with a nitric oxide donor indicating that PknE plays a cytoprotective role. In addition, proliferation of *Δpkn*E mycobacteria inside macrophages as well as the cytokine response of TNF-α and IL-6 were considerably reduced (Jayakumar et al., 2007).

Protein kinase H (PknH)

Adjacent to the C-terminus of its kinase domain, PknH features a proline-rich region with 38 proline residues distributed over a stretch of 107 amino acids. This region was proposed to function as a linker region or to mediate substrate binding. Like other mycobacterial serine/threonine kinases, PknH was shown to undergo autophosphorylation in the presence of divalent ions and to phosphorylate histones as exogenous substrate (Molle et al., 2003; Sharma et al., 2004).

Low pH values and heat shock (42°C) decrease PknH expression significantly, but oxidative stress, hypoxia or nutrient deprivation have no influence on transcription levels. The fact that *pkn*H is not present in non-pathogenic species, such as *M. smegmatis*, and the observation that its expression is induced under certain stress conditions suggests that PknH could play a role in sensing stress factors occurring in a hostile environment (Sharma et al., 2004).

The *pkn*H gene is located downstream of the *emb*R gene, that encodes a putative transcriptional activator assigned to the OmpR-like family. EmbR was proposed to control the transcription of the *emb* operon, which in *M. tuberculosis* consists of the *emb*A, *emb*B and *emb*C genes (Sharma et al., 2006). The corresponding proteins are arabinosyltransferases involved in the synthesis of arabinan, which is a complex homopolymer integrated in the cell wall components arabinogalactan or lipoarabinomannan (LAM), the latter one being an important virulence factor (Molle et al., 2003). The structure of EmbR revealed the existence of a N-terminal helix-turn-helix DNA binding domain, a central bacterial transcription activation domain and a C-terminal forkhead-associated domain containing the phosphothreonine recognition motif (Alderwick et al., 2006). Autophosphorylation of the activation loop of PknH has a regulatory role and is required for activation of the kinase. Furthermore, EmbR phosphorylation by PknH is mediated by the FHA domain of EmbR, as proved in assays with mutated EmbR versions (Molle et al., 2003).

Phosphorylation dependent DNA binding activity of EmbR is necessary for positive

regulation of the *emb*CAB operon. High levels of arabinosyltransferases result in a high LAM:lipomannan (LM) ratio which is directly correlated with an increase in mycobacterial virulence (Sharma et al., 2006). A high LAM:LM ratio allows the bacteria to suppress the immune response of the host, since the arabinan domain of LAM inhibits the proinflammatory activity of LM on macrophages (Sharma et al., 2006). In addition, expression levels during the transition phase from extracellular to intracellular lifestyle were studied. Interestingly, it was found that PknH expression is significantly upregulated within host cells (Sharma et al., 2006).

Recently, a genomic region was identified in *M. tuberculosis* CDC1551, which encoded a gene highly homologous to EmbR (Molle et al., 2007). This gene, termed *emb*R2, is not present in *M. tuberculosis* H37Rv. Although the domain organization and crucial amino acid residues within the FHA domain are similar, EmbR2 is not a substrate of PknH *in vitro*. However, other serine/threonine kinases tested were partially able to phosphorylate EmbR2, indicating a different substrate specificity. Since an interaction between PknH and EmbR2 as well as potential docking sites within PknH were found, it was assumed that EmbR2 acts as an inhibitor of PknH. By performing kinase assays, dose-dependent inhibition of PknH autophosphorylation, as well as inhibition of EmbR substrate phosphorylation was confirmed. These findings suggest that EmbR2 might act as a key regulator of PknH activity which in turn mediates phosphorylation of EmbR. Furthermore, an ATP-competitive CDK inhibitor named O6-cyclohexylmethylguanine was found to efficiently inhibit PknH activity. PknD and PknE, which, based on their amino acid sequence, are closely related to PknH, were inhibited as well, but no inhibition was observed for the kinases PknA, PknB, PknF, PknK and PknL (Molle et al., 2008).

To identify a possible role of PknH in free-growing bacteria or during infection, a strain with a *pkn*H deletion was constructed and tested. Since the phosphorylation state of PknH is likely to be regulated by intracellular signals, such as reactive oxygen species and nitric oxide produced by the host, the bacteria were assayed for survival under these conditions. The Δ*pkn*H strain displayed a higher tolerance to acidified sodium nitrite, but was more sensitive to peroxide and superoxide, and showed decreased viability compared to the control strains. However, infection of mice with *M. tuberculosis* lacking *pkn*H resulted in a higher bacterial load compared to the load obtained in mice infected with wildtype *M. tuberculosis;* this effect of increased *in vivo* growth and survival was even more pronounced at late time points

of infection. These results suggest that PknH plays an important role in mycobacterial growth in the chronic phase of infection (Papavinasasundaram et al., 2005).

To identify potential substrates, 40 candidate proteins were selected by a bioinformatics approach. DacB1 and Rv0681, both proteins which do not possess a FHA domain, were analyzed in detail (Zheng et al., 2007). DacB1 is a membrane-bound protein, a penicillin-binding protein/carboxypeptidase, which is implicated in cell wall biosynthesis in *B. subtilis* (Buchanan et al., 1992). Rv0681 is a transcriptional regulatory protein possessing a TetR-type helix-turn-helix motif (Zheng et al., 2007). Direct phosphorylation of DacB1 and Rv0681 was confirmed by performing *in vitro* kinase assays (Zheng et al., 2007).

1.3.3 Group III Serine/Threonine Kinases: Protein Kinases F, I and J

Protein kinase F (PknF)

PknF, a protein of 476 amino acids, has been found to localize to the cell envelope (Koul et al., 2001). The operon to which *pkn*F belongs, contains another gene, Rv1747, encoding a putative ATP binding cassette transporter. These transporters are translocators responsible for the uptake and export of various molecules across the cell membrane, in a process coupled to ATP hydrolysis. Since phosphorylation is known to regulate stability and activity of ABC transporters, a functional relationship between PknF and Rv1747 was investigated. Interestingly, Rv1747 is the only protein in the *M. tuberculosis* genome possessing two forkhead-associated domains, suggesting that its function may be extensively regulated through phosphorylation. PknF phosphorylates Rv1747 *in vitro*, and mutation of each of the two N-terminally located FHA domains on Rv1747 results in a significant decrease in phosphorylation (Molle et al., 2004).

A physiological role for PknF was analyzed by an antisense approach in *M. tuberculosis*, as well as by expressing PknF in *M. smegmatis*, which normally does not express PknF. *M. tuberculosis* expressing antisense RNA against PknF had a shorter generation time and the cells had bulbous ends and abnormal septa (Deol et al., 2005). Conversely, expression of PknF in *M. smegmatis* resulted in reduced growth and in drastic morphological changes. These observations suggest that PknF is involved in the regulation of cell division at different

stages eg. septum formation and elongation (Deol et al., 2005). Interestingly, the *M. tuberculosis* antisense strain showed an increased uptake of ^{14}C glucose compared to wildtype, suggesting an additional role of PknF in the negative regulation of glucose uptake mediated through the ABC transporter Rv1747 located within the same operon (Deol et al., 2005). While the growth of a Rv1747 deletion mutant is normal *in vitro,* mice infected with the mutant strain displayed significantly less colony forming units in lungs and spleen (Curry et al., 2005), suggesting the ABC transporter function is important for normal growth *in vivo*.

Protein kinase I (PknI)

Few studies have been carried out on PknI, a 585 amino acid protein encoded in an operon containing genes involved in cell division (*dac*B and *fts*Y) as extrapolated from other bacterial species like *B. subtilis* and *E. coli* (Av-Gay and Everett, 2000; Popham et al., 1995; Popham and Young, 2003). PknI is the only mycobacterial kinase whose active site contains an asparagine instead of the usual lysine in the catalytic loop (Av-Gay and Everett, 2000). Cellular fractionation revealed that PknI distributes to the cytosolic fraction despite the presence of a transmembrane domain (Singh et al., 2006). Apart from this rather striking finding, PknI showed typical kinase properties such as autophosphorylation, phosphorylation of myelin basic protein as well as activity dependence on Mn^{2+} (Gopalaswamy et al., 2004). Analysis of PknI expression levels during the course of infection of human THP-1 macrophage-like cells with *M. tuberculosis* suggests that PknI expression is initially low and decreases even more at later times (Singh et al., 2006) although the significance of this expression pattern remains unknown.

Protein kinase J (PknJ)

PknJ is a 61.6 kDa protein with a predicted transmembrane region. Its genomic localization is defined by several nearby transposon genes (Av-Gay and Everett, 2000). PknJ is only present in species of the *M. tuberculosis* complex and does not seem to harbor any specific features. Nevertheless, ongoing studies on PknJ may clarify functions and properties of the kinase.

1.3.4 Group IV Serine/Threonine Kinases: Protein Kinases K and G

Protein kinase K (PknK)

With a molecular weight of 119.4 kDa, PknK is the largest serine/threonine kinase identified in *M. tuberculosis*. PknK, together with PknG, does not possess a transmembrane domain and is therefore predicted to be localized in the cytosol of the bacilli. Thus far, the kinase itself has not been biochemically characterized, hence the only conclusions regarding PknK function can be drawn from its genomic localization and domain architecture. PknK contains an additional ATP binding pocket within the kinase domain as well as an ATP binding motif (Av-Gay and Everett, 2000). This particular AAA domain comprises a so-called PDZ domain, which has been shown to be required for targeting signalling molecules to sub-membranous sites (Ponting et al., 1997). PknK is further characterized by a C-terminal region which displays homology to regulatory regions found in transcriptional regulators of the LuxR family (Av-Gay and Everett, 2000). This regulatory region further encompasses a helix-turn-helix motif as well as a tetratricopeptide domain which often mediates protein-protein interactions. The genomic localization of *pkn*K upstream of a gene homologous to members of the LuxA family (involved in flavin monucleotide metabolism) supports the hypothesis that PknK might play a role in the regulation of secondary metabolism. However, *pkn*K is also closely localized to the transcriptional regulator *vir*S, implicated in virulence (Av-Gay and Everett, 2000; Narayan et al., 2007). The elucidation of a physiological function of PknK will require more extensive analysis.

Protein kinase G (PknG)

PknG, a 82 kDa protein displaying autophosphorylation activity, is different from the other mycobacterial kinases in that it has an extended N-terminal region which precedes the kinase domain. Moreover, it does not contain a transmembrane domain, suggesting that this protein, like PknK, is located in the cytoplasm. Within the N-terminal domain of PknG are two CXXC motifs whereas at the C-terminus, a tetratricopeptide (TPR)-like region is present (figure 1.5). CXXC motifs are essential for the catalysis of redox reactions since the cysteines can reversibly form disulfide bonds

Figure 1.5. The domain architecture of PknG. The kinase domain (blue) covering one third of the protein is flanked by an N-terminal domain characterized by two CXXC motifs and by a C-terminal region containing a tetratricopeptide repeat.

(Laboissiëre et al., 1995; Walker et al., 1996). The ubiquitously distributed CXXC motifs enable proteins to carry out several functions which are based on protection against stress, such as the control of correct folding or removal of peroxides (Tinsley et al., 2004).
TPR-like regions are motifs of 34 amino acids that are usually three-16 times repeated. These motifs are predominantly found in eukaryotic proteins where they mediate protein-protein interactions.

The *pkn*G gene locus has been shown to be present and conserved throughout the mycobacterial genus (Narayan et al., 2007). Interestingly, PknG is not expressed in non-pathogenic mycobacteria such as *M. smegmatis* (Walburger et al., 2004). When *pkn*G is deleted in pathogenic mycobacteria, no apparent phenotype is observed in mutant strains grown *in vitro* compared to wildtype mycobacteria (Nguyen et al., 2005). However, upon infection of macrophages, bacilli lacking PknG are rapidly transferred to lysosomes and killed, whereas wildtype mycobacteria can survive within non-lysosomal phagosomes (Walburger et al., 2004). At this point it should be noted that preventing or delaying phagosome-lysosome fusion is an important strategy utilized by pathogenic mycobacteria to ensure their survival (Hart, 1975; Nguyen and Pieters, 2005; Pieters, 2001). To analyze whether this capacity of PknG to prevent lysosomal delivery is related to its kinase activity, a kinase-dead molecule was overexpressed in wildtype *M. bovis* BCG. Overexpression of this mutant, PknG-K/M, resulted in rapid transfer to lysosomes and intracellular killing of these bacteria, suggesting that the kinase activity of protein kinase G is essential for its ability to modulate phagosome-lysosome transfer and to confer mycobacterial survival inside macrophages (figure 1.6).

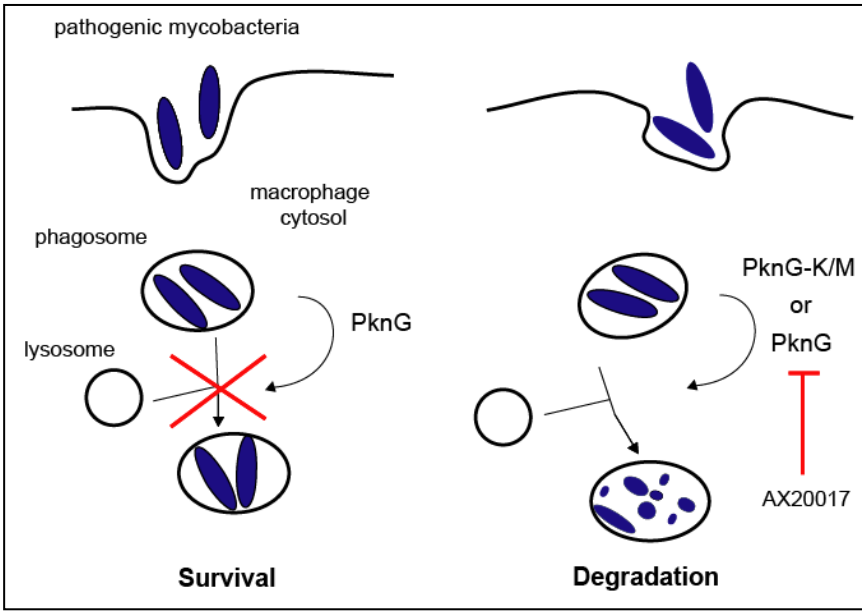

Figure 1.6. Trafficking of mycobacteria expressing PknG.
Upon phagocytosis of pathogenic mycobacteria, PknG is secreted into the cytosol and prevents the fusion of the mycobacterial phagosome with lysosomes resulting in survival of the bacilli (left panel). However, mycobacteria expressing a kinase-dead version of PknG or bacteria treated with the inhibitor AX20017 are incapable of blocking phagosome maturation, finally leading to degradation of the mycobacteria (right panel).

PknG is actively secreted into the macrophage cytosol upon infection (Walburger et al., 2004), presumably phosphorylating substrates present in the macrophage cytosol. Importantly, PknG does not possess a classical signal sequence that would allow secretion in a sec-dependent manner through the mycobacterial membrane. Therefore, it is likely that PknG is secreted by a thus far undefined specialized secretion system. In addition, it needs to be established, how PknG is translocated from phagosomes into the cytosol.

The relocation of PknG-deficient pathogenic mycobacteria from phagosomes to lysosomes, resulting in mycobacterial killing, makes this kinase a promising drug target. A screen for small molecular weight compounds identified a tetrahydrobenzothiophene, termed AX20017, that efficiently blocks PknG kinase activity *in vitro* (Walburger et al., 2004). AX20017 is highly effective in re-directing mycobacteria to lysosomes and inducing killing of *M. tuberculosis* in macrophages (figures 1.6 and 1.7).

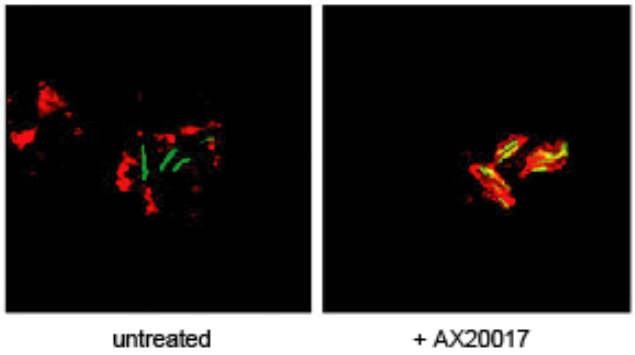

Figure 1.7. Intracellular trafficking of mycobacteria upon treatment with the PknG inhibitor AX20017. Macrophages (J774) were infected for 1 h with wildtype *M. bovis* BCG expressing GFP in the presence or absence of the inhibitor (20 µM). After a 2 h chase, the cells were fixed, permeabilized and stained with antibodies against the lysosomal marker LAMP 1 (red). When macrophages are treated with the PknG specific inhibitor AX20017, mycobacteria predominantly localize within lysosomes (Walburger et al., 2004)

In *Corynebacterium glutamicum*, an actinobacterium related to *M. tuberculosis*, a mutant depleted of a PknG homologue was found to be impaired in glutamine utilization. Proteome analysis of wildtype and mutant strains led to the identification of Odh1 as putative substrate of corynebacterial PknG. This 15 kDa FHA domain-containing protein represents the homolog of mycobacterial GarA and is a key enzyme of the tricarboxylic acid cycle in Corynebacteria. It has been shown that phosphorylation of Odh1 on amino acid residue T14 is essential for proper glutamine utilization and efficient glutamate production (Niebisch et al., 2006; Schultz et al., 2007).

In the genome of *M. bovis* BCG, *pknG* is located in a putative operon containing *glnH*, encoding a protein potentially playing a role in glutamine uptake. However, deletion of pknG did neither affect glutamine uptake nor intracellular glutamine concentrations suggesting that glutamine metabolism is not controlled by PknG in *M. bovis* BCG (Nguyen et al., 2005).

In conclusion, PknG has been shown to promote survival of mycobacteria within macrophages by preventing phagosome-lysosome fusion and is therefore considered as an important virulence factor. Identification of PknG substrates and secretion machinery as well as elucidation of the structure of PknG may help to substantiate the mode of function of PknG.

1.4 Protein kinases in the context of drug design

1.4.1 Tuberculosis-a global threat to human health

With 2.2 billion infected individuals and over 2 million TB-related deaths per year, tuberculosis remains to be the world's most infectious bacterial disease (www.who.int/tb). It has been prognosticated that 200 million people will become newly infected within the next 20 years if current trends continue (Global alliance for TB drug development). *M. tuberculosis*, the causative agent of tuberculosis, possesses an almost impermeable cell wall and specialized defense systems providing intrinsic tolerance towards antibiotics (Nguyen and Pieters, 2008). The recent emergence of extensively drug-resistant (XDR) *M. tuberculosis* strains raises concerns of a future TB epidemic. These highly virulent strains are characterized by being resistant to at least isoniazid and rifampicin (i. e. multidrug-resistant or MDR-TB), plus resistance to any fluroquinolones and anyone of the injectable second-line anti-TB drugs like amikacin, kanamycin or capreomycin. To date, the existence of XDR strains has been confirmed in 41 countries (www.who.int/tb). In order to restrict TB dissemination, the development of novel drugs and efficient vaccines is of utmost importance.

1.4.2 Inhibition of mycobacterial kinases

In addition to proteins involved in control of cell wall synthesis or cell division, kinases implicated in signalling are intensively studied as potential anti-mycobacterial targets (Janin, 2007). Currently, mycobacterial kinases having important physiological functions or those involved in virulence are being evaluated as potential drug targets.

Effective inhibition can be achieved by either blocking ATP binding or by preventing protein-protein interactions as well as by RNA-based approaches leading to downregulation of kinase expression levels (Melnikova, 2004).

The existing knowledge about structure and function of several mycobacterial kinases combined with the fact that prokaryotic and eukaryotic serine/threonine kinases share with < 30% only low sequence identities, provide a good basis for the development of anti-mycobacterial drugs (Cohen, 2002; Wehenkel et al., 2008).

1.4.3 Requirements for the development of potent kinase inhibitors

Structure-based design of inhibitors might result in the development of potent drugs, whereas "potency" is defined by the degree of specificity and selectivity of a certain inhibitor towards the kinase.

In general, targeting a kinase in its inactive conformation seems attractive since unique conformations of the kinase domain can be blocked. However, targeting the active conformation might be beneficial as well, since an active conformation requires conservation of the 3D structure and is therefore less tolerant of potential resistant mutations. The potency of the inhibitor increases by targeting different conformations of a particular kinase but at the expense of selectivity (Noble et al., 2004). Selectivity of mycobacterial kinase inhibitors is a crucial aspect due to the presence of 518 putative human protein kinases (Manning et al., 2002) implicated in various important signal pathways which must not be affected. High selectivity can be achieved when a combination of residues at the ligand-binding forming a uniquely shaped binding pocket is targeted. For the development of inhibitors, targeting a less conserved additional pocket or non-catalytic domains as well as single residues has major advantages regarding selectivity (Noble et al., 2004).
Apart from being efficient and selective, potential tuberculosis drugs must fulfil several requirements to be considered for clinical studies. The Global Drug Alliance proposed the following criteria (www.stoptb.org):

- high efficiency to reduce the treatment duration which usually lasts for 6 months
- potency against resistant strains
- inhibition of dormant mycobacteria
- compatibility with existing TB drugs

- action on new targets
- no interference with other drugs

Many of the eleven kinases expressed by *M. tuberculosis* have been reported to regulate redundant physiological processes. However, kinases essential for survival of mycobacteria such as PknA and PknB, as well as those implicated in virulence such as PknH and PknG are attractive drug targets. For PknB and PknG, efficient inhibitors with minimal inhibitory concentrations in the micromolar range have already been identified (Scherr et al., 2007; Wehenkel et al., 2006). Efforts are ongoing which aim at the identification and optimization of potent PknB inhibitors (Drews et al., 2001). A multi-targeted approach by combining two inhibitors targeting different kinases might be beneficial in terms of efficacy and prevention of resistance.

1.5 Synopsis and concluding remarks

Due to their complex life style, mycobacteria are likely to possess elaborate signalling networks in which the serine/threonine kinases perform important tasks. Recent work has revealed the involvement of several of these kinases in controlling cell shape, cell division, transport, metabolism as well as virulence (figure 1.8).

	Operon	Conser./ Essent.	Features	Substrate	Phys. role	Virulence	Regulation	Inhibitor	Structure
PknA	*pkn*B, *php*A, *rod*A, *mst*P	Yes/Yes	-	DivIVA Rv1422 mFtsZ EmbR KasA/B mtFabD	cell division	?	Mstp	-	-
PknB	*pkn*A, *php*A, *rod*A, *mst*P	Yes/Yes	PASTA	GarA PBPA Rv1422 EmbR Rv0020c Rv 1747 KasA/B	cell division	?	Mstp	Mito-xantrone	KD, KD+Inh
PknL	cell division genes	Yes/?		Rv2175c	regulation of cell division?	?	?	-	-
PknD	*pst*S, *pst*A	No/?	NHL-ß-prop.	Rv0516c MmpL7 GarA	transcription, transport	?	Mstp, dimeriza-tion	SP600125, O6-cyclo-hexyl-methyl guanine	SD
PknE		No/No	CXXC	GarA Rv 1747 KasA/B	stress response apoptosis	?	Mstp	O6-cyclo-hexyl-methyl guanine	KD
PknH	*emb*R	No/No	Pro-rich region	EmbR Dac1B Rv0681 KasA/B	stress resp., infection, arabinan metabolism	yes	Mstp, Embr2	O6-cyclo-hexyl-methyl guanine	-
PknF	Rv1747	No/?	-	Rv 1747 GarA KasA/B	cell division, glucose-uptake, transport	?	Mstp	-	-
PknI	*dac*B, *fts*Y	No/?	catalytic Asp	Not EmbR	cell division?	?	?	-	-
PknJ	transposon genes	No/?	-	?	?	?	?	-	-
PknK	*lux*A like	No/?	PDZ, TPR	?	secondary metabolism	?	?	-	-
PknG	*gln*H, Rv0412c	Yes/No	CXXC, TPR	GarA? not EmbR	pathogenicity	yes	CXXC	AX20017	wt-ΔN +Inh

Figure 1.8. The eleven serine/threonine kinases of *M. tuberculosis* and their characteristics. The table shows the eleven serine/threonine kinases of *M. tuberculosis* listed according to their relationship and provides an overview of the individual properties of each kinase. The forkhead-associated domain containing substrates are underlined. Abbreviations: Conser.: conserved; Essent.: essential; Phys. Role: physiological role, KD: kinase domain, SD: sensor domain, Inh: inhibitor, wt-ΔN: part of the N-terminus missing).

Future work focussing on the identification of interacting molecules, as well as substrates, may help to specify the role of individual kinases and lead to a better understanding of signalling processes in mycobacteria. In the long-term, these results may provide a basis for the development of novel and potent drugs which are urgently needed in the fight against disease.

1.6 References

Alderwick, L. J., Molle, V., Kremer, L., Cozzone, A. J., Dafforn, T. R., Besra, G. S., and Futterer, K. (2006). Molecular structure of EmbR, a response element of Ser/Thr kinase signaling in Mycobacterium tuberculosis. Proceedings of the National Academy of Sciences *103*, 2558-2563.

Av-Gay, Y., and Everett, M. (2000). The eukaryotic-like Ser/Thr protein kinases of Mycobacterium tuberculosis. Trends Microbiol *8*, 238-244.

Av-Gay, Y., Jamil, S., and Drews, S. J. (1999). Expression and characterization of the Mycobacterium tuberculosis serine/threonine protein kinase PknB. Infect Immun *67*, 5676-5682.

Boitel, B., Ortiz-Lombardia, M., Duran, R., Pompeo, F., Cole, S. T., Cervenansky, C., and Alzari, P. M. (2003). PknB kinase activity is regulated by phosphorylation in two Thr residues and dephosphorylation by PstP, the cognate phospho-Ser/Thr phosphatase, in Mycobacterium tuberculosis. Mol Microbiol *49*, 1493-1508.

Chaba, R., Raje, M., and Chakraborti, P. K. (2002). Evidence that a eukaryotic-type serine/threonine protein kinase from Mycobacterium tuberculosis regulates morphological changes associated with cell division. Eur J Biochem *269*, 1078-1085.

Chopra, P., Singh, B., Singh, R., Vohra, R., Koul, A., Meena, L. S., Koduri, H., Ghildiyal, M., Deol, P., Das, T. K.*, et al.* (2003). Phosphoprotein phosphatase of Mycobacterium tuberculosis dephosphorylates serine-threonine kinases PknA and PknB. Biochemical and Biophysical Research Communications *311*, 112-120.

Cohen, P. (2002). Protein kinases - the major tagets of the twenty-first century? Nat Rev Drug Discov *1*, 309-315.

Cole, S. T., Brosch, R., Parkhill, J., Garnier, T., Churcher, C., Harris, D., Gordon, S. V., Eiglmeier, K., Gas, S., Barry, C. E., 3rd*, et al.* (1998). Deciphering the biology of Mycobacterium tuberculosis from the complete genome sequence. Nature *393*, 537-544.

Cole, S. T., Eiglmeier, K., Parkhill, J., James, K. D., Thomson, N. R., Wheeler, P. R., Honore, N., Garnier, T., Churcher, C., Harris, D.*, et al.* (2001). Massive gene decay in the leprosy bacillus. Nature *409*, 1007-1011.

Curry, J. M., Whalan, R., Hunt, D. M., Gohil, K., Strom, M., Rickman, L., Colston, M. J., Smerdon, S. J., and Buxton, R. S. (2005). An ABC transporter containing a forkhead-associated domain interacts with a serine-threonine protein kinase and is required for growth of Mycobacterium tuberculosis in mice. Infect Immun *73*, 4471-4477.

Dar, A. C., Dever, T. E., and Sicheri, F. (2005). Higher-order substrate recognition of eIF2[alpha] by the RNA-dependent protein kinase PKR. Cell *122*, 887-900.

Dasgupta, A., Datta, P., Kundu, M., and Basu, J. (2006). The serine/threonine kinase PknB of Mycobacterium tuberculosis phosphorylates PBPA, a penicillin-binding protein required for cell division. Microbiology *152*, 493-504.

Deol, P., Vohra, R., Saini, A. K., Singh, A., Chandra, H., Chopra, P., Das, T. K., Tyagi, A. K., and Singh, Y. (2005). Role of Mycobacterium tuberculosis Ser/Thr Kinase PknF: implications in glucose transport and cell division. J Bacteriol *187*, 3415-3420.

Drews, S. J., Hung, F., and Av-Gay, Y. (2001). A protein kinase inhibitor as an antimycobacterial agent. FEMS Microbiology Letters *205*, 369-374.

Dubnau, E., Chan, J., Raynaud, C., Mohan, V. P., Laneelle, M.-A., Yu, K., Quemard, A., Smith, I., and Daffe, M. (2000). Oxygenated mycolic acids are necessary for virulence of Mycobacterium tuberculosis in mice. Molecular Microbiology *36*, 630-637.

Duran, R., Villarino, A., Bellinzoni, M., Wehenkel, A., Fernandez, P., Boitel, B., Cole, S. T., Alzari, P. M., and Cervenansky, C. (2005). Conserved autophosphorylation pattern in activation loops and juxtamembrane regions of Mycobacterium tuberculosis Ser/Thr protein kinases. Biochem Biophys Res Commun *333*, 858-867.

Durocher, D., and Jackson, S. P. (2002). The FHA domain. FEBS Lett *513*, 58-66.

Dutta, R., Qin, L., and Inouye, M. (1999). Histidine kinases: diversity of domain organization. Mol Microbiol *34*, 633 - 640.

Gay, L. M., Ng, H.-L., and Alber, T. (2006). A conserved dimer and global conformational changes in the structure of apo-PknE Ser/Thr protein kinase from Mycobacterium tuberculosis. Journal of Molecular Biology *360*, 409-420.

Good, M. C., Greenstein, A. E., Young, T. A., Ng, H. L., and Alber, T. (2004). Sensor domain of the Mycobacterium tuberculosis receptor Ser/Thr protein kinase, PknD, forms a highly symmetric beta propeller. J Mol Biol *339*, 459-469.

Gopalaswamy, R., Narayanan, P. R., and Narayanan, S. (2004). Cloning, overexpression, and characterization of a serine/threonine protein kinase pknI from Mycobacterium tuberculosis H37Rv. Protein Expression and Purification *36*, 82-89.

Greenstein, A. E., Echols, N., Lombana, T. N., King, D. S., and Alber, T. (2007). Allosteric activation by dimerization of the PknD receptor Ser/Thr protein kinase from Mycobacterium tuberculosis. J Biol Chem *282*, 11427-11435.

Greenstein, A. E., MacGurn, J. A., Baer, C. E., Falick, A. M., Cox, J. S., and Alber, T. (2007). M. tuberculosis Ser/Thr protein kinase D phosphorylates an anti-anti-sigma factor homolog. PLoS Pathog *3*, e49.

Grundner, C., Gay, L. M., and Alber, T. (2005). Mycobacterium tuberculosis serine/threonine kinases PknB, PknD, PknE, and PknF phosphorylate multiple FHA domains. Protein Sci *14*, 1918-1921.

Han, G., and Zhang, C.-C. (2001). On the origin of Ser/Thr kinases in a prokaryote. FEMS Microbiology Letters *200*, 79-84.

Hanks, S. K., and Hunter, T. (1995). Protein kinases 6. The eukaryotic protein kinase superfamily: kinase (catalytic) domain structure and classification. FASEB J *9*, 576-596.

Hart PD, Y. M. (1975). Interference with normal phagosome-lysosome fusion in macrophages, using ingested yeast cells and suramin. Nature *256*, 47-49.

Janin, Y. L. (2007). Antituberculosis drugs: Ten years of research. Bioorganic & Medicinal Chemistry *15*, 2479-2513.

Jayakumar, D., Jacobs, W. R. J., and Narayanan, S. (2007). Protein kinase E of Mycobacterium tuberculosis has a role in the nitric oxide stress response and apoptosis in a human macrophage model of infection. Cellular Microbiology.

Kang, C.-M., Abbott, D. W., Park, S. T., Dascher, C. C., Cantley, L. C., and Husson, R. N. (2005). The Mycobacterium tuberculosis serine/threonine kinases PknA and PknB: substrate identification and regulation of cell shape. Genes Dev *19*, 1692-1704.

Koul, A., Choidas, A., Tyagi, A. K., Drlica, K., Singh, Y., and Ullrich, A. (2001). Serine/threonine protein kinases PknF and PknG of Mycobacterium tuberculosis: characterization and localization. Microbiology *147*, 2307-2314.

Laboissière, M. C. A., Sturley, S. L., and Raines, R. T. (1995). The essential function of protein-disulfide isomerase is to unscramble non-native disulfide bonds. J Biol Chem *270*, 28006-28009.

Leonard, C. J., Aravind, L., and Koonin, E. V. (1998). Novel families of putative protein kinases in bacteria and archaea: evolution of the "eukaryotic" protein kinase superfamily. Genome Res *8*, 1038-1047.

Madec, E., Laszkiewicz, A., Iwanicki, A., Obuchowski, M., and Seror, S. (2002). Characterization of a membrane-linked Ser/Thr protein kinase in Bacillus subtilis, implicated in developmental processes. Mol Microbiol *46*, 571 - 586.

Manning, G., Whyte, D. B., Martinez, R., Hunter, T., and Sudarsanam, S. (2002). The protein kinase complement of the human genome. Science *298*, 1912 - 1934.

Melnikova, I. G. J. (2004). Targeting protein kinases. Nat Rev Drug Discov *3*, 993-994.

Molle, V., Brown, A. K., Besra, G. S., Cozzone, A. J., and Kremer, L. (2006). The condensing activities of the Mycobacterium tuberculosis type II fatty acid synthase are differentially regulated by phosphorylation. J Biol Chem *281*, 30094-30103.

Molle, V., Girard-Blanc, C., Kremer, L., Doublet, P., Cozzone, A. J., and Prost, J. F. (2003a). Protein PknE, a novel transmembrane eukaryotic-like serine/threonine kinase from Mycobacterium tuberculosis. Biochem Biophys Res Commun *308*, 820-825.

Molle, V., Kremer, L., Girard-Blanc, C., Besra, G. S., Cozzone, A. J., and Prost, J. F. (2003). An FHA phosphoprotein recognition domain mediates protein EmbR phosphorylation by PknH, a Ser/Thr protein kinase from Mycobacterium tuberculosis. Biochemistry *42*, 15300-15309.

Molle, V., Reynolds, R. C., Alderwick, L. J., Besra, G. S., Cozzone, A. J., Fütterer, K., and Kremer, L. (2008). EmbR2, a structural homologue of EmbR, inhibits the Mycobacterium tuberculosis kinase/substrate pair PknH/EmbR. Biochemical Journal 410, 309-317.

Molle, V., Soulat, D., Jault, J.-M., Grangeasse, C., Cozzone, A. J., and Prost, J.-F. (2004). Two FHA domains on an ABC transporter, Rv1747, mediate its phosphorylation by PknF, a Ser/Thr protein kinase from Mycobacterium tuberculosis. FEMS Microbiology Letters *234*, 215-223.

Molle, V., Zanella-Cleon, I., Robin, J. P., Mallejac, S., Cozzone, A. J., Becchi, M. . (2006). Characterization of the phosphorylation sites of Mycobacterium tuberculosis serine/threonine protein kinases, PknA, PknD, PknE, and PknH by mass spectrometry. PROTEOMICS *6*, 3754-3766.

Munoz-Dorado, J., Inouye, S., and Inouye, M. (1991). A gene encoding a protein serine/threonine kinase is required for normal development of M. xanthus, a gram-negative bacterium. Cell *67*, 995-1006.

Narayan, A., Sachdeva, P., Sharma, K., Saini, A. K., Tyagi, A. K., and Singh, Y. (2007). Serine threonine protein kinases of mycobacterial genus: phylogeny to function. Physiol Genomics *29*, 66-75.

Nguyen, L., and Pieters, J. (2005). The Trojan horse: survival tactics of pathogenic mycobacteria in macrophages. Trends Cell Biol *15*, 269-276.

Nguyen, L., and Pieters, J. (2008). Mycobacterial subversion of chemotherapeutic reagents and host defense tactics: challenges in tuberculosis drug development. *In press*.

Nguyen, L., Scherr, N., Gatfield, J., Walburger, A., Pieters, J., and Thompson, C. J. (2007). Antigen 84, an effector of pleiomorphism in Mycobacterium smegmatis. J Bacteriol *189*, 7896-7910.

Nguyen, L., Walburger, A., Houben, E., Koul, A., Muller, S., Morbitzer, M., Klebl, B., Ferrari, G., and Pieters, J. (2005). Role of protein kinase G in growth and glutamine metabolism of Mycobacterium bovis BCG. J Bacteriol *187*, 5852-5856.

Niebisch, A., Kabus, A., Schultz, C., Weil, B., and Bott, M. (2006). Corynebacterial protein kinase G controls 2-oxoglutarate dehydrogenase activity via the phosphorylation status of the OdhI protein. J Biol Chem *281*, 12300-12307.

Noble, M. E. M., Endicott, J. A., and Johnson, L. N. (2004). Protein kinase inhibitors: insights into drug design from structure. Science *303*, 1800-1805.

Ochman, H., Lawrence, J. G., and Groisman, E. A. (2000). Lateral gene transfer and the nature of bacterial innovation. Nature *405*, 299-304.

Ogawara, H., Aoyagi, N., Watanabe, M., and Urabe, H. (1999). Sequences and evolutionary analyses of eukaryotic-type protein kinases from Streptomyces coelicolor A3(2). Microbiology *145 (Pt 12)*, 3343-3352.

Ortiz-Lombardia, M., Pompeo, F., Boitel, B., and Alzari, P. M. (2003). Crystal structure of the catalytic domain of the PknB serine/threonine kinase from Mycobacterium tuberculosis. J Biol Chem *278*, 13094-13100.

Otter, M., Zockova, P., Kuiper, J., van Berkel, T. J., Barrett Bergshoeff, M. M., and Rijken, D. C. (1992). Isolation and characterization of the mannose receptor from human liver potentially involved in the plasma clearance of tissue-type plasminogen activator. Hepatology *16*, 54-59.

Pallen, M., Chaudhuri, R., and Khan, A. (2002). Bacterial FHA domains: neglected players in the phospho-threonine signalling game? Trends Microbiol *10*, 556-563.

Papavinasasundaram, K. G., Chan, B., Chung, J.-H., Colston, M. J., Davis, E. O., and Av-Gay, Y. (2005). Deletion of the Mycobacterium tuberculosis pknH gene confers a higher bacillary load during the chronic phase of infection in BALB/c Mice. J Bacteriol *187*, 5751-5760.

Parkinson, J. S. (1993). Signal transduction schemes of bacteria. Cell *73*, 857-871.

Peirs, P., Lefevre, P., Boarbi, S., Wang, X.-M., Denis, O., Braibant, M., Pethe, K., Locht, C., Huygen, K., and Content, J. (2005). Mycobacterium tuberculosis with disruption in genes encoding the phosphate binding proteins PstS1 and PstS2 is deficient in phosphate uptake and demonstrates reduced in vivo virulence. Infect Immun *73*, 1898-1902.

Peirs, P., Parmentier, B., De Wit, L., and Content, J. (2000). The Mycobacterium bovis homologous protein of the Mycobacterium tuberculosis serine/threonine protein kinase Mbk (PknD) is truncated. FEMS Microbiology Letters *188*, 135-139.

Perez, J., Garcia, R., Bach, H., de Waard, J. H., Jacobs, J. W. R., Av-Gay, Y., Bubis, J., and Takiff, H. E. (2006). Mycobacterium tuberculosis transporter MmpL7 is a potential substrate for kinase PknD. Biochemical and Biophysical Research Communications *348*, 6-12.

Pieters, J. (2001). Evasion of host cell defense mechanisms by pathogenic bacteria. Curr Opin Immunol *13*, 37-44.

Ponting, C. P., Aravind, L., Schultz, J., Bork, P., and Koonin, E. V. (1999). Eukaryotic signalling domain homologues in archaea and bacteria. Ancient ancestry and horizontal gene transfer. Journal of Molecular Biology *289*, 729-745.

Ponting, C. P., Phillips, C., Davies, K. E., and Blake, D. J. (1997). PDZ domains: targeting signalling molecules to sub-membranous sites. Bioessays *19*, 469-479.

Popham, D. L., Illades-Aguiar, B., and Setlow, P. (1995). The Bacillus subtilis dacB gene, encoding penicillin-binding protein 5*, is part of a three-gene operon required for proper spore cortex synthesis and spore core dehydration. J Bacteriol *177*, 4721-4729.

Popham, D. L., and Young, K. D. (2003). Role of penicillin-binding proteins in bacterial cell morphogenesis. Current Opinion in Microbiology *6*, 594-599.

Sassetti, C. M., Boyd, D. H., and Rubin, E. J. (2003). Genes required for mycobacterial growth defined by high density mutagenesis. Mol Microbiol *48*, 77-84.

Schultz, C., Niebisch, A., Gebel, L., and Bott, M. (2007). Glutamate production by Corynebacterium glutamicum: dependence on the oxoglutarate dehydrogenase inhibitor protein OdhI and protein kinase PknG. Applied Microbiology and Biotechnology *76*, 691-700.

Sharma, K., Chandra, H., Gupta, P. K., Pathak, M., Narayan, A., Meena, L. S., D'Souza, R. C. J., Chopra, P., Ramachandran, S., and Singh, Y. (2004). PknH, a transmembrane Hank's type serine/threonine kinase from Mycobacterium tuberculosis is differentially expressed under stress conditions. FEMS Microbiology Letters *233*, 107-113.

Sharma, K., Gupta, M., Pathak, M., Gupta, N., Koul, A., Sarangi, S., Baweja, R., and Singh, Y. (2006). Transcriptional control of the mycobacterial embCAB operon by PknH through a regulatory protein, EmbR, in vivo. J Bacteriol *188*, 2936-2944.

Shenkenberg, T. D., and Von Hoff, D. D. (1986). Mitoxantrone: a new anticancer drug with significant clinical activity. Annals of Internal Medicine *105* 67-81.

Singh, A., Singh, Y., Pine, R., Shi, L., Chandra, R., and Drlica, K. (2006). Protein kinase I of Mycobacterium tuberculosis: cellular localization and expression during infection of macrophage-like cells. Tuberculosis *86*, 28-33.

Stock, A. M., Robinson, V. L., and Goudreau, P. N. (2000). Two-component signal transduction. Annu Rev Biochem *69*, 183-215.

Thakur, M., and Chakraborti, P. K. (2006). GTPase activity of mycobacterial FtsZ is impaired due to its transphosphorylation by the eukaryotic-type Ser/Thr kinase, PknA. J Biol Chem *281*, 40107-40113.

Tinsley, C. R., Voulhoux, R., Beretti, J.-L., Tommassen, J., and Nassif, X. (2004). Three homologues, including two membrane-bound proteins, of the disulfide oxidoreductase DsbA in Neisseria meningitidis: effects on bacterial growth and biogenesis of functional type IV pili. J Biol Chem *279*, 27078-27087.

Udo, H., Inouye, M., and Inouye, S. (1996). Effects of overexpression of Pkn2, a transmembrane protein serine/threonine kinase, on development of Myxococcus xanthus. J Bacteriol *178*, 6647-6649.

Udo, H., Inouye, M., and Inouye, S. (1997). Biochemical characterization of Pkn2, a protein Ser/Thr kinase from Myxococcus xanthus, a Gram-negative developmental bacterium. FEBS Letters *400*, 188-192.

Villarino, A., Duran, R., Wehenkel, A., Fernandez, P., England, P., Brodin, P., Cole, S. T., Zimny-Arndt, U., Jungblut, P. R., Cervenansky, C., and Alzari, P. M. (2005). Proteomic identification of M. tuberculosis protein kinase substrates: PknB recruits GarA, a FHA domain-containing protein through activation-loop mediated interactions. J Mol Biol *350*, 953-963.

Walburger, A., Koul, A., Ferrari, G., Nguyen, L., Prescianotto-Baschong, C., Huygen, K., Klebl, B., Thompson, C., Bacher, G., and Pieters, J. (2004). Protein kinase G from pathogenic mycobacteria promotes survival within macrophages. Science *304*, 1800-1804.

Walker, K. W., Lyles, M. M., and Gilbert, H. F. (1996). Catalysis of oxidative protein folding by mutants of protein disulfide isomerase with a single active-site cysteine. Biochemistry *35*, 1972-1980.

Wehenkel, A., Bellinzoni, M., Grana, M., Duran, R., Villarino, A., Fernandez, P., Andre-Leroux, G., England, P., Takiff, H., Cervenansky, C.*, et al.* (2008). Mycobacterial Ser/Thr protein kinases and phosphatases: Physiological roles and therapeutic potential. Biochimica et Biophysica Acta (BBA) *1784*, 193-202.

Wehenkel, A., Fernandez, P., Bellinzoni, M., Catherinot, V., Barilone, N., Labesse, G., Jackson, M., and Alzari, P. M. (2006). The structure of PknB in complex with mitoxantrone, an ATP-competitive inhibitor, suggests a mode of protein kinase regulation in mycobacteria. FEBS Lett *580*, 3018-3022.

Yeats, C., Finn, R. D., and Bateman, A. (2002). The PASTA domain: a beta-lactam-binding domain. Trends Biochem Sci *27*, 438.

Young, T. A., Delagoutte, B., Endrizzi, J. A., Falick, A. M., and Alber, T. (2003). Structure of Mycobacterium tuberculosis PknB supports a universal activation mechanism for Ser/Thr protein kinases. Nat Struct Biol *10*, 168-174.

Zhang, W., Munoz-Dorado, J., Inouye, M., and Inouye, S. (1992). Identification of a putative eukaryotic-like protein kinase family in the developmental bacterium Myxococcus xanthus. J Bacteriol *174*, 5450-5453.

Zheng, X., Papavinasasundaram, K. G., and Av-Gay, Y. (2007). Novel substrates of Mycobacterium tuberculosis PknH Ser/Thr kinase. Biochemical and Biophysical Research Communications *355*, 162-168.

1.7 Aim of the thesis

Mycobacterium tuberculosis, causing 2 millions deaths per year, is a highly successful bacterial pathogen having evolved several tactics to persist within the hostile environment of its host. One of the strategies relies on the activity of a eukaryotic-like serine/threonine kinase, protein kinase G (PknG), which is released within host macrophages where it actively blocks the fusion of phagosomes with lysosomes, thereby allowing intracellular survival of the bacteria. PknG, one of eleven eukaryotic-like serine/threonine kinases of *M. tuberculosis*, displays a unique domain architecture by containing a N-terminal rubredoxin motif and a C-terminal tetratricopeptide repeat both flanking the kinase domain. A first aim was to further understand the mode of action and the molecular structure of PknG. Therefore, the protein was crystallized and analyzed by x-ray crystallography.

Autophosphorylation is a common characteristic attributing different properties to a kinase. In most other mycobacterial kinases, autophosphorylation is a self-regulatory mechanism leading to activation of the kinase. Not much is known about the role of PknG autophosphorylation *in vitro* and its implications *in vivo*. A second aim of this work was to analyze autophosphorylation of PknG and the role of autophosphorylation in kinase activity.

PknG has been shown to be secreted into the cytosol of macrophages; however, the exact function of the kinase has not been determined. Therefore, a third aim of the work presented was the localization of PknG within eukaryotic cells. Preliminary data are presented which suggest that PknG contains signals that allow specific localization within mammalian cells.

The fourth aim was the functional characterization of a *M. smegmatis* protein named Ag84, a homologue of eubacterial DivIVA-like proteins. *Bacillus subtilis* DivIVA was found to be involved in cell division by interacting with the MinCD system and directing septum formation. Due to the absence of a corresponding MinCD system in mycobacteria, a different function for Ag84 was proposed. Studies were carried out in order to elucidate the role of Ag84 in mycobacteria.

Taken together, the aim of this thesis was to contribute to a better understanding of the complex network of signal transduction pathways in mycobacteria - on the one hand by investigating the structure and function of PknG, and in addition, by characterizing the role of Ag84.

- CHAPTER 2 -

Material and Methods

2.1 Reagents

Acetic acid	Merck
Acetone	Merck
Acrylamide	Bio-Rad
Agarose	Eurobio
Adenosine-5'-triphosphate (ATP)	Boehringer Mannheim
Albumine, bovine, 96% pure	Sigma
Alkaline phosphatase (calf intestine)	Boehringer Mannheim
Ammonium persulfate (APS)	Bio-Rad
Amikacin (20mg/ml)	Sigma
Ampicillin	Sigma
Antipain	Sigma
Aprotinin	Merck
Bacto-Agar	Difco
Bacto-Tryptone	Difco
Bacto-Yeast Extract	Difco
Bicinchonic acid (BCA)	Pierce
Bisacrylamide (N,N'-methylen bisacrylamide)	Bio-Rad
Bovine serum albumine (BSA)	Equitech-Bio
Bromophenole blue	Merck
Calcium chloride ($CaCl_2x4H_2O$)	Sigma
Chloroform	Merck
Chymostatin	Merck
α-Chymotrypsin TLCK (10 mg/ml in 1mM HCl, 2 mM $CaCl_2$)	Sigma
Colloidal blue	Invitrogen
Coomassie brilliant blue G-250	Bio-Rad
Coomassie brilliant blue R-250	Bio-Rad
Cycloheximide	Calbiochem
Desoxynucleotides (dNTPs)	Roche Diagnostics
Diethyl ether	Merck
N, N'-dimethyl formamide	Merck
Dimethylsulfoxide (DMSO)	Fluka
Dithiotreitol (DTT)	Sigma

T4 DNA Ligase	NEB
DNA standard markers	Roche Diagnostics
Ethanol, absolute, p.a.	Merck
Ethidium bromide	Sigma
Ethylene diamine tetraacetate (EDTA)	Fluka
FluoroGuard antifade reagent	Bio-Rad
Formaldehyde (37%)	Fluka
Gel filtration standard (1.35 kDa-670 kDa)	Bio-Rad
G418	Calbiochem
D(+)glucose-monohydrate	Merck
Glutaraldehyde	Sigma
Glycine	Fluka
Glycerol (100%)	Fluka
4-(2-hydroxyethyl)-1-piperazineethanesulfonic acid (HEPES)	AppliChem
Horseradish peroxidase	Sigma
Hydrochloric acid (HCl)	Merck
Hygromycin B	Roche Diagnostics
Imidazole	Fluka
Isobutanol	Merck
Isopropanol	Merck
Isopropyl-thiogalactoside (IPTG)	AppliChem
Kanamycin	Sigma
Leupeptin	Fluka
Manganese chloride ($MnCl_2$)	Sigma
Magnesium chloride ($MgCl_2$)	Sigma
β-mercaptoethanol	Fluka
Methanol	Merck
Milk powder (low fat)	Coop
Mineral oil	Sigma
Restriction enzymes	NEB/Roche diagnostics
Paraformaldeyhde, 95% pure	Sigma
Pepsin (from pig, stock 10 mg/ml H_2O)	Sigma
Pepstatin	Fluka
Phenylmethylsulfonylfluoride (PMSF)	Sigma

Phosphoserine	Sigma
Phosphothreonine	Sigma
Phosphotyrosine	Sigma
Ponceau S	Sigma
Potassium chloride (KCl)	Sigma
Potassium hydroxide (KOH)	Sigma
Potassium dihydrogen phosphate (KH_2PO_4)	Merck
Proteinase K	Roche
Saponin (from Quillaja bark)	Sigma
SDS-PAGE molecular weight standards	Bio-Rad
SDS-PAGE molecular weight prestained standards	Bio-Rad
SDS-PAGE molecular weight rainbow standards	Bio-Rad
Shrimp alkaline phosphatase (SAP)	Roche Diagnostics
Sodium acetate	Merck
Sodium acide	Fluka
Sodium carbonate (Na_2SO_3)	Fluka
Sodium citrate	Fluka
Sodium chloride	Fluka
Sodium dihydrogen phosphate (NaH_2PO_4)	Fluka
Sodium hydroxide	Merck
Subtilisin A (stock 10 mg/ml H_2O)	Sigma
N,N,N',N'tetramethylenethylenediamine (TEMED)	Bio-Rad
Thermolysin (stock 10 mg/ml H_2O)	Sigma
Thrombin (1U/µl)	Sigma
Tricloric acid (TCA)	Merck
Tris(hydroxymethyl)aminomethane (Tris)	Sigma
Triton X-100	Boehringer Mannheim
Trypan blue (0.4 %)	Sigma
Trypsin (bovine pancreas, stock 10 mg/ml H_2O)	Roche
Trypsin inhibitor	Boehringer Mannheim
Tween 20	Fluka
Tween 80	Fluka
Xylene Cyanol	Sigma

2.2 Kits

BCA protein detection Kit	Pierce
Big Dye1.1® Terminator v1.1 Cycle sequencing Kit	Perkin Elmer
Bradford protein detection Kit	Bio-Rad
Crystallization Kits:	
Basic Crystallography Kit	Sigma
Extension Kit	Sigma
Low Ionic Strength Kit	Sigma
Protein Crystallization Cryo Kit	Sigma
Additive Screen I, II and III	Hampton
Detergent Screen I, II and III	Hampton
PEG Screen	Hampton
Membrane Kit	Hampton
Wizard I+II	Emerald BioSystems
Enhanced Chemoluminescence (ECL) Kit	Amersham Biosciences
Expand High Fidelity PCR System	Roche
Expand Long Template PCR System	Roche
GenElute Plasmid Miniprep Kit	Sigma
HiSpeed Plasmid Midi Kit	Qiagen
HiSpeed Plasmid Maxi Kit	Qiagen
jetPEI™ DNA transfection agent	Polyplus
jetPEI™-Macrophage DNA transfection agent	Polyplus
MycoAlert mycoplasma detection Kit	Cambrex
pGEM®-T-Easy Vector Kit	Promega
QIAprep Spin Miniprep Kit	Qiagen
QIAquick gel extraction Kit	Qiagen
QIAquick PCR purification Kit	Qiagen
QuikChange® Site-Directed Mutagenesis Kit	Stratagene
Taq polymerase and PCR buffer Kit	Pharmacia

2.3 Columns

HiLoad 16/60^{TM} Superdex 200 prep grade	GE Healthcare
HiLoad 26/60^{TM} Superdex 200 prep grade	GE Healthcare
Hi-Trap^{TM} Protein A HP 1ml	GE Healthcare
His-Trap^{TM} HP 1 ml / 5 ml	GE Healthcare
His-Trap^{TM} FF 1 ml / 5ml	GE Healthcare
His-Trap^{TM} FF crude 1 ml	GE Healthcare
PD-10 columns	GE Healthcare
Superdex 200 PC 3.2/30	GE Healthcare

2.4 Radiochemicals

EasyTag^{TM}EXPRESS ^{35}S Protein Labeling Mix	Perkin Elmer
Rainbow^{TM}[^{14}C]-methylated protein marker standard	GE Healthcare
Redivue adenosine 5'-[γ-^{32}P] triphosphate	GE Healthcare
[methyl-^{3}H] Thymidine	GE Healthcare
[5,6-^{3}H] Uracil	GE Healthcare

2.5 General buffers and solutions

Acrylamide	30% acrylamide 0.8% N'-methylene-bis-acrylamide
Coomassie staining solution (0.25%)	2.5 g Coomasie Brilliant Blue R-250 dissolved in 1L fix-destain solution
CLAAP (100x)	25 mg/ml antipain in H_2O 25 mg/ml aprotinin in PBS 10 mg/ml chymostatin in DMSO 25 mg/ml leupeptin in H_2O 20 mg/ml pepstatin in DMSO
DNA loading buffer (6x)	0.25% bromphenol blue 0.25% xylene cyanol FF 1 mM EDTA pH 8.0 30% glycerol anhydrous
Fix-destain solution	45% ddH_2O 45% Methanol 10% Acetic acid
PBS (pH 7.2)	137 mM NaCl 2.7 mM KCl 8 mM Na_2HPO_4 1.5 mM KH_2PO_4
PBS-T (pH 7.2)	PBS + 0.2% (v/v) Tween 20
Paraformaldehyde (3%)	90 ml ddH_2O and 30 µl 1 M NaOH added to 3.0 g PFA, stirring on hot plate until PFA is dissolved, 10 ml 10x PBS were added, mixed, cooled to 37°C and pH adjusted to 7.2
PMSF (100x)	100 mM PMSF in isopropanol (100%) (17.4 mg PMSF/ml isopropanol)
SDS-PAGE running buffer (10x)	250 mM Trizma base 1.9 M glycine 0.1% SDS
SDS-PAGE transfer buffer (10x)	480 mM Trizma base 390 mM glycine 0.375% SDS 20% methanol

SDS-SB (5x)	300 mM Tris/HCl pH 6.8 500 mM DTT 10% SDS 20% glycerol 0.015% bromophenol blue
Stripping buffer	62.5 mM Tris pH 6.7 100 mM β-mercaptoethanol 2% SDS
TBE (10x)	108 g Tris 55 g boric acid 40 ml of 0.5 M Na_2EDTA (pH 8.0) ad 1 L with dH_2O
TB	10 mM PIPES 15 mM $CaCl_2$ 250 mM KCl dissolve in H_2O adjust pH to 6.7 with KOH/HCl add 55 mM $MnCl_2$ ad 1 L with dH_2O
TE	10 mM Tris/HCl pH 8.0 1 mM EDTA
TEN buffer	75 mM Tris pH 8.8 4 mM EDTA 100 mM NaCl
Tris solution	30.3 g (for pH 6.8) or 121.1 g (for pH 8.8) ad 0.5L
TX-100 buffer	50 mM Tris-HCl (pH 7.5) 137 mM NaCl 2 mM EDTA 10% glycerol 1% Triton X-100

2.6 Bacterial media and supplements

LB agar	10 g tryptone (Difco) 5 g yeast extract (Difco) 10 g NaCl 15 g Bacto agar (Difco) dissolve in 1 L H_2O, autoclave if required: add antibiotics and/or sterile 0.1% glucose, pour plates and store at 4°C
LB broth	LB medium as described, without agar
Middlebrook 7H11 agar with glycerol	21 g 7H11 (Difco) 900 ml H_2O 5 ml glycerol dissolve at 120°C (stirring on a hot plate until solution becomes clear (1.5 h) after autoclaving let cool to 55-60°C add 100 ml OADC (Difco) if required: add antibiotics, pour plates and store at 4°C
Middlebrook 7H9 agar with glycerol	Difco
OADC Middlebrook supplement	home-made
SOC	2% trypton (w/v) 0.5% yeast extract (w/v) 10 mM NaCl 10 mM $MgCl_2$ 10 mM $MgSO_4$ 2.5 mM KCl dissolve in 1 L H_2O and autoclave add 20 mM sterile glucose
Tween 80	Fluka
Ampicillin	Sigma, stock 100 mg/ml (1000x)
Kanamycin	Sigma, stock 50 mg/ml (1000 or 2000x)
Hygromycin B	Calbiochem, stock 50 mg/ml (1000x)

2.7 Eukaryotic cell culture media and supplements

DMEM	Sigma
DMEM Glutamax	Gibco BRL
Fetal bovine serum (FBS)	Gibco BRL
L929 supernatant	home-made
L-glutamin (200 mM)	Gibco BRL
ß-mercaptoethanol (50 mM)	Sigma
Sodium pyruvate (100 mM)	Sigma
Trypsin/EDTA (0.05%) in HBBS	Gibco BRL
Ciproxin (0.2%)	Bayer

2.8 Vectors

Name (kb)	Vector	Insert	Reference	Application
pGEM vector (3.0 kb)	pGEM®-T Easy (Promega) Amp^R	-	Promega	subcloning
pGEM-PknG	pGEM®-T Easy (Promega) Amp^R	*pknG*	Anne Walburger	subcloning
pGEM-NS1	pGEM®-T Easy (Promega) Amp^R	*pknG* (N-term)	Nicole Scherr	subcloning
pGEM-NS2	pGEM®-T Easy (Promega) Amp^R	*pknG* (kin domain)	Nicole Scherr	subcloning
pGEM-NS3	pGEM®-T Easy (Promega) Amp^R	*pknG* (C-term)	Nicole Scherr	subcloning
pGEM-NS4	pGEM®-T Easy (Promega) Amp^R	*pknG* (kin+C-term)	Nicole Scherr	subcloning
pGEM-ΔN	pGEM®-T Easy (Promega) Amp^R	*pknG* (N-terminal deletion)	Nicole Scherr	subcloning
pGEM-inh	pGEM®-T Easy (Promega) Amp^R	*pknG* (I87S/A92S)	Nicole Scherr	mutagenesis and subcloning
pGEM-P-mut	pGEM®-T Easy (Promega) Amp^R	*pknG* T21/23/26/32/63/64A	Nicole Scherr	subcloning
pET15b vector (5.7 kb)	pET-15b (Novagen) Amp^R	-	Novagen	expression in *E. coli* BL21 and purification
pET15b-PknG	pET-15b (Novagen) Amp^R	*pknG*	Anne Walburger	expression in *E. coli* BL21 and purification
pET15b-NS1	pET-15b (Novagen) Amp^R	*pknG* (N-term)	Nicole Scherr	expression in *E. coli* BL21 and purification
pET15b-NS2	pET-15b (Novagen) Amp^R	*pknG* (kin domain)	Nicole Scherr	expression in *E. coli* BL21 and purification
pET15b-NS3	pET-15b (Novagen) Amp^R	*pknG* (C-term)	Nicole Scherr	expression in *E. coli* BL21 and purification
pET15b-NS4	pET-15b (Novagen) Amp^R	*pknG* (kin+C-term)	Nicole Scherr	expression in *E. coli* BL21 and purification
pET15b-ΔN	pET-15b (Novagen) Amp^R	*pknG* (N-terminal deletion)	Nicole Scherr	expression in *E. coli* BL21 and purification
pET15b-K181M	pET-15b (Novagen) Amp^R	*pknG* (K181M kinase dead)	Philipp Müller	expression in *E. coli* BL21 and purification
pET15b-inh	pET-15b (Novagen) Amp^R	*pknG* (I87 and A92 to S)	Nicole Scherr	expression in *E. coli* BL21 and purification
pET15b-P-mut	pET-15b (Novagen) Amp^R	*pknG* T21/23/26/32/63/64A	Nicole Scherr	expression in *E. coli* BL21 and purification
pET15b-C1/2	pET-15b (Novagen) Amp^R	*pknG* (C106/109/128/131S)	Philipp Müller	expression in *E. coli* BL21 and purification
pMV361 (4.4 kb)	pMV361 Kan^R	-	Stover et al. (1991)	subcloning, control
pMV361-PknG	pMV361 Kan^R	*pknG*	Anne Walburger	expression in mycobacteria
pMV361-ΔN	pMV361 Kan^R	*pknG* (N-terminal deletion)	Martin Bratschi/ Edith Houben	expression in mycobacteria
pMV361-P-mut	pMV361 Kan^R	*pknG* T21/23/26/32/63/64A	Damir Perisa	expression in mycobacteria
pMV361-C1/2	pMV361 Kan^R	*pknG*: (C106/109/128/131S)	Philipp Müller	expression in mycobacteria
pGEM-ΔN2	pGEM®-T Easy (Promega) Amp^R	*pknG* (N-terminal deletion)	Nicole Scherr	subcloning
pGEM-kin	pGEM®-T Easy (Promega) Amp^R	*pknG* (kinase domain)	Nicole Scherr	subcloning
pGEM-ΔC1	pGEM®-T Easy (Promega) Amp^R	*pknG* (C-terminal deletion)	Nicole Scherr	subcloning
pGEM-ΔC2	pGEM®-T Easy (Promega) Amp^R	*pknG* (C-terminal deletion)	Nicole Scherr	subcloning
pGEM-ΔC3	pGEM®-T Easy (Promega) Amp^R	*pknG* (C-terminal deletion)	Nicole Scherr	subcloning

pIRES vector (5.1 kb)	pIRESpuro3 (Clontech) $Amp^R/Puro^R$	-	Clontech	control, subcloning
pIRES-PknG	pIRESpuro3 (Clontech) $Amp^R/Puro^R$	*pknG*	Nicole Scherr	expression in mammalian cells
pIRES-K181M	pIRESpuro3 (Clontech) $Amp^R/Puro^R$	*pknG* (K181M kinase dead)	Nicole Scherr	expression in mammalian cells
pIRES-ΔN1	pIRESpuro3 (Clontech) $Amp^R/Puro^R$	*pknG* (N-terminal deletion)	Nicole Scherr	expression in mammalian cells
pIRES-ΔN2	pIRESpuro3 (Clontech) $Amp^R/Puro^R$	*pknG* (N-terminal deletion)	Nicole Scherr	expression in mammalian cells
pIRES-kin	pIRESpuro3 (Clontech) $Amp^R/Puro^R$	*pknG* (kinase domain)	Nicole Scherr	expression in mammalian cells
pIRES-ΔC1	pIRESpuro3 (Clontech) $Amp^R/Puro^R$	*pknG* (C-terminal deletion)	Nicole Scherr	expression in mammalian cells
pIRES-ΔC2	pIRESpuro3 (Clontech) $Amp^R/Puro^R$	*pknG* (C-terminal deletion)	Nicole Scherr	expression in mammalian cells
pIRES-ΔC3	pIRESpuro3 (Clontech) $Amp^R/Puro^R$	*pknG* (C-terminal deletion)	Nicole Scherr	expression in mammalian cells
pIRES-P-mut	pIRESpuro3 (Clontech) $Amp^R/Puro^R$	*pknG* T21/23/26/32/63/64A	Nicole Scherr	expression in mammalian cells
pIRES-C1/2	pIRESpuro3 (Clontech) $Amp^R/Puro^R$	*pknG*: (C106/109/128/131S)	Nicole Scherr	expression in mammalian cells
pGEX-PknG	pGEX-5x-3 Amp^R	*pknG*	Koul A. (2001)	subcloning
pGEX-PknG-K181M	pGEX-5x-3 Amp^R	*pknG* (K181M kinase dead)	Koul A. (2001)	subcloning
pGEM-PknG	pGEM®-T Easy (Promega) Amp^R	*pknG*	Nicole Scherr	subcloning
FLAG vector (6.3 kb)	p3XFLAG-CMV-10 (Sigma) Amp^R/Neo^R	-	Sigma	expression in mammalian cells
pGEM-FLAG-PknG	pGEM®-T Easy (Promega) Amp^R	*3xFLAG::pknG*	Nicole Scherr	subcloning
pSD5-PknG	pSD5 Kan^R	*pknG*	Jain S. (1991)	subcloning
pSD5-FLAG-PknG	pSD5 Kan^R	*3xFLAG::pknG*	Nicole Scherr	expression in mycobacteria
FLAG-PknG-wt	p3XFLAG-CMV-10 (Sigma) Amp^R/Neo^R	*pknG*	Nicole Scherr	subcloning, expression in mammalian cells
FLAG-K181M	p3XFLAG-CMV-10 (Sigma) Amp^R/Neo^R	*pknG* (K181M kinase dead)	Nicole Scherr	expression in mammalian cells
FLAG-ΔN1	p3XFLAG-CMV-10 (Sigma) Amp^R/Neo^R	*pknG* (N-terminal deletion)	Nicole Scherr	expression in mammalian cells
FLAG-ΔN2	p3XFLAG-CMV-10 (Sigma) Amp^R/Neo^R	*pknG* (N-terminal deletion)	Nicole Scherr	expression in mammalian cells
FLAG-kin	p3XFLAG-CMV-10 (Sigma) Amp^R/Neo^R	*pknG* (kinase domain)	Nicole Scherr	expression in mammalian cells
FLAG-ΔC1	p3XFLAG-CMV-10 (Sigma) Amp^R/Neo^R	*pknG* (C-terminal deletion)	Nicole Scherr	expression in mammalian cells
FLAG-ΔC2	p3XFLAG-CMV-10 (Sigma) Amp^R/Neo^R	*pknG* (C-terminal deletion)	Nicole Scherr	expression in mammalian cells
FLAG-ΔC3	p3XFLAG-CMV-10 (Sigma) Amp^R/Neo^R	*pknG* (C-terminal deletion)	Nicole Scherr	expression in mammalian cells
FLAG-P-mut	pIRESpuro3 (Clontech) $Amp^R/Puro^R$	*pknG* T21/23/26/32/63/64A	Nicole Scherr	expression in mammalian cells
FLAG-C1/2	pIRESpuro3 (Clontech) $Amp^R/Puro^R$	*pknG*: (C106/109/128/131S)	Nicole Scherr	expression in mammalian cells
pCB6-TACO-CHA	pCB6 Amp^R	*coronin 1::HA*	John Gatfield	expression in mammalian cells
pNDL1	pMV361 Kan^R	$wag31_{MS}$*::gfp*	Liem Nguyen	expression in mycobacteria
pNDL2	pMV361 Kan^R	$wag31_{MS}$*::gfp* (for integration)	Liem Nguyen	expression in mycobacteria
pNDL4	pMV361 Kan^R	$wag31_{MS}$	Liem Nguyen	expression in mycobacteria
pNDL8	pMV361 Kan^R	$wag31_{TB}$	Liem Nguyen	expression in mycobacteria

2.9 Primers

Primers used for cloning

Name	Sequence (5'-3')	Source	Application
NS-PknG-N-term-f	CAT ATG GCC AAA GCG TCA GAG ACC GAA CG	*pknG*	cloning PknG-N-terminus
NS-PknG-N-term-r	CTC GAG TTA GAC GAT GTC CCC GGG ATT TAG	*pknG*	cloning PknG-N-terminus
NS-PknG-Kin-f	CAT ATG CTA AAT CCC GGG GAC ATC GTC GC	*pknG*	cloning PknG-kin-domain
NS-PknG-Kin-r	CTC GAG TTA CTC CCG CAA CAC GCC	*pknG*	cloning PknG-kin-domain
NS-PknG-C-term-f	CAT ATG CTG CAG GCC ACG GTG CTC TCC	*pknG*	cloning PknG-C-terminus
NS-PknG-C-term-r	CTC GAG TTA GAA CGT GCT GGT GGG CCG	*pknG*	cloning PknG-C-terminus
NS-PknG–C-term-neu-r	CAT ATG CTG GGC GGC GGC CTG GTG	*pknG*	cloning PknG-ΔN
NS-inh-Ser-2	CAG TAG TCC CTG AGT TCG CCT AGC CTT AGC CCG CGG	*pknG*	site-directed mut. PknG-inhibitor
NS-inh-Ser-1	GTC ATC AGG GAC TCA AGC GGA TCG GAA TCG GGC GCC	*pknG*	site-directed mut. PknG-inhibitor
NS-PknG-dC1-NotI-r	GCG GCC GCT TAC TGT TCC TCG GTG ACT TC	*pknG*	cloning PknG-ΔC1
NS-PknG-dC2-NotI-r	GCG GCC GCT TAC AGC GCG CGG ACT TCC C	*pknG*	cloning PknG-ΔC2
NS-PknG-dC3-NotI-r	GCG GCC GCT TAC ACG ATC TCG TTG GCG GTC	*pknG*	cloning PknG-ΔC3
NS-PknG-dN2-EcoRI-f	GAA TTC ATG CCG TAT TCG TTC CTG CCG CAG	*pknG*	cloning PknG-ΔN2
NS-PknG-EcoRI-fw	GAA TTC ATG GCC AAA GCG TCA GAG ACC GAA CG	*pknG*	cloning PknG-FL
NS-PknG- NotI-r	GCG GCC GCT TAG AAC GTG CTG GTG GGC CG	*pknG*	cloning PknG-FL
NS-PknG-HindIII-fw	AAG CTT ATG GCC AAA GCG TCA GAG ACC GAA CG	*pknG*	cloning 3xFLAG-PknG
NS-PknG-EcoRI-rev	GAA TTC TTA GAA CGT GCT GGT GGG CCG	*pknG*	cloning 3xFLAG-PknG
3-FLAG-NdeI-fw	CAT ATG ACC ATG GAC TAC AAA GAC CAT GAC	*pknG*	cloning 3xFLAG-PknG
3-FLAG-EcoRI-fw	GAA TCC ACC ATG GAC TAC AAA GAC CAT GAC	*pknG*	cloning 3xFLAG-PknG
PknG-ScaI-rev	AGT ACT TTA GAA CGT GCT GGT GGG CCG	*pknG*	cloning 3xFLAG-PknG

Primers used for Sequencing and Colony-PCR

Name	**Sequence (5'-3')**	**Source**	**Application**
T7 promotor seq	TAA TAC GAC TCA CTA TAG GG	pGEM-T-easy Promega	sequencing primer pGEM
M13-forward	CGC CAG GGT TTT CCC AGT CAC GAC	pGEM-T-easy Promega	sequencing primer pGEM
M13-reverse	TCA CAC AGG AAA CAG CTA TGA C	pGEM-T-easy Promega	sequencing primer pGEM
pknG Seq1 5'	GAC TCG GAG ACC AAG GGA GCT TC	*pknG* (bp349-bp371)	sequencing primer *pknG*
pknG Seq1 3'	CCC TTG GTC TCC GAG	*pknG* (bp365-bp351)	sequencing primer *pknG*
pknG Seq2 5'	CCC GTC GCG GAG GCC ATC G	*pknG* (bp745-bp771)	sequencing primer *pknG*
pknG Seq2 3'	GCT CAG CGC CGG CAG	*pknG* (bp795-bp781)	sequencing primer *pknG*
pknG Seq3 5'	CCG CGG CAA CGG TTC ACC AC	*pknG* (bp1132-bp1151)	sequencing primer *pknG*
pknG Seq3 3'	CGG ACA TCT CTT CGG	*pknG* (bp1168-bp1154)	sequencing primer *pknG*
pknG Seq4 5'	GGA CGC CGA CGG CGT CGA C	*pknG* (bp1473-bp1491)	sequencing primer *pknG*
pknG Seq4 3'	CGG GTG GCC TTG GCC	*pknG* (bp1568-bp1554)	sequencing primer *pknG*
pknG Seq5 5'	GGC ACG GCT GAC CAG CGC G	*pknG* (bp1914-bp1932)	sequencing primer *pknG*
pknG Seq5 3'	CGG TGA CTT CAC TCG	*pknG* (bp1972-bp1958)	sequencing primer *pknG*
pknG Seq6 5'	CCG CGC CCT GGT GCT GGG	*pknG* (bp2043-bp2060)	sequencing primer *pknG*
pknG EN 5'	GGA ATT CCA TAT GGC CAA AGC GTC AGA GAC CGA AC	*pknG*	colony PCR for presence of *pknG*
pknG XNH 3'	CTC GAG CAT ATG AAG CTT TTA GAA CGT GCT GGT GGG CCG GAC	*pknG*	colony PCR for presence of *pknG*

2.10 Antibodies and dyes

Primary antibodies

Name	Isotype	Antigen/Target	Source	Culture conditions
antiserum 17	rabbit	PknG	Anne Walburger	Immunoblotting (1:1000)
antiserum 18	rabbit	PknG	Anne Walburger	Immunoblotting (1:1000)
ProteinA purified antiserum 18	rabbit	PknG	Edith Houben	Immunoblotting (1:1000) Immunofluorescence (1:500)
Affinity purified antiserum 18	rabbit	PknG	Jean Pieters	Immunofluorescence (1:500)
antiserum 45	rabbit	PknG-C-terminus	Eurogentec	Immunoblotting (1:20.000)
anti-FLAG-M2®	mouse	FLAG-tagged proteins (PknG mutants)	Sigma	Immunoblotting Immunofluorescence (1:500)
anti-Coronin 1	rat	Coronin1	Rajesh Jayachandran	Immunofluorescence (1:200)
anti-phospho- HistoneH3 (Ser10)	rabbit	Chromatin (mitosis marker)	upstate	Immunofluorescence (1:100)
F126-2	mouse	Ag84	obtained from A. Kolk, KIT, Amsterdam/NE	Immunoblotting (1:10.000)
AI-75320	mouse	GroEL	MRL, Fort Collins, Colorado/USA	Immunoblotting (1:500)
F29-47	mouse	Lipoprotein	obtained from A. Kolk, KIT, Amsterdam/NE	Immunoblotting (1:5000)
anti-GFP	mouse	GFP-tagged proteins	Roche	Immunoblotting (1:2000)
anti-His	mouse	His-tagged proteins	Amersham Biosciences	Immunoblotting (1:2000)

Secondary antibodies

anti-rabbit-HRP (1mg/ml)	goat	Rabbit IgG (H+L)	Southern Biotech	Immunoblotting (1:20.000)
anti-mouse-HRP (1mg/ml)	goat	Mouse IgG (H+L)	Southern Biotech	Immunoblotting (1:20.000)
anti-mouse-Alexa Fluor™-488 (2mg/ml)	goat	Mouse IgG (H+L)	Molecular Probes	Immunofluorescence (1:200)
anti-rat-Alexa Fluor™-488 (2mg/ml)	goat	Rat IgG (H+L)	Molecular Probes	Immunofluorescence (1:200)
anti-rabbit-Alexa Fluor™-488 (2mg/ml)	goat	Rabbit IgG (H+L)	Molecular Probes	Immunofluorescence (1:200)
Alexa Fluor™-568 goat-anti-rabbit IgG (H+L), (2mg/ml)	goat	Rabbit IgG (H+L)	Molecular Probes	Immunofluorescence (1:200)

Dyes

DRAQ5	-	DNA (nucleus)	Biostatus limited	Immunofluorescence (1:2500)
Alexa Fluor®-Phalloidin -488	-	F-Actin	Molecular Probes	Immunofluorescence (1:100)

2.11 Bacterial strains and culture conditions

Name	Source	Culture medium	Culture condition	Application
E. coli DH10β	Silvia Arber	LB medium	37°C, 180 rpm	cloning
E. coli DH5α	Invitrogen	LB medium	37°C, 180 rpm	cloning
E. coli BL21(DE)	Jean Pieters	LB medium	37°C, 180 rpm	protein expression
M. bovis BCG-phsp60::gfp „Montreal“	V. Deretic, Michigan, USA	7H9 + 10% OADC	37°C, 90 rpm, dark	biochemistry
M. bovis BCG-*ΔpknG*-phsp60 „Montreal“	Liem Nguyen	7H9 + 10% OADC	37°C, 90 rpm, dark	biochemistry
M. bovis BCG „Pasteur-1173P2“	Roland Brosch Pasteur/Paris	7H9 + 10% OADC	37°C, 90 rpm, dark	expression growth survival assay
M. bovis BCGΔ*pknG* „Pasteur-1173P2“	Edith Houben	7H9 + 10% OADC	37°C, 90 rpm, dark	expression growth survival assay
M. bovis BCGΔ*pknG* *pMV361::pknG-ΔN*	Martin Bratschi, Nicole Scherr,	7H9 + 10% OADC (25 µg/µl Kanamycin)	37°C, 90 rpm, dark	expression growth survival assay
M. bovis BCGΔ*pknG* *pMV361::pknG-P-mut*	Damir Perisa	7H9 + 10% OADC (25 µg/µl Kanamycin)	37°C, 90 rpm, dark	expression growth survival assay
M. bovis BCGΔ*pknG* *pMV361::pknG-CXXC-mut*	Nicole Scherr	7H9 + 10% OADC (25 µg/µl Kanamycin)	37°C, 90 rpm, dark	expression growth survival assay
M. bovis BCGΔ*pknG* *pSD5::3xFLAG::pknG*	Nicole Scherr	7H9 + 10% OADC (25 µg/µl Kanamycin)	37°C, 90 rpm, dark	expression microscopy
M. smegmatis mc²155	ATCC	7H9 + 10% OADC	37°C, 90 rpm, dark	expression biochemistry microscopy
M. smegmatis BCG*ΔpknG* *pSD5-3xFLAG::pknG*	Nicole Scherr	7H9 + 10% OADC (25 µg/µl Kanamycin)	37°C, 90 rpm, dark	expression microscopy
M. smegmatis mc²155 NDL1 *pMV361::wag31$_{MS}$::gfp*	Liem Nguyen	7H9 + 10% OADC	37°C, 90 rpm, dark	expression biochemistry microscopy
M. smegmatis mc²155 NDL4 *pMV361::wag31$_{MS}$*	Liem Nguyen	7H9 + 10% OADC	37°C, 90 rpm, dark	expression biochemistry microscopy
M. smegmatis mc²155 NDL8 *pMV361::wag31$_{TB}$*	Liem Nguyen	7H9 + 10% OADC	37°C, 90 rpm, dark	expression biochemistry microscopy
M. tuberculosis H37Rv	Roland Brosch Pasteur/Paris	7H9 + 10% OADC	37°C, 90 rpm, dark (Med. Microbiology)	culture maintenance expression
M. tuberculosis H37Rv *ΔpknG* *clones 2,7,8*	Liem Nguyen	7H9 + 10% OADC	37°C, 90 rpm, dark (Med. Microbiology)	culture maintenance expression complementation
M. tuberculosis H37Rv *ΔpknG, pMV361::pknG* *clones B2a(2), B3a,b,d(7)* *B4-I/III(8)*	Liem Nguyen/ Nicole Scherr	7H9 + 10% OADC (50 µg/µl Kanamycin)	37°C, 90 rpm, dark (Med. Microbiology)	culture maintenance expression

2.12 Eukaryotic cells and culture conditions

Name	Cell type	Source	Culture medium	Culture conditions	Application
BMM	bone marrow derived macrophages	C57/BL6 mice	DMEM 10% FBS 2 mM L-glutamine 1 mM Na-pyruvate 50 µM β-Mercaptoethanol 30% L929 cond. medium	37°C 5% CO_2 for 5-7 days on Teflon dishes	Survival assay
J774A.1	mouse macrophage-like cell line	ATCC	DMEM 10% FBS 2 mM L-glutamine	37°C 5% CO_2	Survival assay Translation Proliferation Transfections and Immunofluorescence
HEK293	human embryonic kidney cell line	ATCC	Glutamax 10% FBS 1 mM Na-pyruvate 0.002% Ciproxin	37°C 5% CO_2	Transfections and Immunofluorescence Microscopy
HeLa	human cervical cancer cell line	ATCC	Glutamax 10% FBS 1 mM Na-pyruvate 0.002% Ciproxin	37°C 5% CO_2	Transfections and Immunofluorescence Microscopy
Mel JuSo	human melanoma cell line	Johnson et al. (1981), Pieters et al. (1991)	Glutamax 10% FBS 1 mM Na-pyruvate 0.002% Ciproxin	37°C 5% CO_2	Transfections and Immunofluorescence Microscopy

2.13 MOLECULAR GENETICS METHODS

2.13.1 Preparation of ultracompetent *E. coli* DH10β

Ultracompetent cells were prepared according to Inoue et al., 1990. A 5 ml pre-culture derived from a single colony and grown for 16 h (at 37°C, 180 rpm) was used to inoculate 250 ml SOC medium. The culture was grown under vigorous shaking to an OD_{600} = 0.5 and placed on ice for 10 min. The following steps were performed at 4°C with pre-cooled materials. Bacteria were spun at 7280*x*g (10 min, 4°C) and the pellet was gently resuspended in 80 ml ice-cold TB solution and put on ice for 10 min. After a further centrifugation step 20 ml ice-cold TB and 1.4 ml ice-cold DMSO were added and the cells gently resuspended. Aliquots (50µl) were frozen in liquid nitrogen and stored at -80°C.

2.13.2 Preparation of electrocompetent *E. coli* DH5α/BL21

A 5 ml pre-culture derived from a single colony and grown o/n (at 37°C, 180 rpm) was used to inoculate 1L LB medium. The culture was grown until an OD_{600} of 0.5-0.8 was reached. The flask was placed on ice for 15-30 min. All subsequent steps were carried out at 4°C with

pre-cooled materials. The bacteria were washed three times, first with 1L ice-cold dH_2O, then with 0.5 L dH_2O, followed by washing with 20 ml ice-cold 10% glycerol. In between, the bacteria were pelleted by spinning at 7280*x*g (15 min, 4°C). After the last washing step, the bacteria were resuspended in a final volume of 2 ml ice-cold 10% glycerol, aliquoted, frozen in liquid nitrogen and stored at -80°C.

2.13.3 Preparation of electrocompetent *M. bovis* and *M. tuberculosis* (Parish and Stoker, 1998)

Hundred ml 7H9 medium containing 10% OADC were inoculated with 1 ml of a saturated culture (OD_{600}>1.0) and incubated shaking at 160 rpm (37°C) until an OD_{600} of 0.5 was reached (1-2 weeks). Bacteria were pelleted by centrifugation at 1500*x*g for 10 min and gently resuspended in 10% glycerol. This washing step was repeated 3 times before the pellet was resuspended in 4.5 ml 10% glycerol. Aliquots of 200 µl were frozen in liquid nitrogen and stored at -80°C.

Remark: Electrocompetent *M. tuberculosis* cells were prepared in a biosafety level 2+ laboratory according to the special safety rules.

2.13.4 Preparation of electrocompetent *M. smegmatis* (Parish et al., 1998)

Two ml 7H9 medium containing 10% OADC and 0.05% Tween 80 were inoculated from a glycerol stock and bacteria were grown o/n at 37°C (150 rpm) up to saturation (OD_{600}=4.5). A main culture was prepared by using 1 ml of the saturated culture as inoculum for 100 ml 7H9 medium containing 10% OADC and 0.5% Tween 80. The cultures were grown o/n at 37°C (70 rpm). At OD_{600} of 0.8-1.0, the bacteria were placed on ice for 20 min and handled at 4°C for the whole procedure. Cells were pelleted at 1500*x*g (10 min, 4°C) and gently resuspended in 100 ml 10% glycerol, which was added drop-wise to the pellet by using two pipetboys at once. This step was repeated three times and the pellet was finally resuspended in 2 ml 10% glycerol. Aliquots of 100 µl were quickly frozen in liquid nitrogen and stored at -80°C.

2.13.5 Transformation of ultracompetent *E. coli* DH10β

Ultracompetent cells were thawed on ice, then plasmid DNA or an aliquot of the ligation mix was added to the cells and incubated on ice for 5 min. Then, the mixture was plated out on pre-warmed agar plates containing the appropriate antibiotic and incubated o/n at 37°C.

2.13.6 Transformation of electrocompetent *E. coli* DH5α/BL21

Electrocompetent cells were thawed while electroporation cuvettes (0.2 µm, Bio-Rad or Eppendorf) were pre-cooled on ice. Plasmid DNA or an aliquot of the ligation mix was added to the cells, the mixture was transferred to the cuvette and electorporated at 1800 mV. Immediately, 500 µl pre-warmed LB medium were added and the cell suspension was transferred to an Eppendorf tube. After a recovery time of 1h (180 rpm, 37°C), the cells were plated on pre-warmed LB plates with the required antibiotic and incubated o/n at 37°C.

2.13.7 Transformation of *M. bovis BCG and M. tuberculosis*

M. bovis BCG or *M. tuberculosis* competent cells (200 µl) were thawed and electroporation cuvettes (0.2 µm, Bio-Rad) were pre-cooled on ice. A 15 ml Falcon tube with 1 ml 7H9 (10% OACD) was prepared for recovery of the cells after transformation. Around 500 ng of DNA was added to the cells and the mixture was transferred to the pre-cooled electroporation cuvette. Electroporation (Bio-Rad Gene Pulser^{TM}) was performed at 2.5 V, 1000 Ω and 25 µF (time constant ideally 18-22 ms). Quickly, 1 ml ice-cold 7H9 (10% OADC) was added to the cells and the suspension transferred to the prepared 15 ml Falcon tube. For recovery, the cells were incubated 16-24 h at 130 rpm and 37°C. The next day, different volumes were spread onto selective 7H10 (10% OADC) agar plates and incubated for 2-4 weeks at 37°C.
Remark: Transformation of *M. tuberculosis* cells was performed under supervision in a biosafety level 2+ laboratory according to the special safety rules.

2.13.8 Transformation of *M. smegmatis*

M. smegmatis electrocompetent cells (100 µl) were thawed and electroporation cuvettes (0.2 µm, Bio-Rad) were pre-cooled on ice. For recovery, a 15 ml Falcon tube with 1 ml 7H9 (10% OADC) was prepared. 200 ng of DNA was added to the cells and the mixture was transferred to the pre-cooled electroporation cuvette. Electroporation (Bio-Rad Gene Pulser^{TM}) was performed at 2.5 V, 1000 Ω and 25 µF (time constant ideally 18-22 ms). Immediately, 1 ml ice-cold 7H9 (10% OADC) was added to the cells and the suspension transferred to the prepared 15 ml Falcon tube. The cells were incubated for 3 h at 130 rpm and 37°C for recovery. Then, different volumes were plated out onto selective 7H10 (10% OADC) agar plates and incubated for 1-2 days at 37°C.

2.13.9 Preparation of bacterial stocks

Exponentially growing bacteria were diluted to a final concentration of 15% (*E. coli*) or 20% (Mycobacteria) glycerol and aliquots of 1 ml were prepared. The stocks were snap-frozen in liquid nitrogen and stored at -80°C.

2.13.10 Agarose gel electrophoresis

Agarose gel electrophoresis was performed for either analytical or preparative purposes by preparing 0.8-2.0 % agarose gels in 0.5x TBE containing ethidium bromide (final conc. 1.0 µg/ml). The gels were run in 0.5x TBE at 50 or 100 V using the Mupid® electrophoresis system (Eurogentec) and analyzed using a BioDoc-It™ Imaging System (UVP).

2.13.11 Preparation of plasmid DNA from *E. coli* cultures

Plasmid DNA was prepared by using commercially available kits from QIAGEN (Maxi, Midi) and Sigma (Mini) according to the manufacturer's protocols.

2.13.12 Digestion of plasmid DNA by restriction enzymes

Restriction digests were performed to analyze plasmids or to prepare DNA for ligation. Usually, 0.5-5 µg DNA were digested in the appropriate buffer using 1-5 U enzyme/µg DNA for 1-3 h at 37°C.

2.13.13 Dephosphorylation of DNA

Re-ligation of digested plasmid DNA was prevented by incubating the DNA with 5 U shrimp alkaline phosphatase (SAP) in 1x SAP buffer for 1 h at 37°C. SAP was inactivated by heating the reaction mixture for 10 min at 65°C. Dephosphorylated linearized vectors were applied to preparative agarose gels and purified.

2.13.14 Purification of DNA from agarose gels

Under UV illumination (312 nm, TFX 20M UV transilluminator), the bands of interest were quickly excised from the gel and purified from agarose gels using the Qiaquick gel extraction kit (QIAGEN) according to the manufacturer's protocol.

2.13.15 Ligation of insert and vector

Ligation of DNA fragments with sticky ends was performed in a reaction volume of 15 µl using 1U T4 DNA ligase and buffer from New England Biolabs (NEB). The molar vector-

insert ratio varied from 1:2 to 1:8. The ligation reaction mixture was incubated o/n at 16°C (cold room) to obtain a maximal number of transformants.

2.13.16 Precipitation of DNA

Plasmid DNA was precipitated by adding 0.1 volume of 3 M sodium acetate pH 5.2 and 3 volumes of 100 % ethanol. The mixture was incubated for at least 15 min at -20°C. The precipitated DNA was spun (20,800*x*g, 15 min, 4°C) and the DNA pellet was washed once with 100% ethanol, air-dried and dissolved in H_2O DW-trigB (Albatros).

2.13.17 Sequencing

Sequencing reactions were set up in a 0.5 ml tube by mixing 4 µl of the BigDye (Perkin Elmer) Terminator Ready reaction buffer with 0.5 µl primer (10 pmol/µl) and 200-400 ng template DNA, completed to a total volume of 10 µl. For the amplification of DNA, the following protocol was used:

A. preheating:	96°C	1 min
B. denaturation:	96°C	10 sec
C. annealing:	50°C	5 sec
D. elongation:	60°C	4 min, 25 cycles
E. cooling:	4°C	

The extension products were purified by ethanol precipitation as follows: 90 µl H_2O DW-trigB (Albatros), 10 µl 125 mM EDTA pH 8.0, 10 µl 3 M Na-acetate pH 4.6 and 250 µl 95% EtOH were added to each reaction, mixed and placed in the dark for 10 min at RT. DNA was pelleted by centrifugation at 20,800*x*g and RT for 20 min. The supernatant was carefully removed and the pellet was washed with 350 µl 70% ethanol and centrifuged again for 5 min at maximum speed. This washing step was repeated once. The pellet was air-dried and stored at 4°C.

Sequencing was performed by the in house sequencing facility and the obtained sequences were analyzed using the Mac Vector™ software (version 7.2.2).

2.13.18 Polymerase chain reaction (PCR)

In general, a PCR designated to amplify DNA for the construction of new vectors was set up as follows:

- 100 ng template

- 1.5 µl forward primer (10 µM)
- 1.5 µl reverse primer (10 µM)
- 1.0 µl 25 mM dNTP
- 5.0 µl 10x Expand buffer 1 or 10x Easy-A® buffer
- 0.75 µl Expand Long Template Enzyme (Roche) or Easy-A® polymerase (Promega)
- 0.75 µl DMSO (1-2%)
- x µl ddH_2O (ad 50 µl final volume)

Following standard program was used:

A. Initial denaturation:	95°C	2 min
B. Denaturation:	95°C	15 sec
C. Annealing:	x °C	30 sec ($T_{melting}$ -10%)
D. Elongation:	68°C (*)	x min (1kb = 1min), 25-30 cycles
E. Final elongation:	68°C (*)	7 min
F. Cooling:	4°C	until usage

(*) for Easy-A®-Polymerase, an elongation temperature of 72°C was required.

2.13.19 Colony PCR

Colony PCRs were performed as a first assay to test colonies of transformed *M. bovis* for the presence of *pknG* and mutant constructs. The PCR was set up by mixing:

- 1.25 µl forward primer (12.5 µM), *pknG* EN 5'
- 1.25 µl reverse primer (12.5 µM), *pknG* XNH 3'
- 0.4 µl 25 mM dNTP
- 2.5 µl 10x PCR reaction buffer 3
- 0.25 µl Expand Long Template Enzyme mix
- 18.35 µl ddH_2O
- colony material

The standard program was as follows:

A. Initial denaturation:	95°C	3 min	
B. Denaturation:	95°C	40 sec	
C. Annealing:	66°C	30 sec	
D. Elongation:	68°C	2 min 20 sec	30 cycles
E. Final elongation:	68°C	7 min	
F. Cooling:	4°C	until usage	

2.13.20 Site-directed mutagenesis

Site-directed mutagenesis was performed using components of the QuikChange II site-directed mutagenesis kit (Stratagene). The basic procedure utilizes a supercoiled double-stranded DNA vector with an insert of interest and two synthetic oligonucleotide primers (Microsynth), both containing the desired mutation. The primers, each complementary to opposite strands of the vector, are extendend during temperature cycling by *PfuUltra* HF (high fidelity) DNA polymerase withouth primer displacement. Extension of the primers generates a mutated plasmid containing staggered nicks. Following temperature cycling, the product is treated with *Dpn*I. The *Dpn*I endonuclease is specific for methylated and hemimethylated DNA that exclusively occurs in DNA isolated from *E. coli*, but not in *in vitro* amplified DNA, and is used to digest the parental DNA template and to select for mutation-containing synthesized DNA.

The reaction was set up in thin-walled tubes as follows:

- 1 µl DNA (50 ng)
- 1 µl (10 µM) Primer 1 (HPLC purified NS-inh-Ser-1)
- 1 µl (10 µM) Primer 2 (HPLC purified NS-inh-Ser-2)
- 1 µl 25 mM dNTPs
- 5 µl 10x Pfu reaction buffer
- 1 µl Pfu-Ultra HP-Polymerase (2.5 U)
- x µl ddH_2O (ad 50 µl final volume)

The following program was run:

A. Preheating lid:	100°C		
B. Initial denaturation:	95°C	30 sec	
C. Denaturation:	95°C	30 sec	
D. Annealing:	55°C	60 sec	20 cycles
E. Elongation:	68°C	8 min	
F. Cooling:	25°C	3 min	

Then, the reaction was digested with 10 U *Dpn*I (NEB) for 2 h at 37°C. Ultracompetent DH5α cells were transformed with 5 µl of the PCR mixture and plated on LB-Amp agar. The

colonies were picked, the plasmid DNA isolated and the sequence analyzed for correctly introduced point mutations.

2.13.21 Construction of different expression vectors

a) Construction of vectors for expression of truncated PknG versions in *E. coli*

Different PknG domains were cloned into vector pET-15b for subsequent expression and purification from *E. coli*: PknG-N-term, PknG-kin-domain, PknG-c-term, PknG-kin-c-term and PknG-ΔN.

By introducing *Nde*I and *Xho*I restriction sites, *pknG* was amplified from genomic DNA (*M. bovis* BCG) using Easy-A® polymerase (Promega). The PCR product was T/A cloned into pGEM®-T Easy vector (Promega), and the sequence was verified. The DNA fragments were then cut out by *Nde*I/*Xho*I and ligated into the expression vector pET-15b (Novagen).

In addition, *pknG* was mutated by site-directed mutagenesis (to obtain PknG-I87S/A92S with mutated inhibitor binding sites), subcloned into pGEM®-T Easy and sequenced. Using *Nde*I and *Xho*I restriction sites PknG was transferred into pET-15b.

b) Construction of vectors for expression of PknG mutants in mammalian cells - I

For expression in HEK, HeLa and Mel JuSo cells, several PknG truncated sequences were cloned into pIRESpuro3 (Clontech) to express the following mutant proteins:

PknG-wt, PknG-K181M: *pknG* inserts were excised from pGEX vectors using *Eco*RI and *Not*I restriction sites and ligated into pIRESpuro3.

PknG-ΔN: *pknG-ΔN* fragment was cut out from *pGEM::ΔN* by *Eco*RI and inserted into pIRESpuro3. The orientation was checked by *Bam*H1 digestion.

PknG-C/S and PknG-P-mut: *pknG* was amplified from *pMV361::pknG-C/S* and *pMV361::pknG-P-mut* using Easy-A polymerase by introducing *EcoR*I and *Not*I restriction sites, cloned into pGEM®-T Easy and sequenced. The inserts were excised by *Eco*RI and *Not*I and put into pIRESpuro3.

PknG-ΔC1, ΔC2, ΔC3, ΔN2 and kin: *pknG* was amplified from *pET-15b::pknG* adding *Eco*RI and *Not*I restrictions sites. The truncated *pknG* sequences were cloned into pGEM®-T Easy, excised by *Eco*RI and *Not*I and ligated into pIRESpuro3.

c) Construction of vectors for expression of PknG mutants in mammalian cells - II

PknG-wt and mutants were cloned into a vector allowing the expression of following FLAG-tagged proteins in eukaryotic cells. PknG-wt: *pknG* was amplified from *pGEX::pknG* by adding *Hind*III/*Not*I sites, cloned into pGEM®-T Easy and transferred to 3xFLAG® vector.

PknG-K181M: The *pknG* insert carrying the point mutation was cut out from *eGFP::pknG-K181M* by *Hind*III/*Not*I and ligated into the 3xFLAG® vector (Sigma).

PknG-ΔN: The *pknG-ΔN* insert was excised from *pGEM::pknG-ΔN* by *Not*I and ligated into 3xFLAG® vector. The orientation was tested by digestion with *Bam*H1.

PknG-Pmut, PknG-CXXC: *pknG* was amplified by Expand Long Template polymerase from *pMV361::pknG-Pmut* and *pMV361::pknG-C/S* and *Hind*III/*Not*I restriction sites were added. The amplified DNA was directly digested by *Hind*III/*Not*I and inserted into the 3xFLAG® vector.

PknG-ΔC1, ΔC2, ΔC3, ΔN2 and kin: The *pknG* fragments were excised from pGEM®-T Easy by *Not*I restriction and cloned into the 3xFLAG® vector. The orientation was verified by restriction digests with either *EcoR*V or *BamH*1.

d) Construction of a vector for PknG expression in mycobacteria

A construct was designed which allowed the expression of 3xFLAG-tagged PknG by mycobacteria.

3xFLAG-PknG: DNA was amplified using the FLAG vector containing *pknG* as template; *Nde*I and *Sca*I restriction sites were added and the *3xFLAG::pknG*-fragment was T/A-cloned into pGEM®-T Easy. To verify the presence of the 3xFLAG-tag, different clones were analyzed by sequencing the N-terminal region. One positive clone was selected for sequencing of full length *pknG*. The *3xFLAG::pknG* fragment was excised by *Nde*I and *Sca*I and cloned in the mycobacterial vector pSD5.

2.14. CELL CULTURE METHODS

2.14.1 Thawing eukaryotic cells

To recover cells from liquid nitrogen, the stocks were thawed at 37°C (water bath). The cells were immediately diluted in 9 ml of pre-warmed medium and centrifuged (200*x*g, 5 min). The pellet was gently resuspended in medium, transferred to a culture dish and incubated at 37°C (5% CO_2) for 24 h. Then the cells were microscopically checked, the medium exchanged or the cells splitted into new cultures.

2.14.2 Determination of cell numbers

The number of viable cells was determined using a Neubauer counting chamber (0.1 mm depth). An aliquot of cell suspension was diluted 1:2 with trypan blue solution (0.4 %, Sigma) and the non-stained cells in 4 big squares (each containing 16 small fields) were counted. The density in cells/ml was calculated by multiplying the mean number of cells per big square by 2×10^4.

2.14.3 Splitting of J774 macrophages

The cells were washed with PBS, removed from the dishes using a cell scraper or a bend glass pipette, and the cell suspensions were transferred to Falcon tubes. After centrifugation (5 min, 200*x*g), pellets were resuspended in fresh medium and the cells were distributed onto new culture dishes.

2.14.4 Trypsinization of adherent cells

Adherent cells (Mel JuSo, HeLa, HEK) were washed once with PBS or medium and trypsin/EDTA was added. The culture dish was incubated for 3-5 min at 37°C. The digestion was quenched by adding medium before spinning the cell suspension for 5 min at 200*x*g. The cell pellet was resuspended in medium and splitted into new cultures.

2.14.5 Preparation of cell stocks

A cell suspension from several dishes was prepared, centrifuged (200*x*g, 5 min) and the pellet was resuspended in freezing medium (FBS with 10% DMSO) at a cell density of 5-10x 10^6 cells/ml. The cell suspension was aliquoted (1 ml) into cryotubes which were placed into a pre-cooled (4°C) freezing box containing isopropanol, and stored at -80°C for 1-2 days before the tubes were transferred to the liquid nitrogen tank for long-term storage.

2.14.6 Preparation of murine bone marrow derived macrophages

The femur bones of a mouse killed by CO_2 asphyxiation were isolated, cleaned and cut open on one side and placed inside a yellow tip. The tip was transferred into a 5 ml tube containing 500 µl bone marrow macrophage medium. Pluripotent bone marrow cells were obtained by spinning at 200*x*g for 10 min. The bone marrow of one bone was added to Teflon dishes (Rowatec) containing bone marrow medium. After an incubation period of 5-7 days (at 37°C, 5 % CO_2) the differentiated cells (ca. 5-10x10^6 cells/bone) were used for further analysis.

2.14.7 Testing cells for mycoplasma contamination

Possible mycoplasma contamination in cell cultures was tested using the Mycoalert kit (Cambrex) according to the manufacturer's protocol. A luminometer (Biotek) was used to read out the bioluminescence which is generated in case of a contamination.

2.14.8 Transfection of cells

Mel JuSo, HeLa and HEK cells were transfected using jetPEI^{TM} (Polyplus), a polymer forming stable aggregates with DNA. Accordingly, macrophages were transfected by jetPEI^{TM} macrophages. Transfections were performed according to the Polyplus transfection protocol. In general, 400,000-600,000 cells were seeded in 6 cm dishes and grown to 60 % confluency (up to 24 h). Then, 5 µg plasmid DNA complexed to jetPEI^{TM} was added to the cells and the transfected cultures were further cultivated for 24-48 h. The cells were seeded on disinfected Teflon-coated 10 well-microscopy slides (4000-6000 cells / 50 µl) and incubated for 12-16 h (2 h for macrophages) to allow adherence.

Alternatively, 5 µl of the transfection mixture (containing 50 ng DNA) were added directly to the cells seeded on slides and incubated for 24-48 h.

2.14.9 Infection of J774 and bone marrow macrophages

Mycobacterial cultures (OD_{600}=0.5-1.0) were washed twice in PBS before washing and resuspension in macrophage medium. Suspensions were left for 20-30 min to obtain a supernatant devoid of mycobacterial aggregates.

Macrophages were seeded on Teflon-coated 10-well microscopy slides > 2 h prior to infection. The medium was removed and replaced by 50 µl of the bacterial suspension (OD_{600} of infection variable). Slides were incubated for 4 or 24 h at 37°C (5 % CO_2).

2.15. BIOCHEMICAL METHODS

2.15.1 Determination of protein concentrations

The concentration of proteins was determined by either the Bradford (Bradford, 1976) or the BCA (Smith et al., 1985) method. In general, a calibration curve was prepared by pipetting different volumes (1, 2, 4, 6, 8 and 10 µl) of a protein standard (bovine gamma globulin, 1 mg/ml, Bio-Rad) in duplicates into 96-well flat bottom plates (BD Falcon). For the unknown sample, aliquots of 1-5 µl in duplicates or triplicates were analyzed. To start the reaction, 200

µl Bradford reagent (Bio-Rad) or BCA reagent (Pierce) were added to the wells and the plate was incubated for 10 min at RT (Bradford) or for 30 min at 37°C (BCA). The protein concentration was measured at A_{595} (Bradford) or A_{562} (BCA) using a microplate reader (bucher biotec) with SoftMax®Pro software (version 4.0). Finally, the protein amount was calculated based on the standard curve.

2.15.2 Discontinuous SDS polyacrylamide gel electrophoresis (SDS-PAGE)

SDS-PAGE (Laemmli, 1970) was carried out using the Bio-Rad Protean II system. Usually, minigels (7cm x 10cm x 0.75mm) were prepared. After assembling the glass plates, the components for the separating gel were mixed, poured into the assembly and overlaid with water-saturated butanol. The concentration of acrylamide was selected dependent on the molecular weight of the protein to be analyzed (quantities for 7.5-15% gels are given in the table below). After polymerization of the lower gel, butanol was removed and the stacking gel mixture was poured on top of the lower gel, followed by immediate insertion of the comb with 10 slots.

Samples for SDS-PAGE were treated with 5x SDS-containing sample buffer, boiled for either 7 min (purified proteins) or 10-15 min (lysates), cooled to RT, centrifuged and loaded using a Hamilton pipet (50 µl/100 µl). The samples were run at 80V until the samples entered the separating gel, then the voltage was set to 120V.

component	**7.5 %**	**10%**	**12.5 %**	**15 %**	**stacking gel**
30% acrylamide, 0.8% bisacrylamide	2.5 ml	3.3 ml	4.2 ml	5 ml	0.65 ml
2 M Tris/HCl, pH 8.8	2 ml	2 ml	2 ml	2 ml	-
0.5 M Tris/HCl, pH 6.8	-	-	-	-	1.25 ml
20 % SDS	50 µl	50 µl	50 µl	50 µl	25 µl
dH_2O	5.4 ml	4.6 ml	3.7 ml	2.9 ml	3.05 ml
10% APS	50 µl	50 µl	50 µl	50 µl	25 µl
TEMED	10 µl	10 µl	10 µl	10 µl	5 µl

2.15.3 Western Blotting

Following gel electrophoresis, proteins were transferred onto a positively charged nitrocellulose membrane using the semi-dry transfer technique (Bio-Rad Trans-Blot® SD Cell). The blot was assembled on the lower electrode (anode) as follows: thick filter paper

(MN440, Macherey&Nagel), thin filter paper (3MM, Whatman®), nitrocellulose membrane (Hybond™-C super, Amersham Biosciences), gel, thin filter paper, thick filter paper and the upper electrode (cathode). Upon removal of air bubbles the transfer was run at 0.6 h at 2.5 mA/cm^2 = 0.17 A/minigel. Afterwards the proteins on the membrane were stained shaking in Ponceau S (Sigma) for 2 min and destained in dH_2O until bands were visible. The molecular weight standard bands were marked with a pen and the membrane was scanned for documentation.

The membrane was blocked under agitation in PBS-T containing 5% milk (low fat milk powder) for 2 h or o/n. The membrane was incubated with primary antibody diluted in PBS-T milk for 30 min or 1 h at RT, followed by 6x 5 min washing steps in PBS-T milk. The incubation with HRP-coupled-secondary antibody (diluted in PBS-T milk) was performed for 30 min at RT. The membrane was washed 4x 5 min with PBS-T milk and 2x 5 min with PBS-T, then rinsed in PBS. For immunodetection, the membrane was covered for 1-2 min with reagents enhancing chemiluminescence (ECL, Amersham). The membrane was dried with tissue paper, placed in a plastic bag and exposed to ECL films for different times.

2.15.4 Stripping of membranes for reprobing

In order to remove primary and secondary antibodies, the membrane was first washed twice in PBS-T and then incubated under agitation in stripping buffer (20% SDS, 100 mM β-mercaptoethanol, 67 mM Tris/HCl pH 6.7) for 30 min at 50°C. After 3x 10 min washing steps in PBS-T, the membrane was blocked in PBS-T with 5 % milk before the incubation with primary antibodies was continued as described above.

2.15.5 Expression of PknG

For expression of His-tagged PknG wt, PknGΔN, PknG-N-term, PknG-I87S/A92S and PknG-C/S, 50 µl competent *E. coli* BL21(DE3) cells were transformed with 200 ng/µl *pET15b::his::pknG*. After 1 h recovery in LB medium, the cells were spread on two LB-Amp plates and incubated o/n at 37°C.

The colony material was scratched from the agar plates by adding LB medium, the cell suspension was pooled and distributed equally among four 2 L-Erlenmeyer flasks (with 1L LB-Amp medium). The cultures were incubated while shaking at 37°C and 180 rpm until OD_{600}=0.5-0.6 was reached. Then, PknG expression was induced with IPTG (final conc. 0.1 mM) and incubated for 16 h at 22°C. The cultures were incubated shaking at 180 rpm for 15-16 h at 22°C using an aqua shaker (coldroom).

2.15.6 Purification of PknG

Cells were harvested (7280*x*g for 25 min at 4°C), resuspended in 50 ml 20 mM Tris pH 7.5, 500 mM NaCl, 40 mM imidazole including protease inhibitors (50x Roche protease inhibitor cocktail, 1 mM PMSF) and homogenized by four passages at 1000 psi (cell type 40 K) through a French® pressure cell press (Thermo, Electron corporation). The lysate was cleared by subsequent centrifugation steps at 20,000 rpm (SS34 Sorvall rotor, 20 min at 4°C) and at 41,000 rpm (TST 41.14 Kontron rotor, 30 min, 4°C). The supernatant was filtered and applied to a 5 ml HisTrap™ HP column (GE Healthcare) attached to a FPLC system (Pharmacia). The column was washed with ca. 150 ml of 20 mM Tris pH 7.5, 500 mM NaCl, 40 mM imidazole and His-PknG was eluted from the column by switching to 200 mM imidazole in 20 mM Tris pH 7.5, 500 mM NaCl. The collected 1 ml fractions were tested by loading 1 µl on a 10% SDS-PAGE (Laemmli, 1970). Fractions containing high PknG amounts were pooled and gel filtrated using the ÄKTA FPLC system (GE Healthcare) with attached Superdex 200 HiLoad 16/60 column (GE Healthcare) equilibrated in 20 mM Tris pH 7.5, 500 mM NaCl to remove imidazole and to obtain pure protein. Fractions containing pure PknG were tested by 10% SDS-PAGE (1-2 µl of the PknG fraction) and concentrated at 2500*x*g and 4°C to 8-18 µg/µl in Vivaspin 20 tubes (30,000 MWCO PES, Vivascience AG). Protein concentration was determined by BCA™ Protein Assay (Pierce). The overall yield of PknG was 15 mg/L *E. coli* culture. The purity of the samples was checked by 10% SDS-PAGE; kinase activity was confirmed by performing *in vitro* autophosphorylation assays. Aliquots of purified PknG were either kept on ice for further usage or frozen in liquid nitrogen and stored at -80°C.

When cleavage of the N-terminal His-Tag was required, the protein concentration of the gel filtration-purified PknG pool was determined and PknG was cleaved with 2U thrombin/mg protein and in sample buffer containing 4 mM $CaCl_2$. The protein sample was incubated for 16 hours at room temperature, centrifuged (20,800*x*g, 5 min, 4°C) and applied to a 1 ml HisTrap™ HP column to remove the His-tag. Fractions were collected, loaded on a 10% SDS-PAGE and analyzed by western blotting to confirm His-Tag cleavage by using an α-His antibody. Thrombin present in the PknG containing fractions was removed by a subsequent size exclusion chromatography step on a Superdex 200 HiLoad 16/60 column equilibrated in 20 mM Tris pH 7.5, 500 mM NaCl. Fractions containing cleaved protein were pooled and concentrated at 4°C to 8-18 mg/ml.

See flow-chart on the next page for overview and timing!

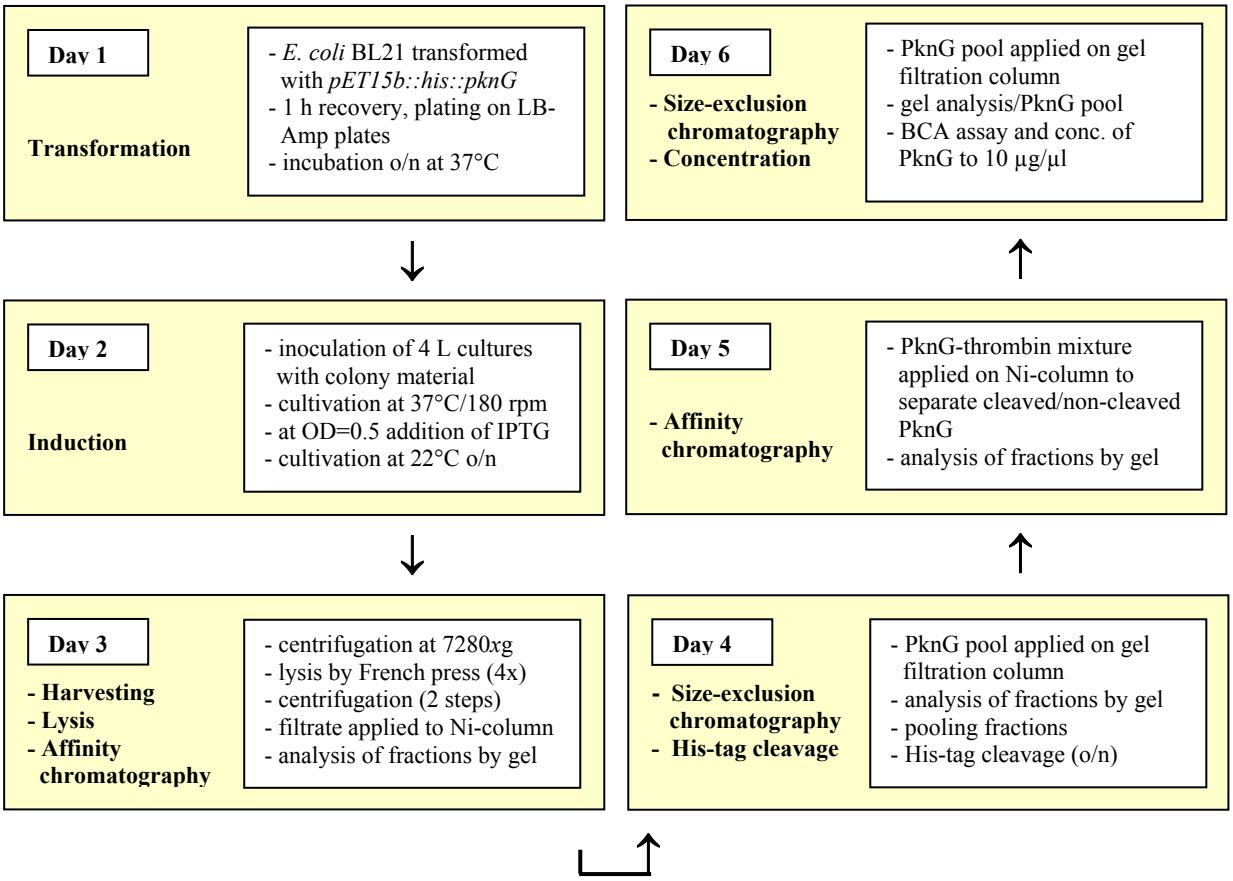

2.15.7 Aging assay

Aging assays were performed on a regular basis to check the quality of PknG. Protein samples were centrifuged at 20,800*x*g for 15 min (4°C). The supernatant was transferred to a new tube. An aliquot of the supernatant and the starting sample as well as the complete pellet fraction were analyzed by 7.5% SDS-PAGE.

2.15.8 Analytical gel filtration

To test the quality of purified PknG, PknG was analyzed by small-scale size exclusion chromatography. Fifty µg protein (in 20 mM Tris pH 7.5, 500 mM NaCl) were injected onto a Superdex 200 PC 3.2/30 gel filtration column attached to the SMART^{TM} System (Pharmacia) and the sample was run and eluted in 20 mM Tris pH 7.5, 500 mM NaCl at a flow rate of 50 µl/min.

To separate PknG monomers and dimers for further analysis, 500 µg PknG full length were loaded on the column. PknG was eluted in 75 µl fractions collected on ice. The concentration of monomer- and dimer peak fractions was determined by BCA^{TM} Protein Assay (Pierce).

2.15.9 Kinase assay

In vitro autophosphorylation of PknG and mutants was performed by incubating 0.3-0.5 µg kinase in 25 mM Tris pH 7.5, 2 mM $MnCl_2$, 1 mM DTT and 0.5 µCi [γ^{32}P]ATP (GE Healthcare) for 30 min at 37°C. To monitor kinase activity of PknGΔN, the protein was combined with 0.5-2 µg PknG-K181M, the kinase-dead version of PknG (Walburger et al., 2004).

Alternatively, PknG mutants (PknG-I87S/A92S and PknG-C/S) were incubated in buffer containing the N-terminal domain of PknG used as an artificial substrate. Sample buffer was added and the phosphorylated proteins were boiled for 7 min at 95°C. The samples were separated on 7.5%, 10% or 12.5 % SDS-PAGE, analyzed by autoradiography (Hyperfilm MP, Amersham) and, if required, quantitated by Phospho-Imaging using a STORM 840 Optical Scanner System and ImageQuant software (Molecular Dynamics, version 5.2).

2.15.10 Inhibitor screen (ProQinase/Freiburg)

To test the selectivity of AX20017, the IC_{50} profile of the inhibitor was determined using different concentrations of PknG and 28 selected mammalian protein kinases representing the six major kinase families (Manning et al., 2002). IC_{50} values were determined performing a radiometric ATP consumptive assay (^{33}PanQinase® Activity Assay, ProQinase) in which 12 concentrations of AX20017 in the range from 5 x 10^{-5} M to 1.5 x 10^{-10} M were tested. For sample preparation, PknG was dissolved in the same storage buffer (50 mM HEPES pH 7.5, 100 mM NaCl, 5 mM DTT and 20% v/v glycerol as the other kinases. All kinase assays were performed in 96-well FlashPlates™ (Perkin Elmer) in 50 µl reaction volume. The reaction cocktails were pipetted by the BeckmanCoulter Biomek 2000/SL robotic system as follows:

- 20 µl assay buffer
- 15 µl ATP solution (in H_2O)
- 5 µl test sample in 10% DMSO
- 10 µl enzyme/substrate mixture (in H_2O)

The mixtures were incubated at 30°C for 80 min. Then the reaction was stopped with 50 µl of 2% (v/v) H_3PO_4 and the plates were aspirated and washed two times with 200 µl 0.9% (w/v) NaCl. The incorporation of $^{33}P_i$ (in cpm) was determined with a microplate scintillation counter.

2.15.11 Phosphorylation and dephosphorylation of PknG

Phosphorylation and dephosphorylation of PknG was visualized by performing band shift assays. PknG was phosphorylated by incubating 2 µg sample for 3 h at 37°C in 20 mM Tris, 500 mM NaCl containing 50 µM ATP, 1mM DTT and 2mM $MnCl_2$. PknG was dephosphorylated by using either bovine alkaline phosphatase (AP) or shrimp alkaline phosphase (SAP). PknG was incubated for 3 h at 37°C in 1x phosphatase buffer containing 0.5 U phosphatase/µg PknG and protease inhibitors (CLAAP, PMSF). As controls, PknG was incubated in buffers lacking ATP, AP or SAP. The reactions were stopped by adding sample buffer, boiled for 7 min and analyzed by 7.5% SDS-PAGE.

2.15.12 Limited proteolysis

PknG (10 mg/ml, in 20 mM Tris pH 7.5, 75 mM NaCl, 10% glycerol) was stored at 4°C. To analyze proteolysis, aliquots were taken at different time points (days) and separated by 7.5% SDS-PAGE. In addition to "natural" degradation, PknG was treated with enzymes. For digestion of PknG (4 mg/ml, in 100 mM Tris pH 7.5, 200 mM NaCl) different enzymes (Trypsin, Proteinase K, Chymotrypsin, Subtilisin, Thermolysin and Pepsin) in varying enzyme-substrate ratios at different temperatures (4°C and 30°C) were tested. The enzyme-substrate mixtures were incubated at 37°C and 2 µl aliquots (3 µg PknG) were removed at different time points (usually 2, 5, 10, 20, 30, 60, 120, 210 min), treated with sample buffer and boiled for 7 min at 95°C to stop the reaction. The samples were analyzed by 10% SDS-PAGE, followed by staining with Coomassie. If required, PknG degradation was further analyzed by performing Western blotting with antibodies directed against the N- and C-terminal part of PknG. In order to identify the degraded products, the samples separated by SDS-PAGE were electroblotted to an Immobilon-P transfer (PVDF) membrane (Millipore).

2.15.13 Electroblotting proteins to PVDF membranes

Before setting up the blot, the PVDF membrane was briefly (2-3 s) immersed in 100% methanol, rinsed with H_2O, and equilibrated in transfer buffer (10 mM CAPS, 10% MeOH, pH 11.0) for at least 15 min. After electrophoresis, the gel was rinsed in transfer buffer for 5 min. Gel and PVDF membrane were sandwiched between Whatman 3MM paper and assembled into the blotting cassette (Bio-Rad Trans-Blot® SD Cell). A backing sheet of PVDF was included to ensure that all proteins were trapped on the membrane. The amperage was doubled by selecting 0.34 A/minigel. After completion of the transfer, the membrane was rinsed several times for each 5 min in H_2O DW-trigB (Albatros) to reduce the level of

contaminants. Proteins on the membrane were stained for 5 min in freshly prepared Coomassie blue R-250 solution (0.1% in 50% methanol) and destained with several changes of the destaining solution (50% MeOH, 10% acetic acid). The membrane was rinsed several times in H_2O DW-trigB (Albatros), air-dried on Whatman paper and the bands of interest were excised using fresh razor blades for each sample. The bands were transferred to Eppendorf tubes and subjected to sequence analysis by Edman degradation (Urs Kämpfer, University of Bern).

2.15.14 Preparation of *M. bovis* BCG lysates

For obtaining *M. bovis* BCG lysates, the cultures were harvested at OD_{600} 0.7-0.9. Cells were washed three times in phosphate buffered saline (PBS), resuspended in PBS or TEN buffer and disrupted in the presence of glass beads and protease inhibitors (1 mM PMSF and 50x complete EDTA-free protease inhibitor cocktail from Roche) by using the Mixer Mill (type MM 300, Retsch, Germany) at frequency 30/s for 20 min with chilling intervals. Cell debris and non-lysed cells were removed by low speed centrifugation (10 min, 10,600*x*g).

Alternatively, bacteria were washed twice in PBS, followed by a final washing step and resuspended in TEN buffer (75 mM Tris pH 8.8, 4 mM EDTA, 100 mM NaCl). Cells were lysed in the presence of protease inhibitors by three passages of FRENCH® press (Thermo, Waltham, USA) treatment. Cell lysate was cleared by centrifugation (10 min, 10,600*x*g).

2.15.15 Cell fractionation of mycobacterial lysates

To analyze subcellular localization of Ag84, total mycobacterial lysate was subjected to a high-speed spin (100,000*x*g, 30-45 min, 4°C) to obtain membrane and soluble fractions. After determination of the protein concentration, equal amounts were loaded on 10 % SDS-PAGE gels and analyzed by Western blotting as described above using Ag84 specific antibody. As controls, monoclonal antibodies GroEL AI-75320 and lipoprotein F29-47 were included.

2.15.16 Size-exclusion chromatography of mycobacterial lysates (SMART system)

Fifty µg *M. bovis* BCG lysate (soluble fraction, prepared as described above) was applied to a gel filtration column pre-equilibrated in PBS. The presence of Ag84 in the collected fractions was detected by immunoblotting. Standard marker proteins allowing the determination of the molecular weight of Ag84 were bovine thyroglobulin (670 kDa), bovine

y-globulin (158 kDa), chicken ovalbumin (44 kDa), horse myoglobin (17 kDa) and vitamin B_{12} (1.35 kDa).

2.15.17 Chemical crosslinking of mycobacterial lysates

To analyze oligomerization of Ag84, purified protein (0.2 mg/ml) or *M. bovis* BCG lysate (1 mg/ml) was added with different concentrations of formaldehyde and incubated for 15 minutes at 37°C. Sample buffer including SDS was added and the samples were loaded (without boiling) on a 10% SDS-PAGE gel followed by Western blotting with Ag84 antibody.

2.15.18 Preparation of lysates from eukaryotic cells

Cells lysates were prepared from 1-2 ml of the undiluted cell culture after centrifugation. The cells were washed twice with ice-cold PBS (5 min, 20,800*x*g, 4°C). 50 µl Triton-X100 lysis buffer containing protease inhibitors was added to the cell pellet, followed by 15 min incubation on ice. The lysate was centrifuged at 4°C and 20,800*x*g for 15 min and the supernatant was transferred to a new tube. The protein concentration of the lysates was determined and equal protein amounts were resuspended in 1x SDS sample buffer followed by SDS-PAGE and Western blotting.

Alternatively, cells were washed twice in PBS and counted using a Neubauer chamber. The cells were spun (5 min, 200*x*g, RT) and lysed by adding SDS sample buffer normalized for the cell number and by boiling for 10 min at 95°C.

2.16. BIOPHYSICAL METHODS

2.16.1 Optimum solubility screen (OSS)

The OSS enables rapid and optimal buffer selection for the sample by simultaneously screening small amounts of protein for solubility in 24 buffers of different pHs. To perform this screen, a PknG (wildtype) sample of high concentration (17.5 µg/µl, in 20 mM Tris, 500 mM NaCl) was prepared. Four different PknG sample buffer conditions were tested (PknG in 200 mM or 500 mM NaCl with or without 10% glycerol), making up 96 conditions under which PknG solubility was analyzed. 5 µl PknG were incubated for 2 h (RT) with 45 µl of screening buffer (100 mM) supplemented with NaCl and, if required, glycerol. Then, PknG was centrifuged for 20 min (RT) at 17,900*x*g and the supernatant was transferred to a new

tube. Protein concentration and possible aggregation were analyzed by measuring the absorption spectrum using a NanoDrop photometer (Thermo Fisher Scientific). The remaining supernatant was pipetted into wells of a 24 well-plate (VDX 24) and the hydrodynamic radius was measured by dynamic light scattering using a DynaPro^{TM}Titan device (Wyatt Technology Europe GmbH) with DYNAMICS^{TM} software (Version 6.7.3). Buffers resulting in a monomodal and monodisperse PknG profile were considered as optimal.

2.16.2 Static light scattering (SLS)

SLS analysis was performed using a miniDAWN TriStar equipped with an Optilab rEX refractometer (Wyatt Technology Corp.) coupled to Superdex 200 10/30 (Amersham Biosciences) gel filtration column run on an Agilent 1100 HPLC. 100 µl of PknG full length (2.5 µg/µl, in 20 mM Tris pH 7.5, 500 mM NaCl) were injected onto the column equilibrated in 20 mM Tris pH 7.5, 500 mM NaCl. Samples were eluted at a constant flow rate of 0.5 ml/min. The shape-independent molecular mass was determined with Wyatt Astra version 4.90.08 software package.

2.16.3 Circular dichroism spectroscopy (C/D)

Circular dichroism spectroscopy was performed in order to verify the structural integrity of several PknG mutants. Protein samples were diluted with buffer (20 mM Tris pH 7.5, 500 mM NaCl) to a final concentration of 0.06-0.08 µg/µl. Measurements were done in 0.1 or 0.2 cm quartz glass cuvettes at 20°C. C/D data were collected on a Jasco J720 spectropolarimeter. Per measurement, 8 scans of spectra ranging from 190-260 nm were recorded and normalized for the buffer.

2.16.4 Crystallization

The crystallization work comprising crystallization assays, assessment of plates, x-ray measurements and structure determination, was carried out at the Paul Scherrer Institut (PSI) in Villigen in collaboration with S. Honnappa and M. Steinmetz.

Freshly purified, non-frozen protein (5-15 µg/µl) was used for the crystallization assays. During storage and transport the sample was kept on ice. PknG was centrifuged for 10 min at 17,900*x*g (4°C) and the supernatant was transferred to a new tube. PknG was pre-incubated for 2h at RT in case inhibitor or ATP analoga were added.

Crystallization was carried out according to the sitting drop vapour diffusion method. Crystals were set up in 24 well plates (Hampton). Various conditions were screened by testing buffers provided by commercial crystallization kits (Sigma, Hampton, Emerald). 300 µl of the individual buffers was pipetted into each well, 2 µl protein sample were pipetted on top of the plateau before 2 µl of the mother liquor (buffer) were added to PknG to initiate the evaporation process. The crystallization plates were usually stored at 20°C and analyzed at different time points. For crystals diffracting to a low resolution, buffer and incubation conditions were further optimized. The scheme below showes the variety of methods applied to obtain well-diffracting 3D-crystals.

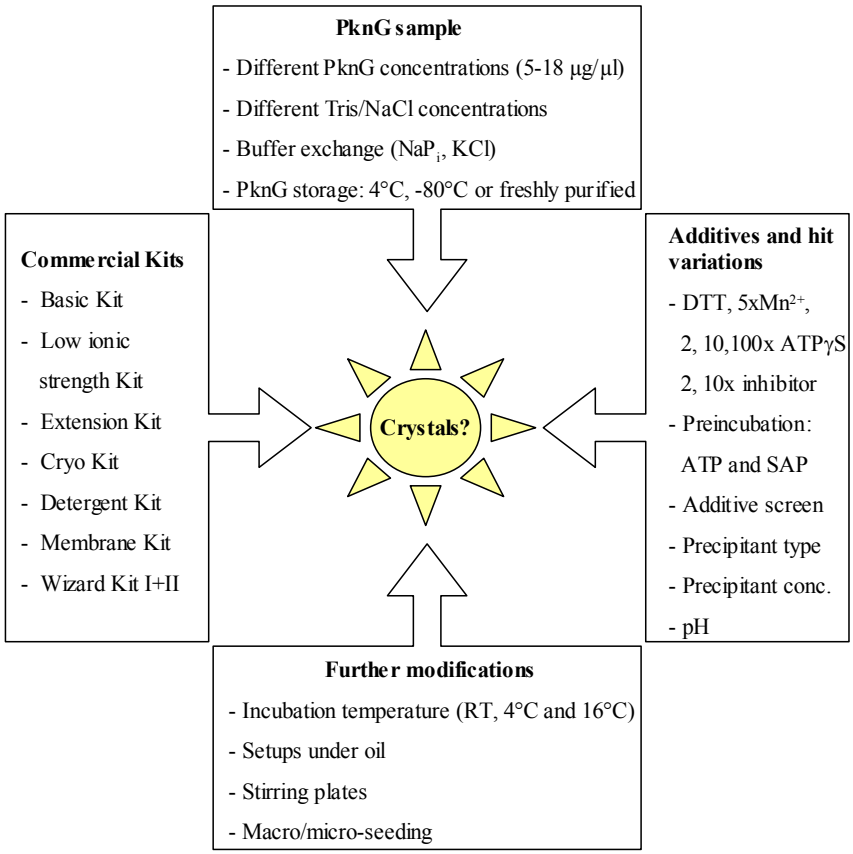

2.16.5 Structure determination

PknGΔN (10 mg/ml) was co-crystallized with AX20017 (135 µM final concentration) by mixing equal volumes of protein/inhibitor (each 2 µl) with the reservoir solution by using the sitting drop method at 20°C. The crystals grew within 1 day in a reservoir solution containing 100 mM sodium citrate at pH 5.5, 1 M $(NH_4)_2HPO_4$, 200 mM NaCl and 10 mM $CdCl_2$. Data sets were collected at the Swiss Light Source (Villigen PSI, Switzerland) protein beam line X10SA on an MAR CCD detector. All x-ray diffraction data were collected at 100 K. A total

of 360 and 240 rotation images of 0.5° were recorded for native and derivative crystals, respectively.

The structure of the PknGΔN-AX20017 complex was solved by single isomorphous replacement anomalous scattering (SIRAS) using a mercury derivative obtained by overnight soaks of crystals in the presence of 0.5 mM thiomersal. Iterative rounds of model building and maximum likelihood refinement resulted in a complete 2.4 Å resolution model for the PknGΔN-AX20017 complex. The final model converged at an R/R_{free} of 0.18/0.22 with very good stereochemistry. Data sets and refinement statistics are given in Table 1.

Figures were prepared with the program PyMOL (De-Lano Scientific LLC, San Carlos, CA, www.pymol.org). Solvent accessible area calculations were carried out with the program NACCESS (http://wolf.bms.umist.ac.uk/naccess/). Determination of the structure was carried out by S. Honnappa and M. Steinmetz.

2.16.6 Crystallographic data and refinement statistics

	Native	**Mercury (at λ p**
Wavelength, Å	1.008503	1.008503
Space group	P65	P65
Resolution, Å	2.4	3.1
Unit cell, *a*, *b*, and *c*, Å	122.6, 122.6 and	122.4, 122.4 and
No. of observed reflections	908,852	283,571
No. of unique reflections	80,540	73,241
R_{sym}*, %	7.3 (80.1)†	6.4 (76.0)†
I/σ (*I*)	20.1 (3.4)†	13.6 (2.1)†
Completeness, %	99.9 (100)†	99.7 (99.6)†
Phasing power (centric/acentri	0.56/0.84	
R_{Cullis} (centric/acentric)§	0.92/0.86	
Figure-of-merit (centric/acentr	0.12/0.14	
No. of refined atoms		
Proteins	9,973	
Water	299	
Ligand/ion	72/3	
R-factor/free *R*-factor‖	0.18/0.23	
R.m.s.d. bond lengths/bond an	0.011/1.4	

*$R_{sym} = \Sigma_h\Sigma_i|I_i(h) - \langle I(h)\rangle|/\Sigma_h\Sigma_i I_i(h)$, where $I_i(h)$ and $\langle I(h)\rangle$ are the *i*th and mean measurement of the intensity of reflection *h*.

†Figures in parentheses indicate the values for the outer shell of the data.

‡Phasing power = $\Sigma F_H^{calc}/\Sigma|F_{PH}^{obs} - F_{PH}^{calc}|$, where F_H^{calc} is the calculated heavy atom amplitude and F_{PH}^{obs} and F_{PH}^{calc} are the observed and calculated heavy-atom derivative structure factor amplitudes, respectively.

§$R_{Cullis} = \Sigma |F_{PH}^{obs} \pm F_P^{obs}| - |F_H^{calc}|/|\Sigma |F_{PH}^{obs} - F_P^{obs}|$, where F_{PH}^{obs} is the observed heavy-atom derivative structure factor amplitude, F_P^{obs} is the observed native structure factor amplitude, and F_H^{calc} is the calculated heavy atom amplitude.
¶Figure-of-merit = $\alpha |\int_\alpha P(\alpha)\exp(i\alpha)d_\alpha/\int_\alpha P(\alpha)d_\alpha|$, with α ranging from 0 to 2π.
‖ $R = \Sigma |F_P^{obs} - F_P^{calc}|/\Sigma F_P^{obs}$, where F_P^{obs} and F_P^{calc} are the observed and calculated structure factor amplitudes, respectively.
**R.m.s.d., root-mean-square-deviation from the parameter set for ideal stereochemistry.
Data measured and calculated by S. Honnappa and M. Steinmetz.

2.16.7 Sequence analysis

To calculate the frequency of occurrence of the four individual AX20017-contacting residues Ile165, Val179, Gly236, and Ile292 of PknG, an alignment of 491 human kinases was used as a reference (Manning et al, 2002). The corresponding positions of the four residues within the alignment was corroborated by superimposing the x-ray structure of PknG with the ones of PKA (PDB ID 1ATP), (PDB ID 2BHE), CaMK1 (PDB ID 1A06), PAK1 (PDB ID 1F3M), TgFβR1 (PDB ID 1B6C), and IRK (PDB ID 1IRK). Identical PknG residues in the alignment were counted and divided by 491 to obtain the frequency of occurrence. Carried out by M. Steinmetz and F. Winkler.

2.17. CELLULAR ASSAYS

2.17.1 Phagocytosis of mycobacteria by J774 macrophages

Phagocytosis was analyzed by treating J774 cells for 30 min with 10 and 20 µM of AX20017, followed by incubating the cells for 2 hours with latex beads (3 µm diameter, Polysciences) at a 10:1 ratio of beads:cells in the continued presence of the inhibitor followed by fixation in 3% paraformaldehyde as described before (Ferrari et al., 1999). Cells were observed with an Axiophot (Zeiss) using a 63X objective. Carried out by G. Kunz.

2.17.2 Proliferation assay

Proliferation of J774 macrophages was determined by measuring ^{3}H-thymidine incorporation as a function of replication (Jayachandran et al., 2007). J774 macrophages (2.5 x 10^4) were seeded in 100 µl of DMEM medium (with 10 % FBS and 2 mM Glutamine) per well in a 96 well plate and allowed to adhere while incubating for 1 h at 37°C, 5 % CO_2. Then, 100 µl medium supplemented with AX20017, (final concentration 12.5 µM and 25 µM), G418 (final concentration 2 mg/ml) or DMSO (same volume as highest inhibitor concentration) were added. At timepoint 0, 24 h and 48 h, 50 µl of tritiated thymidine (0.5 µCi) were added

to each well. To allow incorporation of ^{3}H-thymidine into DNA, the cells were incubated for 12 h at 37°C, 5 % CO_2 and afterwards frozen at -20 °C. For harvesting, the cells were thawed and lysed by hypotonic shock and the DNA isolated using Packard FilterMate Harvester 196, with Unifilter-96, GF/C filter. CPMA numbers were measured using the TopCount (Perkin Elmer) microplate scintillation counter.

2.17.3 Survival assay

Survival of mycobacteria was determined by measuring ^{3}H-Uracil incorporation as a function of transcription. Prior to infection, mycobacteria were washed twice and resuspended in bone marrow macrophage medium (DMEM supplemented with 30 % L929 medium 10% FBS, 2 mM L-glutamine, 1 mM Na-pyruvate, 50 µM β-Mercaptoethanol). Bone marrow derived macrophages were infected with mycobacteria (ODI = 0.05) for 1 h at 37°C. Extracellular bacteria were removed by adding amikacin (200 µg/mL), followed by a 45 min incubation at 37°C. The cells were washed and chased in bone marrow medium. At different time points, the medium was replaced by incorporation medium containing 0.15 % saponin to lyse the macrophages and 1 µCi ^{3}H-Uracil to label RNA. After 24 h incorporation time at 37°C, mycobacteria were killed by NaOH/TCA treatment and the RNA was harvested onto UniFilter-96 GF/C glass fiber filter plates (Packard). The recovered radioactivity was measured by liquid scintillation counting (Microplate Scintillation Counter, Packard).

2.17.4 Protein translation assay

Protein synthesis of J774 macrophages was determined by measuring ^{35}S-Methione and ^{35}S-Cysteine incorporation into proteins (Pieters et al., 1991; Tulp et al., 1993). J774 macrophages (2.5×10^{4}) were seeded in 100 µl of DMEM medium (with 10 % FBS and 2 mM Glutamine) per well in a 96 well plate and let adhere for 12 h. Then, 100 µl medium supplemented with 12.5 µM, 25 µM AX20017, cyclohexamide (100 µg/ml) or DMSO (same volume as highest inhibitor concentration) were added. After 45 min incubation at 37°C, 5 % CO_2, the medium was removed using a pipette and replaced by 100 µl of starvation medium supplemented with the above mentioned concentrations of inhibitor, DMSO or cyclohexamide and pre-incubated for 1 h. To label the cells, 100 µl starvation medium containing 0.4 µCi ^{35}S-Methione and ^{35}S-Cysteine (Easy Tag Express Protein Labeling Mix [^{35}S], Perkin Elmer) as well as inhibitor, DMSO or cyclohexamide was added to each well and the plates were incubated at 37°C, 5 % CO_2. After a chase time of 4 h or 9 h, the cells

were washed 2x in 200 µl PBS^{++} and lysed by adding 100 µl lysis buffer containing 20 mM HEPES pH 7.4, 100 mM NaCl, 5 mM $MgCl_2$, 1 % Triton X-100 and protease inhibitors (Complete EDTA-free protease inhibitor cocktail, Roche). The plates were incubated shaking on ice for 30 min, and lysis efficiency was checked by microscopy. The lysed cells (without nuclei) were carefully transferred from the well to an Eppendorf tube and spun for 15 min at 17,900*x*g. The supernatant was mixed and 5 µl and 10 µl per sample were spotted on Whatman paper pieces. Then, the pieces were washed 2x in 10 % TCA and 2x in diethyl ether and dried for approx. 45 min at 50°C. Then, the pieces were placed in scintillation vials and 10 ml of scintillation fluid (Ultima Gold XR, Perkin Elmer) were added. The samples were mixed (vortexed) and the incorporated ^{35}S was analyzed by counting CPMB numbers using the TRI-CARB Liquid Scintillation Analyzer 1900 TR (Packard).

2.17.5 Cell organelle electrophoresis

Bone marrow derived macrophages were infected for 3 hours with mycobacteria. Cells were washed twice (450*x*g, 7 min), resuspended in 1 ml buffer and homogenized using a cell cracker. The post-nuclear supernatant (240*x*g, 15 min) was trypsinized (25 µg/mg protein) for 5 min at 37°C and the reaction was stopped by adding soybean trypsin inhibitor (Calbiochem, 625 µg per mg protein). After sedimentation of the membranes (100,000*x*g, 60 min), the pellet was resuspended in 0.5 ml homogenization buffer containing 6 % Ficoll-70 (Pharmacia), and loaded in the middle of a 10-0 % Ficoll gradient. During electrophoresis (10.4 mA, 80 min), fractions were collected to be tested for β-hexosaminidase activity and protein amount (Bradford, 1976). Cytospins were performed to analyze the presence of bacteria in the collected fractions. After pelleting the fractions on glass slides, the cells were fixed with paraformaldehyde and acid-fast stained (Becton Dickinson). The slides were analyzed by fluorescence microscopy in order to count the number of bacteria in the fractions (Hasan and Pieters, 1998; Tulp et al., 1993). Carried out by B. Combaluzier.

2.17.6 Video microscopy

Video microscopy was done using a Zeiss Axiovert 100TV and processed using Openlab software (Gatfield and Pieters, 2000). Carried out by R. Jayachandran.

2.17.7 Growth of mycobacteria

An aliquot of a culture (OD_{600} = 0.5-0.6) was used to inoculate 40 ml 7H9 medium supplemented with 10 % OADC (no antibiotics). Per strain, four 100 ml-Erlenmeyer flasks

were prepared and the cultures were adjusted to a start OD_{600} of 0.05. The cultures were incubated shaking orbitally (90 rpm) in the dark at 37°C. Every 12 h, an aliquot (dependent on the OD_{600} 500µl, 100µl or 50µl) was removed, diluted and the OD_{600} was determined. Bacterial growth was observed for about 7-8 days until the cultures reached the stationary phase.

Alternatively, mycobacterial growth was measured in 96-well plates (BD Falcon). First, the cultures were left at RT to allow sedimentation of bacterial clumps. The supernatant was then transferred and diluted to OD_{600} = 0.05. Per strain, 10 wells of 200 µl were prepared. The plates were incubated at 37°C and the OD_{600} was determined every 12 h for 4-5 weeks.

2.18. MICROSCOPY

Microscopy was used to analyze the effects of Ag84 overexpression and to determine the localization of Ag84 within mycobacteria. In addition, PknG localization upon transfection of mammalian cells or upon infection of macrophages was studied by fluorescence microscopy. Furthermore, trafficking of PknG mutants in macrophages was analyzed. All studies described here were carried out using a confocal laser scanning microscope (CLSM 510 META, Zeiss).

2.18.1 Staining cells for immunofluorescence microscopy

Upon transfection or infection, the adhered eukaryotic cells were carefully washed twice with PBS on slide prior to fixation in 100 % MeOH (at -20°C for 4 min). The cells were blocked in PBS with 5 % FBS for 30 min at RT. Incubation with primary antibodies was performed on slide by adding 25 µl blocking buffer (PBS with 5 % FBS) including antibodies, followed by six washing steps in blocking buffer and PBS (5 min each). Staining with secondary antibodies was done by incubating cells with Alexa-antibodies for 30 min in the dark. Cells were washed as previously in blocking buffer and PBS, but were kept in the dark. If required, DNA was stained using intercalating DRAQ5 prior to further washing in PBS (2 x 5 min). FluoroGuard antifade-reagent was added to each well and the slides were covered with cover slips and sealed with nail polish. Slides were stored at 4°C in the dark until usage for microscopy analysis.

Alternatively, cells were fixed with paraformaldehyde (3 % in PBS, pH 7.2) for 30 min at RT and washed 1x 5 min with PBS, 1x with PBS containing 10 mM glycine for quenching of

PFA and again 1x 5 min with PBS. Blocking and lysis was performed in PBS with 2 % BSA and 1 % Triton-X100. Antibody incubations were carried out in blocking buffer (PBS containing 2% BSA, 1% Triton-X100).

2.18.2 Measuring cell length of Ag84 expressing mycobacteria

To measure size, transformed mycobacterial cells from colonies grown on 7H10 agar supplemented with OADC and 25 µg/ml kanamycin were resuspended in 7H9 liquid medium and diluted to a density of 10-20 cells per microscopic focal plane. Cell length (the maximum distance between the two cell poles) and cell width (largest diameter of examined cell) of around 100 bacteria were measured at different times after transformation using the scaling tool provided by the software.

2.18.3 Localization of Ag84 within mycobacteria

To analyze localization of Ag84, *M. smegmatis* overexpressing *wag31*$_{MS}$-*gfp* was grown on 7H10 agar (supplemented with OADC and 25 µg/ml kanamycin). Cells were resuspended in 7H9 medium and ~ 100 cells were analyzed each day during cultivation. Ag84 localization was considered as asymmetric, when the cell poles contained different amounts of Ag84 and regarded as symmetric, when Ag84 was equally distributed at both poles.

2.18.4 Lysosomal trafficking

Bone marrow derived macrophages were seeded on glass slides and infected with bacteria of an ODI = 0.05 for 1 h, followed by a 3 h chase. Cells were fixed in methanol (4 min at -20°C) and incubated with primary antibodies (rat-anti-LAMP1 or polyclonal rabbit-anti-BCG) for 40 min at room temperature, washed in PBS containing 5 % FCS and then incubated with Alexa Fluor 488 or Alexa Fluor 568 (Molecular Probes) coupled to goat anti-rabbit or goat anti-mouse antibodies (Southern Biotech). Coverslips were mounted in FluoroGuard antifade reagent (Bio-Rad). In three independent experiments, 3x100 events per strain were analyzed. Carried out by D. Perisa.

2.19. REFERENCES

Bradford, M. (1976). A rapid and sensitive method for the quantitation of microgram quantities of protein utilizing the principle of protein-dye binding. Anal Biochem *72*, 248-254.

Ferrari, G., Langen, H., Naito, M., and Pieters, J. (1999). A coat protein on phagosomes involved in the intracellular survival of mycobacteria. Cell *97*, 435-447.

Gatfield, J., and Pieters, J. (2000). Essential role for cholesterol in entry of mycobacteria into macrophages. Science *288*, 1647-1651.

Hasan, Z., and Pieters, J. (1998). Subcellular fractionation by organelle electrophoresis: separation of phagosomes containing heat-killed yeast particles. Electrophoresis *19*, 1179-1184.

Inoue, H., Nojima, H., and Okayama, H. (1990). High efficiency transformation of Escherichia coli with plasmids. Gene *96*, 23-28.

Jayachandran, R., Sundaramurthy, V., Combaluzier, B., Mueller, P., Korf, H., Huygen, K., Miyazaki, T., Albrecht, I., Massner, J., and Pieters, J. (2007). Survival of mycobacteria in macrophages is mediated by Coronin 1-dependent activation of calcineurin. Cell *130*, 37-50.

Laemmli, U. (1970). Cleavage of structural proteins during the assembly of the head of bacteriophage T4. Nature *227*, 680-685.

Johnson, J.P, Demmer-Dieckmann, M., Meo, T., Hadam, M.R., Riethmüller, G.(1981). Surface antigens of human melanoma cells defined by monoclonal antibodies. I. Biochemical characterization of two antigens found on cell lines and fresh tumors of diverse tissue origin. Eur J Immunology 11, 825-831.

Manning, G., Whyte, D. B., Martinez, R., Hunter, T., and Sudarsanam, S. (2002). The protein kinase complement of the human genome. Science *298*, 1912 - 1934.

Parish, T., and Stoker, N. (1998). Electroporation of mycobacteria. Methods Mol Biol *101*, 129-144.

Pieters, J., Horstmann, H., Bakke, O., Griffiths, G., and Lipp, J. (1991). Intracellular transport and localization of major histocompatibility complex class II molecules and associated invariant chain. J Cell Biol *115*, 1213-1223.

Smith, P., Krohn, R., Hermanson, G., Mallia, A., Gartner, F., Provenzano, M., Fujimoto, E., Goeke, N., Olson, B., and Klenk, D. (1985). Measurement of protein using bicinchoninic acid. Anal Biochem *150*, 76-85.

Tulp, A., Verwoerd, D., and Pieters, J. (1993). Application of an improved density gradient electrophoresis apparatus to the separation of proteins, cells and subcellular organelles. Electrophoresis *12*, 1295-1301.

Walburger, A., Koul, A., Ferrari, G., Nguyen, L., Prescianotto-Baschong, C., Huygen, K., Klebl, B., Thompson, C., Bacher, G., and Pieters, J. (2004). Protein kinase G from pathogenic mycobacteria promotes survival within macrophages. Science *304*, 1800-1804.

- CHAPTER 3 -

Structural Basis for the Specific Inhibition of Protein Kinase G, a Virulence Factor of *Mycobacterium tuberculosis*

Based on

PNAS (2007), Vol. 104

Nicole Scherr*, Srinivas Honnappa*, Gabriele Kunz, Philipp Müller, Rajesh Jayachandran, Fritz Winkler, Jean Pieters and Michel Steinmetz

3.1 Introduction

Mycobacterium tuberculosis continues to be one of the world's deadliest pathogens, causing a prospected burden of one billion newly infected individuals and 36 million casualties within the next 20 years (http://www.tballiance.org/). Despite the existence of effective chemotherapies, no new drugs have come to the market for more than 40 years. In addition, the rise in drug resistance among *M. tuberculosis* strains is becoming a severe threat to public health, illustrated by the recent emergence of extensively (or extremely) drug resistant tuberculosis (XDR-TB) that has caused a mortality of >98% (Anonymous, 2006; Masjedi et al., 2006).

Virulence of pathogenic mycobacteria is related to their capacity to survive for prolonged times within macrophage phagosomes (Nguyen and Pieters, 2005; Russell, 2001). Whereas normally internalized and phagocytosed bacteria are rapidly degraded within phago-lysosomes, pathogenic mycobacteria have evolved to block lysosomal delivery (Russell, 2001). One strategy by which pathogenic mycobacteria prevent lysosomal maturation is through the activity of mycobacterial protein kinase G (PknG), a eukaryotic-like serine/threonine protein kinase that is not required for mycobacterial growth *per se* but essential for survival within host macrophages (Nguyen et al., 2005; Walburger et al., 2004). PknG is one of the 11 serine/threonine protein kinases found in *M. tuberculosis*, and the only soluble kinase maintained in the genome of *Mycobacterium leprae*, that is believed to have retained the minimal set of genes needed for virulence (Cole et al., 2001). The presence of domains typically found in proteins from eukaryotic species as well as the finding that PknG is dispensable for *in vitro* growth (Av-Gay and Everett, 2000; Nguyen et al., 2005) of *M. tuberculosis* suggests that PknG has arrived in the *M. tuberculosis* genome through horizontal gene transfer and has been maintained as a virulence factor important for its survival inside the eukaryotic host (Leonard et al., 1998).

Importantly, mycobacteria overexpressing a kinase-dead mutant of PknG are rapidly transferred to lysosomes and killed, demonstrating that PknG kinase activity is crucial for mycobacterial survival. The fact that PknG is translocated into the host cytosol suggests that compounds aimed at blocking PknG activity do not require translocation across the only limited permeable mycobacterial cell wall (Walburger et al., 2004). Together, these findings make PknG an attractive and promising drug candidate. Indeed, blocking PknG kinase

activity by a specific small molecular weight inhibitor, the tetrahydrobenzothiophene AX20017, results in a rapid transfer of mycobacteria to lysosomes and killing of the intracellularly residing bacilli (Nguyen and Pieters, 2005; Walburger et al., 2004).

Despite the relatively simple structure of AX20017, it inhibits PknG with high specificity. To explore the mechanism for this specificity we intended to solve the structure of the PknG-AX20017 complex by x-ray crystallography.

3.2 Results

3.2.1 Specificity of the PknG inhibitor AX20017

The inhibitory activity of AX20017 against the 11 known mycobacterial kinases revealed that the compound is highly selective for PknG (Walburger et al., 2004). To test the activity of the drug towards eukaryotic kinases, 24 different archetypical human kinases originating from six major protein kinase groups (Manning et al., 2002) were selected for a performing a radiometric ATP consumption assay (ProQinase/Freiburg). Twelve different AX20017 concentrations in the range from $5x10^{-5}$ and $1.5x10^{-10}$ M were tested and the IC_{50} values were determined. The results (figure 3.1) demonstrate that AX20017 did not affect the human kinases while the activity of PknG was effectively inhibited.

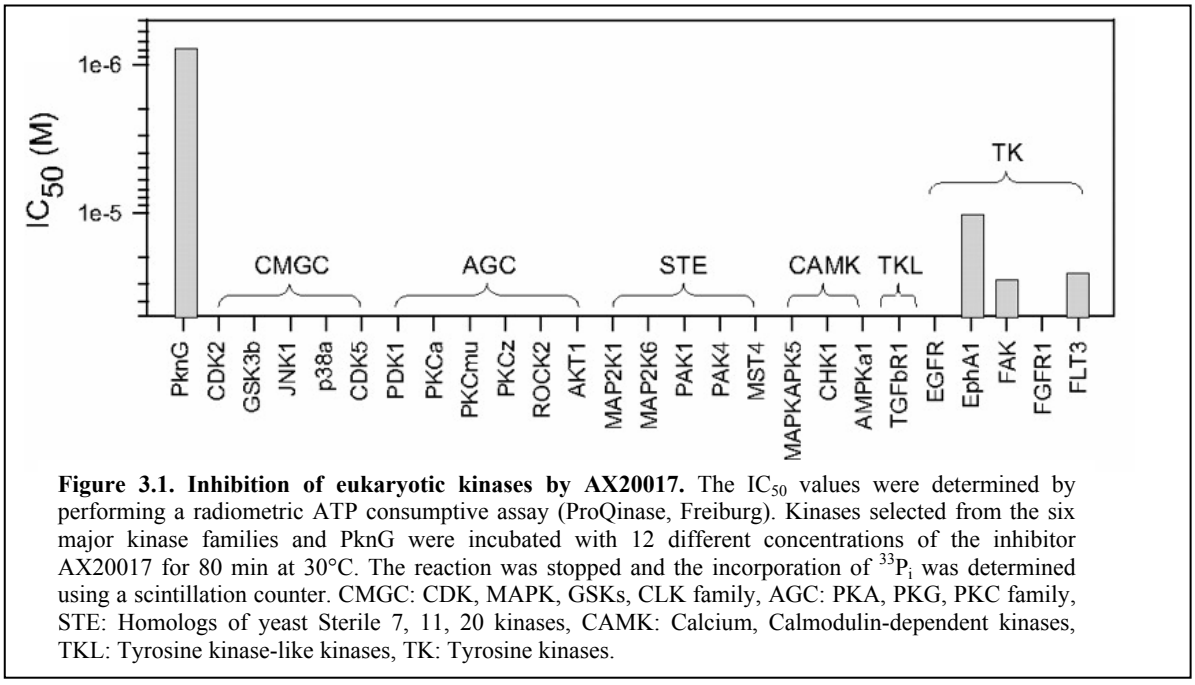

Figure 3.1. Inhibition of eukaryotic kinases by AX20017. The IC_{50} values were determined by performing a radiometric ATP consumptive assay (ProQinase, Freiburg). Kinases selected from the six major kinase families and PknG were incubated with 12 different concentrations of the inhibitor AX20017 for 80 min at 30°C. The reaction was stopped and the incorporation of $^{33}P_i$ was determined using a scintillation counter. CMGC: CDK, MAPK, GSKs, CLK family, AGC: PKA, PKG, PKC family, STE: Homologs of yeast Sterile 7, 11, 20 kinases, CAMK: Calcium, Calmodulin-dependent kinases, TKL: Tyrosine kinase-like kinases, TK: Tyrosine kinases.

To analyze whether AX20017 interferes with kinase-dependent processes within the macrophage host cell, macrophages were left untreated or incubated with AX20017 and analyzed for their capacity to proliferate, synthesize proteins, and phagocytose; activities that are known to depend on host kinase activity (Hamilton, 1997; Vieira et al., 2002; Xaus, 2001). In all experiments similar levels were obtained for the non-treated and treated sample implying that none of these cellular processes was affected by AX20017 (figure 3.2).

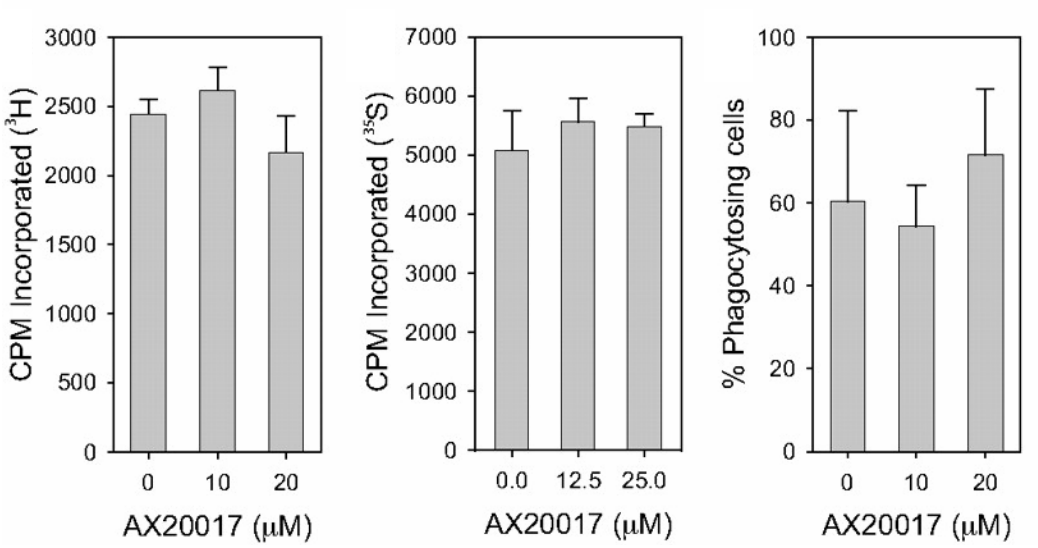

Figure 3.2. Effect of AX20017 on cellular processes in macrophages. Left panel: Proliferation of macrophages in the presence and absence of AX20017, data obtained by R. Jayachandran. Middle panel: Protein translation in macrophages left untreated or treated with AX20017. Right panel: Phagocytosis of latex beads (3 µm, 3 h) in the absence and presence of AX20017. Displayed is the percentage of phagocytosing cells (n=30-50) +/- SD, data obtained by G. Kunz.

In addition, video microscopy revealed that the presence of AX20017 did not affect cellular morphology, membrane ruffling, or macropinocytosis of J774 macrophages (figure 3.3). These results demonstrate that AX20017 is a highly specific inhibitor of PknG. Furthermore, adverse effects regarding essential kinase-dependent processes can be exluded.

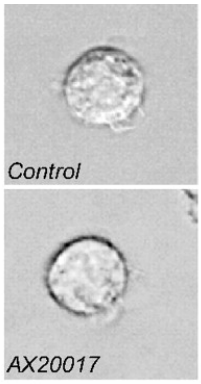

Figure 3.3. Analysis of macrophage morphology upon treatment with AX20017. J774 cells were incubated with 20 µM AX20017 and morphology, membrane ruffling and macropinocytosis were analyzed by video microscopy. Data obtained by R. Jayachandran.

3.2.2 Purification of PknG

The first prerequisite for solving the three-dimensional structure of a protein by x-ray crystallography is a well-ordered crystal that will diffract x-rays strongly. The formation of crystals is critically dependent on a number of different parameters, including pH, temperature, protein concentration, the nature of the solvent and precipitant as well as the presence of added ions or ligands to the protein. A pure and homogeneous (> 97%) protein sample is crucial for successful crystallization. For PknG, a purification protocol was established that yielded large amounts of protein of high purity (see chapter 2).

The purity and homogeneity of purified PknG was analyzed by SDS-PAGE and analytical size-exclusion chromatography (figure 3.4). Besides, kinase activity was usually verified by performing a kinase assay.

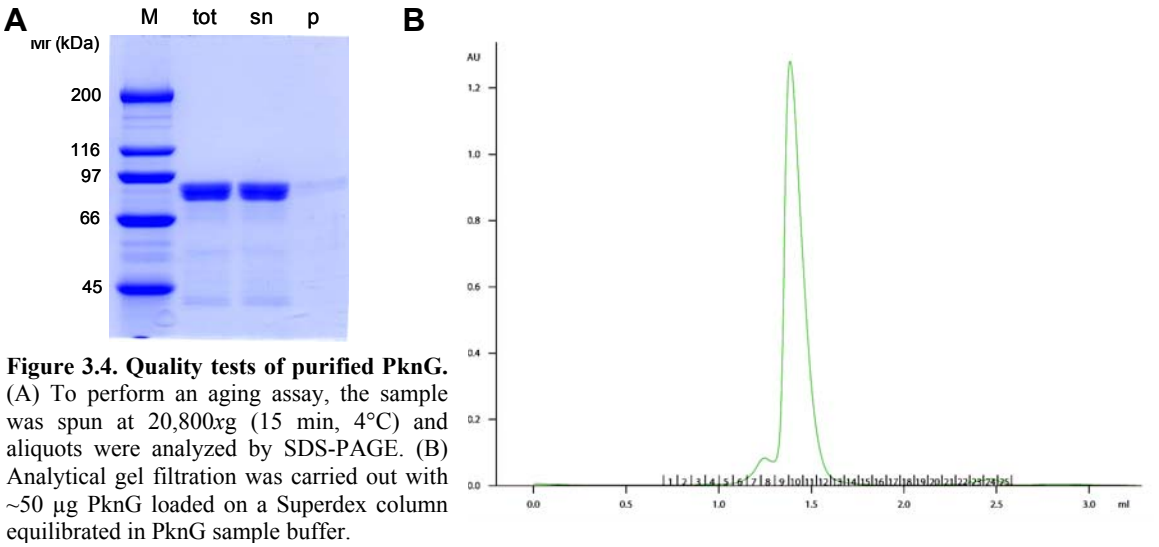

Figure 3.4. Quality tests of purified PknG. (A) To perform an aging assay, the sample was spun at 20,800*x*g (15 min, 4°C) and aliquots were analyzed by SDS-PAGE. (B) Analytical gel filtration was carried out with ~50 µg PknG loaded on a Superdex column equilibrated in PknG sample buffer.

To make sure that the PknG sample buffer (composed of 20 mM Tris pH 7.5, 500 mM NaCl) used so far is ideal to allow growth of well-shaped crystals, an optimal solubility screen (OSS) was performed. This extensive screen is based on an initial incubation step of the sample in several buffers, followed by centrifugation and determination of the protein concentration in the supernatant which then is subjected to dynamic light scattering (DLS) analysis. The scattered light is used to measure the rate of diffusion of protein particles. The data are processed to derive a size distribution for the sample, where the size is given by the hydrodynamic radius of the protein particle which depends on mass and shape. All buffers resulting in a monomodal and monodisperse profile of PknG could in principal be selected for crystallization setups. The evaluation of the screen showed that the buffer (20 mM Tris pH 7.5, 500 mM NaCl) chosen for PknG was optimal (figure 3.5), addition of glycerol or decreasing the NaCl concentration did not further improve the quality of the sample. In several cases, PknG homogeneity was obtained when 10% glycerol was included as a buffer component (figure 3.5). In conclusion, the sample buffer used so far provides good start conditions for the continued crystallization experiments.

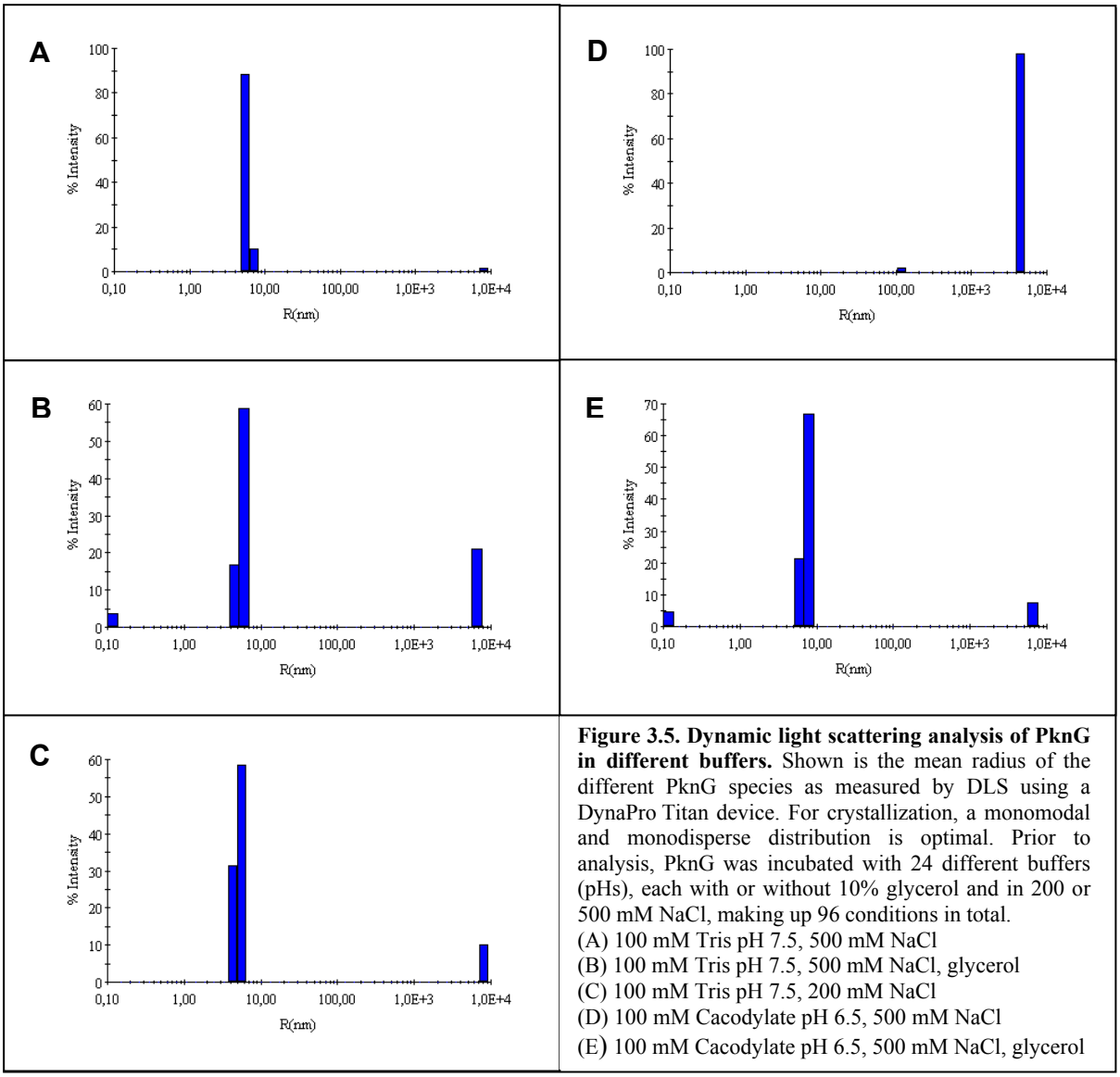

Figure 3.5. Dynamic light scattering analysis of PknG in different buffers. Shown is the mean radius of the different PknG species as measured by DLS using a DynaPro Titan device. For crystallization, a monomodal and monodisperse distribution is optimal. Prior to analysis, PknG was incubated with 24 different buffers (pHs), each with or without 10% glycerol and in 200 or 500 mM NaCl, making up 96 conditions in total.
(A) 100 mM Tris pH 7.5, 500 mM NaCl
(B) 100 mM Tris pH 7.5, 500 mM NaCl, glycerol
(C) 100 mM Tris pH 7.5, 200 mM NaCl
(D) 100 mM Cacodylate pH 6.5, 500 mM NaCl
(E) 100 mM Cacodylate pH 6.5, 500 mM NaCl, glycerol

The crystallization assays were set up manually or by robot according to the sitting drop method. Various buffers were screened until needle-like crystals were obtained; by refining and optimizing the buffer conditions 2D-crystals diffracting to 6 Å were produced, but the quality could not be further improved (figure 3.6).

Figure 3.6. PknG full length crystallization progress.

(A) 1D-crystal, 3 days
(B) 2D-crystal, 10 Å, 5 days
(C) 2D-crystal, 6.5 Å, 1-2 weeks

3.2.3 Defining PknGΔN

Full length PknG expressed in bacteria was found to degrade when stored at 4°C. Since unstable proteins in general are not likely to yield well-diffracting crystals, a limited proteolysis approach was undertaken in order to obtain more stable PknG protein. The rationale of this approach relies on the fact that cleavage of peptide bonds may preferably occur at sites which are either flexible or exposed. Proteolysis of PknG was induced by protease treatments or by natural degradation. To check whether proteolysis occurred at the N-terminus or at the C-terminus, degraded or trypsin digested PknG was analyzed by Western blotting. The results indicate that PknG is cleaved at the N-terminus (figure 3.7).

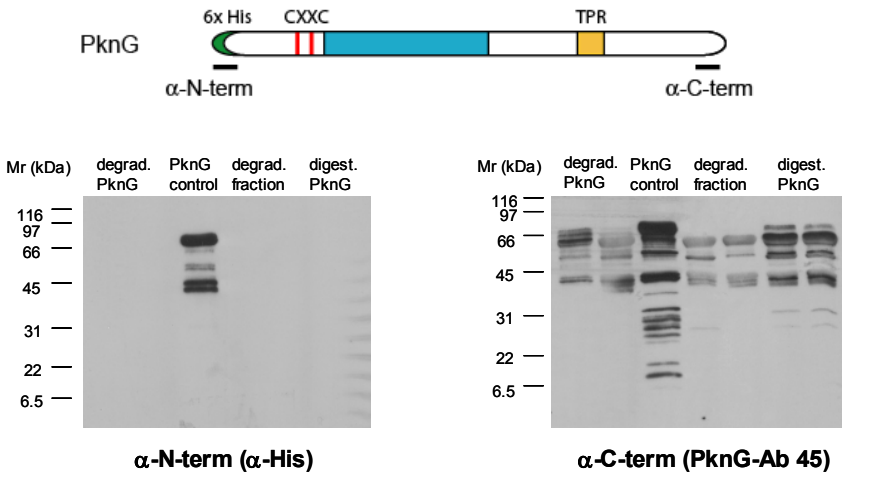

Figure 3.7. Proteolysis of PknG. Degraded and digested PknG samples were loaded on a 10% SDS-PAGE and analyzed by Western blotting using antibodies directed either against the N-terminus (left panel) or the C-terminus (right panel) of PknG.

To analyze degradation of PknG, the sample was kept for several days at 4°C and aliquots were analyzed by SDS-PAGE and blotted to a PVDF membrane (figure 3.8). One prominent stable band of ~70 kDa was excised and analyzed by Edman sequencing. Based on the results, a truncated version of *pknG*, termed *pknG-ΔN*, was cloned into pET-15b.

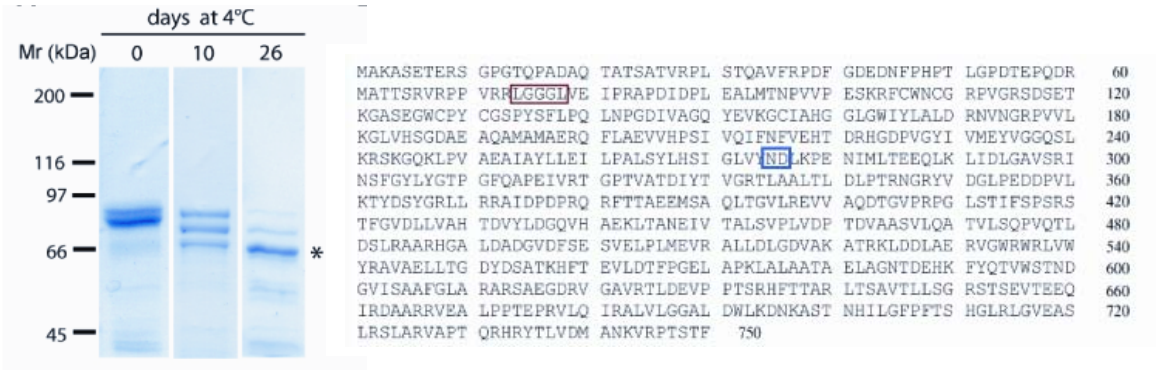

Figure 3.8. Limited proteolysis of PknG. Left panel: Full-length PknG was stored for 4 weeks at 4°C. At different time points (days 0, 10, and 26) aliquots were taken and analyzed for proteolysis on a Coomassie-stained 7.5% SDS-PAGE. Right panel: Amino acid sequence of PknG. The N-terminus of the stable form of the PknG fragment (asterisk in *A*) that was identified by Edman degradation is indicated by a red box. The dipeptide sequence of the catalytic loop, which discriminates between RD- and non-RD kinases is indicated by a blue box.

PknG-ΔN (figure 3.9) was expressed and purified from *E. coli* using the protocol established for PknG wildtype (see chapter 2, material and methods). SDS-PAGE analysis, analytical gel filtration as well as kinase assays (figure 3.10) were performed to analyze the quality of the protein. In contrast to the full length protein, the PknG-ΔN deletion mutant was highly soluble and stable.

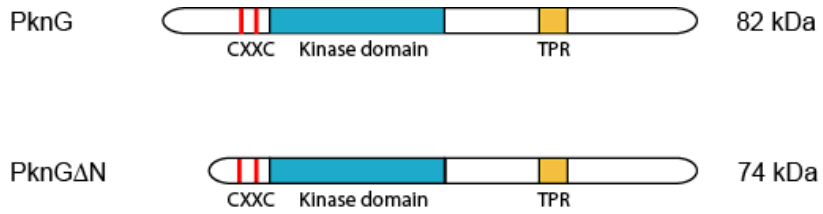

Figure 3.9. Schematic view of PknG full length and PknGΔN. The truncated version of PknG is missing the first 73 amino acids at the N-terminus.

However, PknG-ΔN was not able to autophosphorylate, since the N-terminally located phosphorylations sites were missing. To monitor kinase activity, the kinase-dead version of PknG-K181M was included in the reaction mix (figure 3.10). Using the same experimental setup it was tested whether the inhibitor AX20017 inhibits the activity of PknG-ΔN. As observed for wildtype PknG, the kinase activity was efficiently inhibited (figure 3.10). This finding is relevant for the crystallization studies since the inhibitor is likely to stabilize the kinase which might be crucial for the formation of well-diffracting crystals.

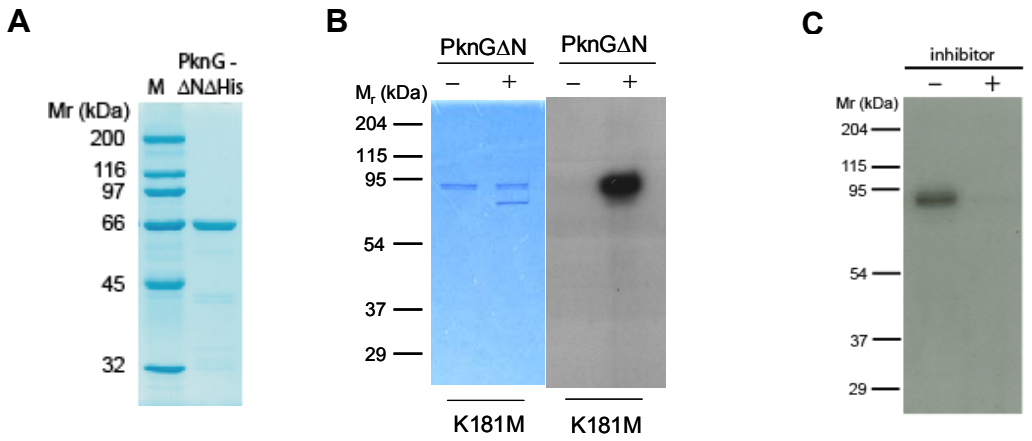

Figure 3.10. Purified PknGΔN, activity and inhibition of PknGΔN. (A) Purified PknGΔN (2.5 µg) analyzed by SDS-PAGE followed by staining with Coomassie. (B) For the *in vitro* kinase assay, 0.5 µg PknGΔN was incubated in reaction buffer containing the PknG-K181M kinase-dead mutant as substrate. Reaction mixtures were analyzed after separation by 10% SDS-PAGE followed by autoradiography. (C) To inhibit PknGΔN, 0.5 µg kinase was incubated in reaction buffer containing PknG-K181M as substrate and 63 µM AX20017 for 30 min at 37°C before the mixture was analyzed by 10% SDS-PAGE and autoradiography.

PknGΔN (10 µg/µl, in 20 mM Tris pH 7.5) treated with thrombin to remove the His-tag was tested for crystallization by first setting up basic crystallization screens before refining the conditions (figure 3.11).

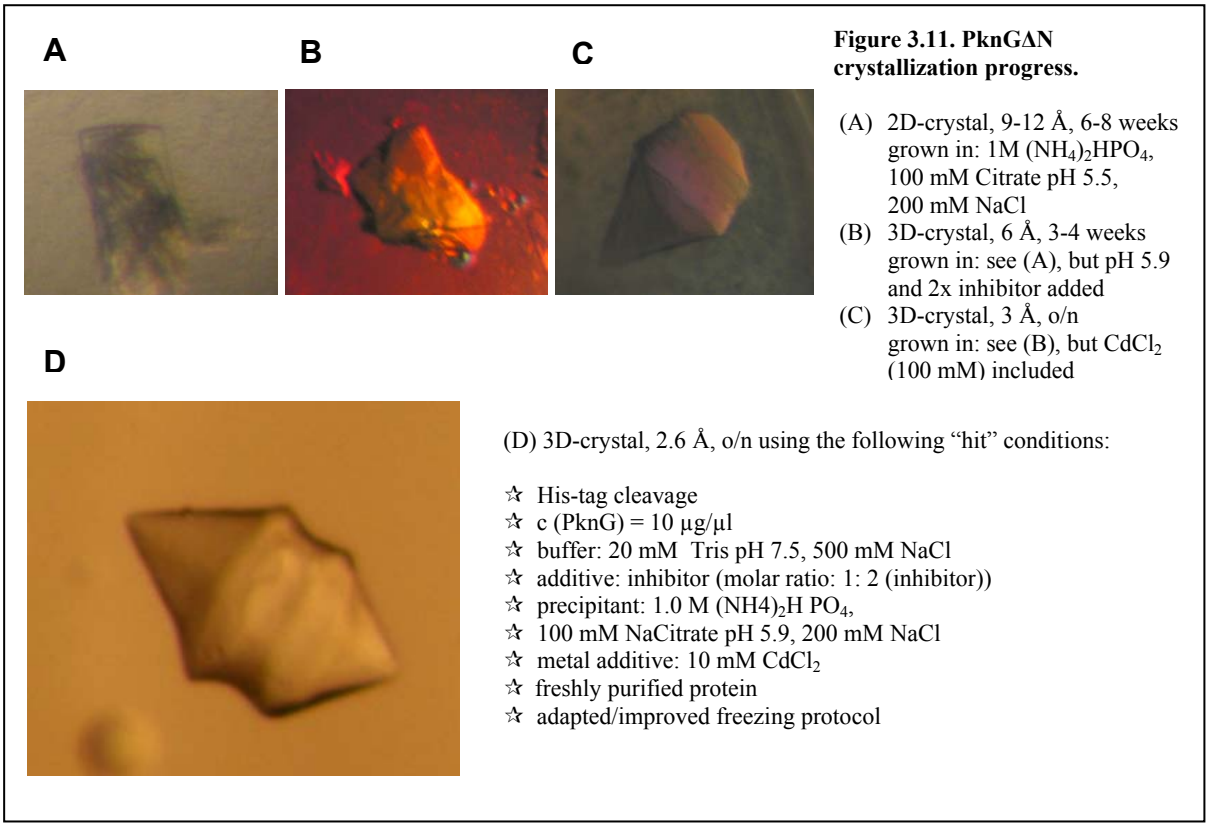

Figure 3.11. PknGΔN crystallization progress.

(A) 2D-crystal, 9-12 Å, 6-8 weeks grown in: 1M $(NH_4)_2HPO_4$, 100 mM Citrate pH 5.5, 200 mM NaCl
(B) 3D-crystal, 6 Å, 3-4 weeks grown in: see (A), but pH 5.9 and 2x inhibitor added
(C) 3D-crystal, 3 Å, o/n grown in: see (B), but $CdCl_2$ (100 mM) included

Crystals diffracting to 2.4-2.6 Å were found and used for further x-ray crystallography analysis.

3.2.4 The Structure of PknG

To define the structural basis of the high specificity of AX20017 for PknG, the crystal structure of the PknG-AX20017 was determined by x-ray crystallography.

PknG in complex with AX20017 (figure 3.12) yielded well diffracting crystals which were used to solve the structure at 2.4 Å resolution by single isomorphous replacement anomalous scattering (SIRAS). The asymmetric unit of the crystal contains two copies of the complex which are related by a non-crystallographic two-fold (RMSD for 571 backbone atoms equals 0.8 Å). PknG consists of three distinct structural domains whose combination to our best knowledge is not found in any other protein kinase.

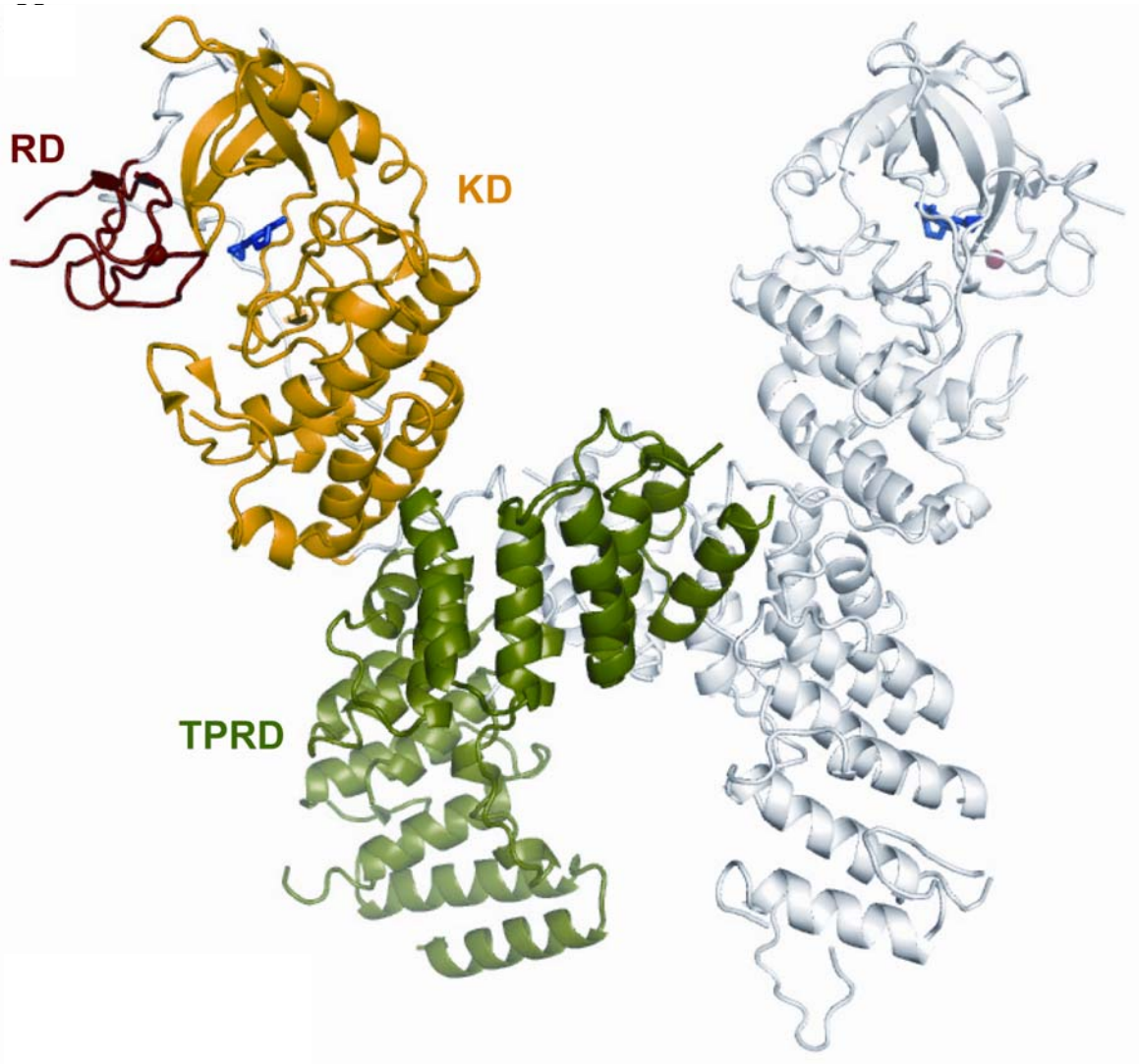

Figure 3.12. X-ray crystal structure of the PknG-AX20017 complex. Overall fold of the dimeric PknG-AX20017 complex (ribbon representation) as seen in the asymmetric unit of the crystal. The three PknG domains of the left subunit are labeled and depicted in different colors (RD, rubredoxin domain with the bound metal, cadmium in the present structure, depicted as sphere; KD, kinase domain; TPRD, tetratricopeptide repeat-containing domain).

3.2.5 The Tetratricopeptide repeat containing domain

The C-terminal half of PknG contains a tetratricopeptide repeat (TPR) and assumes a characteristic extended and curved superhelical fold (D'Andrea, 2003) (figure 3.12). This domain interacts with the tip of the C-terminal lobe of the PknG kinase domain. It forms an extensive intermolecular lateral contact with the TPR domain of the twofold related molecule within the asymmetric unit of the crystal (figure 3.12), consistent with the known function of

TPR domains to mediate protein-protein interactions (D'Andrea, 2003); however, the role of the dimer interface for PknG function is currently not known.

Static light scattering (SLS) analysis was performed in order to analyze whether PknG forms dimers also in solution. It was found that PknG in solution exists in a dimeric form (figure 3.13); two protein peaks were detected which corresponded to a molecular weight of 155 kDa and 78.4 kDa, respectively (figure 3.13). To analyze whether dimeric PknG is catalytically active, a preparative size exclusion chromatography (SMART® system) step was performed. Purified PknG was loaded onto a gel filtration column and fractions were collected. The protein concentration was determined and equal amounts of monomeric and dimeric PknG were used for a kinase assay (figure 3.14). The results showed that PknG in its dimeric form is active.

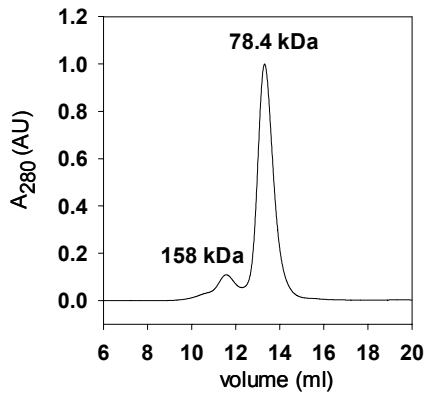

Figure 3.13. Light scattering analysis of full length PknG. 250 µg PknG were loaded on a Superdex 200 column equilibrated in 20 mM Tris pH 7.5, 500 mM NaCl. The molecular weight of PknG was determined using a miniDAWN device (Wyatt).

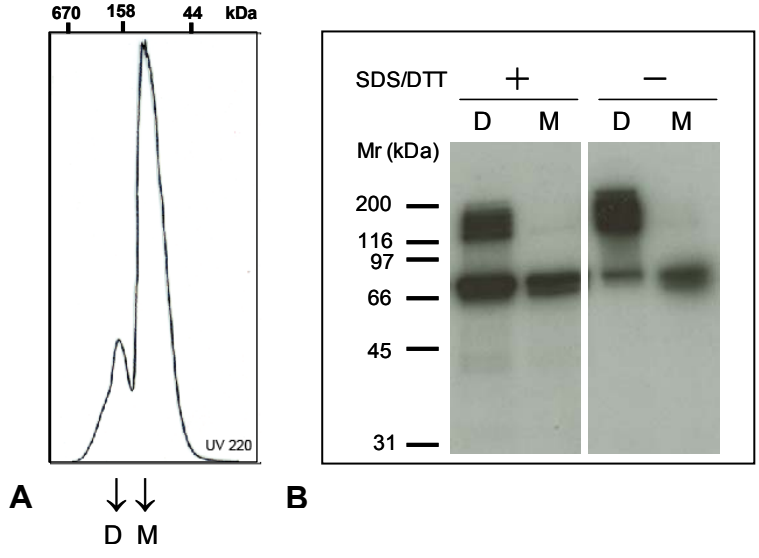

Figure 3.14. Activity of PknG monomers and dimers. (A) Separation of PknG monomers and dimers. 500 µg PknG (in 20 mM Tris pH 7.5, 500 mM NaCl) were loaded on a Superdex 200 gel filtration column. The fractions were collected and the protein concentrations determined. (B) Kinase assay. Equal amounts of PknG were included for the kinase assay. Samples were left untreated or boiled in SDS/DTT, loaded on a SDS-PAGE and then analyzed by autoradiography.
D: Dimer, M: Monomer

3.2.6 The Kinase domain

The kinase domain of PknG is sandwiched between the rubredoxin and the TPR domains (figure 3.12).

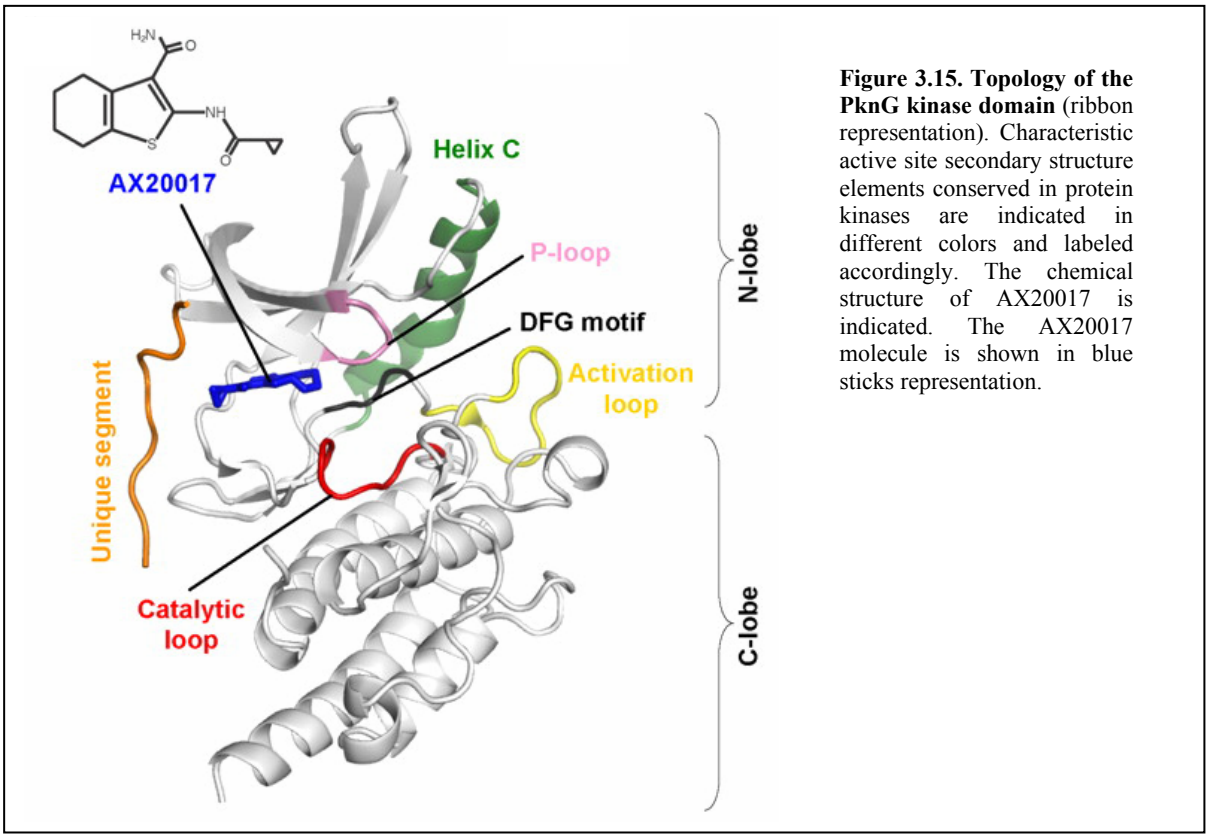

Figure 3.15. Topology of the PknG kinase domain (ribbon representation). Characteristic active site secondary structure elements conserved in protein kinases are indicated in different colors and labeled accordingly. The chemical structure of AX20017 is indicated. The AX20017 molecule is shown in blue sticks representation.

The kinase domain displays the typical two-lobed structure, with a topology reminiscent of serine/threonine kinases (figure 3.15). Importantly, several active site signature sequence elements adopt conformations that are characteristic of an activated state of protein kinases (Huse and Kuriyan, 2002; Johnson et al., 1996; Nolen et al., 2004). First, the activation loop which controls catalytic activity in most kinases by switching between different states is fully ordered and stabilized in an open and extended conformation (figure 3.15). The β9-strand preceding the activation loop forms a short antiparallel β-sheet with the β6-strand preceding the catalytic loop, which provides a site for substrate binding in active states of kinases. Although phosphorylation is the most common mechanism for positioning the activation loop (see, for example, PknB (Ortiz-Lombardia et al., 2003; Young et al., 2003)); it is not phosphorylated in the PknG-AX20017 structure. The absence of an arginine (R) immediately preceding the invariant catalytic aspartate (D) of the catalytic loop (figure 3.8) classifies PknG as a unique mycobacterial non-RD kinase (Johnson et al., 1996; Nolen et al., 2004), explaining the open and extended conformation of the activation loop in the absence of

phosphorylation. Second, the side chains of the functionally important and conserved residues such as Asp276 and Asn281 of the catalytic loop and Asp293 of the highly conserved Asp-Phe-Gly motif (denoted DFG) are positioned and adopt conformations similar to their counterparts, Asp166, Asn171, and Asp184 in the active structural state of protein kinase A (Knighton et al., 1991) (figure 3.16). Likewise, Lys181 of PknG is positioned as Lys72 in the active PKA conformation. However, the ionic interaction observed in PKA between Lys72 and Glu91 (Glu198 in PknG) which is located on the αC helix is not present in PknG due to a tilted and rotated orientation of this α-helix (Figure 3.16). The orientation of the αC helix in the present PknG-AX20017 crystal structure appears to be required to avoid a steric clash with the C-terminal part of the activation loop.

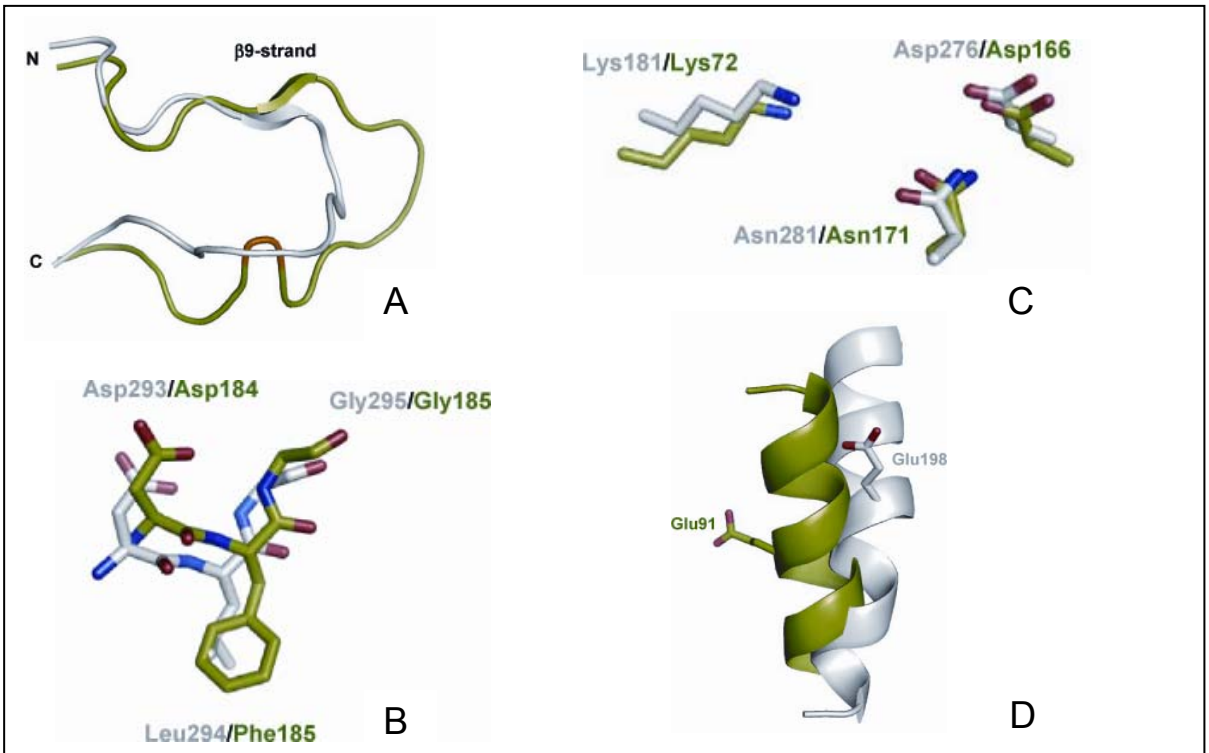

Figure 3.16. AX20017 stabilizes the PknG kinase domain in an active-like conformation. (A-D) Superposition of the AX20017-bound PknG kinase domain and an active structure of protein kinase A (PDB ID 1ATP). The two proteins were first aligned globally over all Cα atoms. Fine tuning was achieved by minimizing the rmsd of Cα atoms from the interlobe kinase cleft. The following conformations of active-site residue side chains (in stick representation and with labels) and elements (in cartoon representation) are shown: segment encompassing the activation loop; the substrate-binding β9-strand is indicated (A); residue side chain conformations of the DFG motif (B); highly conserved residue side chains contacting the substrate and the nucleotide (C); αC helix with the catalytically important glutamate (D). Oxygen and nitrogen atoms of residue side chains are colored in red and blue, respectively. Carbon atoms are colored in grey and green for PknG and PKA, respectively.

3.2.7 The Rubredoxin motif

The N-terminal part contains two iron-binding Cys-X-X-Cys-Gly (X representing any amino acid residue) motifs characteristic of rubredoxin. This small globular domain interacts with both the N- and C-terminal lobes of the PknG kinase domain, packing on top of the active site without blocking its access (figure 3.12). Rubredoxins are used as electron donors in electron-transfer reactions predominantly in certain microorganisms and hence could act as regulatory modules (Sieker et al., 1994).

To test whether the rubredoxin domain could modulate the activity of PknG, the four critical metal coordinating cysteines, Cys106, Cys109, Cys128, and Cys131, were mutated to serines by site-directed mutagenesis. The protein was expressed and purified from *E. coli* in order to check the activity in a kinase assay. Remarkably, the resulting mutant PknG, denoted PknG-C/S, was devoid of activity; no signal was detectable for either autophosphorylated PknG-C/S or for the substrate (figure 3.17). To exclude that this is due to a possible misfolding of the protein, circular dichroism spectroscopy was performed. The mean residue ellipticity was determined, normalized for the buffer and plotted against the wavelength. The overall profile of the PknG-C/S mutant was similar to the one of the wildtype (figure 3.18) suggesting that the modified protein is properly folded.

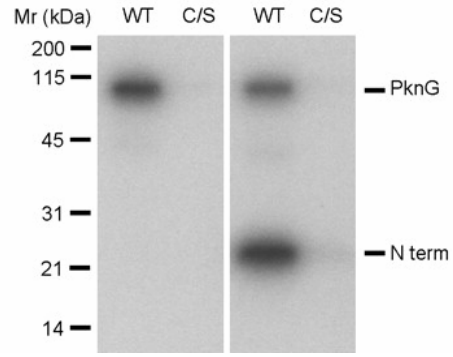

Figure 3.17. *In vitro* kinase assay of PknG (WT) and PknG-C/S (Cys106, Cys109, Cys128, and Cys131 mutated to serines). Reaction mixtures were analyzed after 12.5% SDS-PAGE separation by autoradiography. The N-terminal fragment of PknG was included as a substrate. PknG-C/S construct by P. Müller.

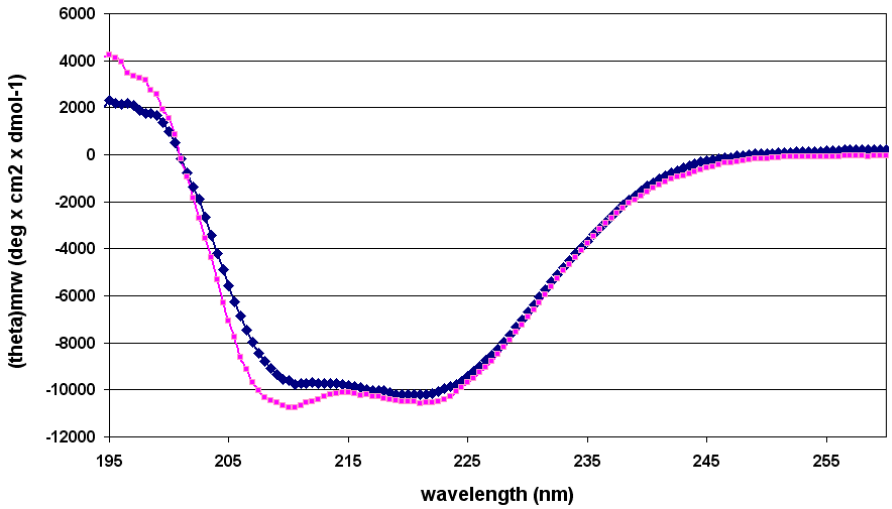

Figure 3.18. Structural integrity of the C/S mutant. Wildtype PknG and PknG-C/S mutant were diluted with buffer (20 mM Tris pH 7.5, 500 mM NaCl) to a concentration of 0.06-0.08 µg/µl and 8 scans in the range of 190-260 nm were recorded using a Jasco spectropolarimeter (J720).
Pink: PknG wildtype
Lilac: PknG-C/S

In addition, analytical gel filtration was performed to test the quality of the purified PknG-C/S mutant. In the chromatogram, PknG-C/S protein appeared as a sharp peak eluted in the same fraction as observed for the wildtype, further confirming that the sample used for the kinase assay was neither degraded nor precipitated (data not shown).

The finding, that the activity of PknG is dependent on the rubredoxin motif is a first indication that PknG might be regulated by the redox status of the environment via the rubredoxin domain.

3.2.8 Structure of the AX20017-binding pocket

The AX20017 inhibitor (figure 3.19) is bound deep within a narrow pocket formed by the interlobe cleft of the kinase domain and a unique peptide segment originating from the N-terminus of PknG (residues Pro85-Met94). Accessible surface area calculations revealed that 90% of the molecular surface of AX20017 is buried within the kinase domain.

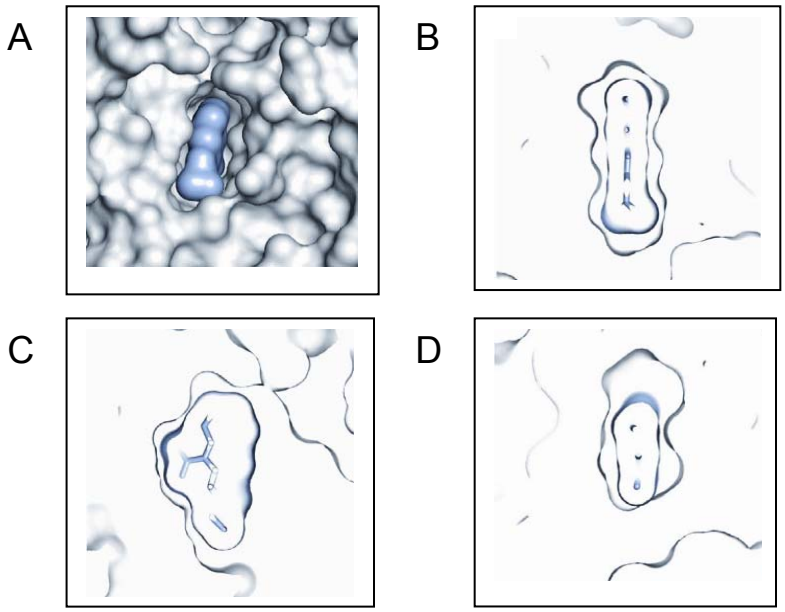

Figure 3.19.
Surface complementarity between the PknG kinase domain and AX20017.
(*A*) View of AX20017 (light blue) buried into the PknG kinase domain-binding pocket. Both molecules are shown as surface representation.
(B, C and D). Three views of a section of the AX20017-PknG interaction (A) 90° apart.

A set of 15 residues originating from both the kinase lobes and the unique N-terminal segment of PknG make extensive polar and non-polar contacts with the inhibitor (figure 3.20).

The almost planar tetrahydrobenzothiophene moiety of the inhibitor occupies the conserved hydrophobic pocket that otherwise binds the adenine base of ATP (Knighton et al., 1991).

The main chain Glu233:O and Val235:NH of PknG form hydrogen bonds to the primary amido substituent of the thiophene ring of the inhibitor reminiscent of the ones made to the adenosine moiety of ATP. An additional hydrogen bond is formed between Val235:O and the secondary amido group substituent of the thiophene ring. This hydrogen bonding network places the tetrahydrobenzothiophene moiety of the inhibitor such that van der Waals contacts are made with the side chains of Ala158, Ile165, Val179, Lys181, Met232, Ile292, and Asp293 of PknG. Apart from the conserved ATP site, the cyclopropyl ring of AX20017 exploits an additional hydrophobic pocket of PknG which is less homologous among protein kinases. This moiety of the inhibitor packs against the side chains of Ile87, Ala92 of the unique N-terminal segment of PknG, and of Ile157, Tyr234, Gly236, and Met283 of the kinase domain (figures 3.20, 3.21).

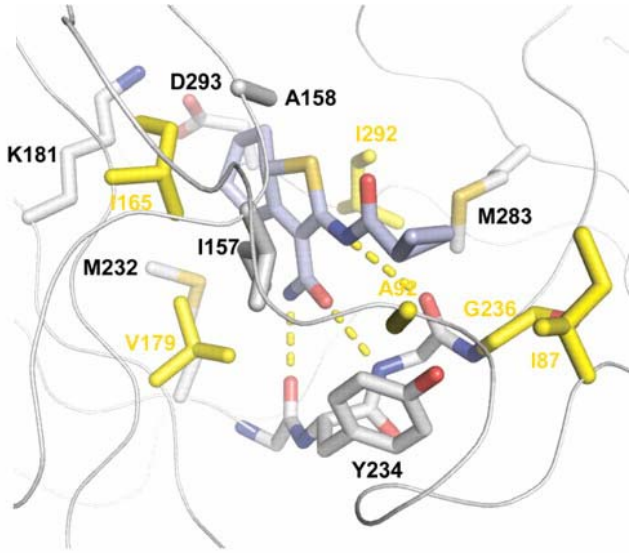

Figure 3.20. Interactions between PknG and inhibitor (sticks representation). PknG (grey carbon atoms)-AX20017 (light blue carbon atoms) binding site. Residue side chains which in combination are unique to PknG are highlighted by yellow carbon atoms. Hydrogen bonds are indicated as dashes. Oxygen, nitrogen, and sulfur atoms are colored in red, blue, and dark yellow, respectively.

Together, these findings show that AX20017 targets both the residues shaping the conserved ATP site as well PknG-specific structural elements adjacent to the ATP site. The remarkable surface complementarities between the PknG kinase domain and inhibitor interfaces (figure 3.19) demonstrate that AX20017 exploits the shape and chemical nature of the PknG binding pocket in a nearly optimal fashion. Sequence comparison of the 11 known *Mycobacterium tuberculosis* serine/threonine protein kinases (Cole et al., 1998) reveals that the identities of four inhibitor contacting residues from the conserved kinase domain are specific to PknG. Sequence analysis of 491 human protein kinases (Manning et al., 2002) unveils that the frequency of occurrence of these four individual inhibitor-contacting residues of the ATP site, Ile165, Val179, Gly236 and Ile292, is 0.037, 0.065, 0.088, and 0.077, respectively. In combination, these four residues are not observed in any human kinase. This finding is

illustrated in figure 3.21 which shows a sequence alignment of selected *Mycobacterium tuberculosis* and human kinase domains originating from six major protein kinase groups (Manning et al., 2002). Together with the two additional inhibitor contacting residues, Ile87 and Ala92, which are unique to PknG, this sequence-to-structure analysis provides a basis for explaining the high specificity of AX20017 for PknG. The precise combination of residues, together with the conformational plasticity of specific structural elements of the PknG kinase domain, appear to generate a uniquely shaped binding pocket for AX20017 not occurring in any other protein kinase.

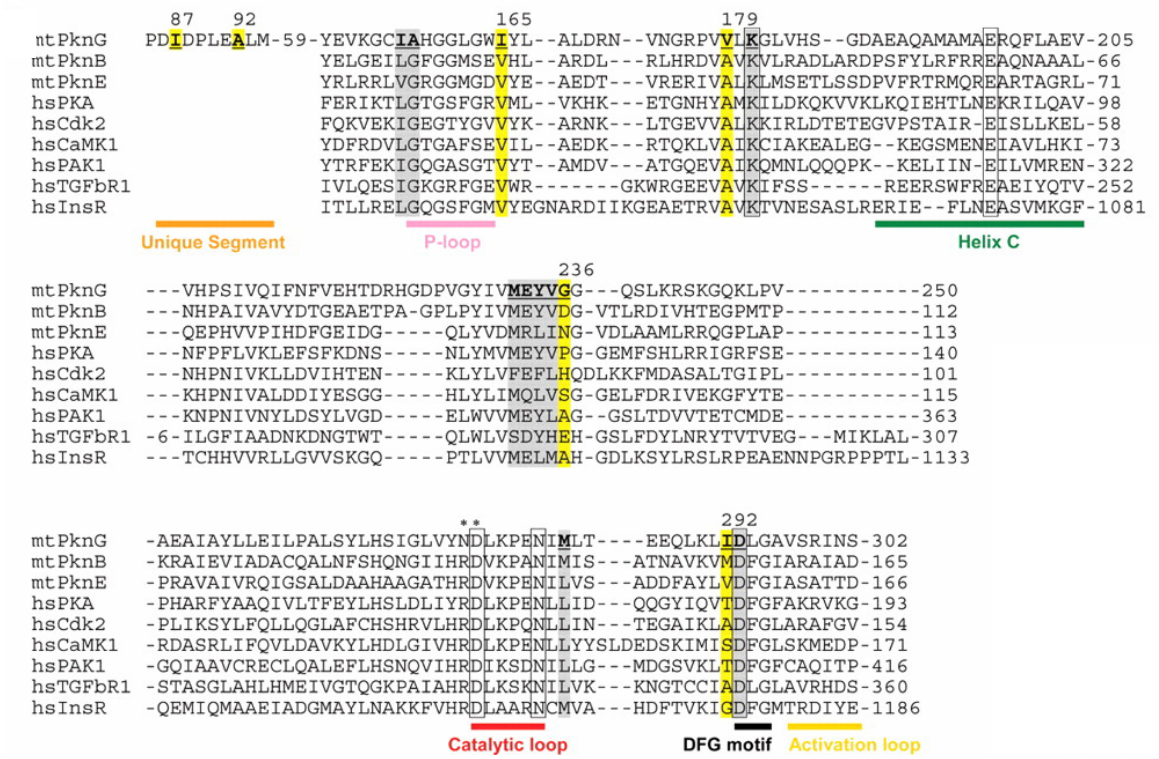

Figure 3.21. Structure-based sequence alignment of three selected *Mycobacterium tuberculosis* (Cole et al., 1998) and six human kinase domains originating from six major kinase groups (Manning et al., 2002). Selected secondary structure elements of kinase domains are indicated on the bottom of the alignment. The fifteen AX20017-interacting residues of PknG and their identity in homologues are indicated in grey (for variable residues) and yellow (for residues which in combination are unique to PknG; residue numbers shown on top correspond to the PknG sequence). Highly conserved catalytic site residues of protein kinases are indicated by boxes. Species identifiers are: mt, *Mycobacterium tuberculosis*; hs, *Homo sapiens*. UniProtKB/Swiss-Prot and Protein Data Bank accession numbers, respectively, are as follows: PknG (Protein kinase G), P65728, 2PZI; PknB (Protein kinase B), P0A5S4, 1O6Y; PknE (Protein kinase E), P72001, 2H34; PKA (cAMP-dependent protein kinase, AGC group), P17612, 1ATP; Cdk2 (Cell division protein kinase 2, CMGC group), P24941, 2BHE; CaMK1 (Calcium/calmodulin-dependent protein kinase type 1, CAMK group), Q14012, 1A06; PAK1 (Serine/threonine-protein kinase PAK 1, STE group), Q13153, 1F3M; TgFβR1 (TGF-β receptor type-1, TKL group), P36897, 1B6C; IRK (Insulin receptor, TK group), P06213, 1IRK.

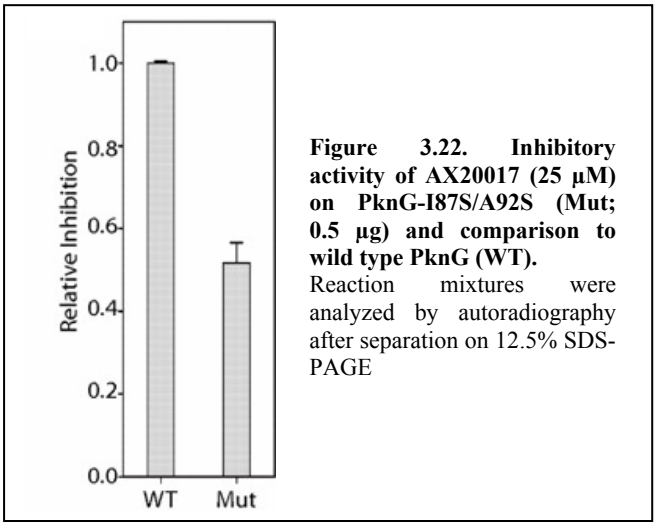

Figure 3.22. Inhibitory activity of AX20017 (25 µM) on PknG-I87S/A92S (Mut; 0.5 µg) and comparison to wild type PknG (WT). Reaction mixtures were analyzed by autoradiography after separation on 12.5% SDS-PAGE

To experimentally test the importance of the two unique PknG inhibitor contacting residues Ile87 and Ala92, both sites were mutated to serines (denoted PknG-I87S/A92S). The double mutation resulted in a >50% loss in the inhibitory capacity of AX20017, indicating that the unique N-terminal segment of PknG is important for AX20017 binding (figure 3.22).

In conclusion, we confirmed that PknG is a multidomain protein consisting of a rubredoxin-, kinase-, and tetratricopeptide repeat domain and found that the rubredoxin domain is essential for the activity of PknG. The structure revealed that the inhibitor binding pocket is shaped by a unique set of amino acid residues which in combination is not found in any human kinase. The structural information presented here explains the highly specific mode of action of AX20017 and provides a basis for the rational design of new PknG drugs aimed at blocking the proliferation of *Mycobacterium tuberculosis*.

3.3 Discussion

Understanding of the virulence factors of pathogenic mycobacteria at the atomic level is required for the development of novel and effective therapeutics for the treatment of diseases caused by these microbes (Goulding CW, 2002; Koul et al., 2004). The eukaryotic-like serine/threonine protein kinase PknG plays a crucial role in the survival mechanism of pathogenic mycobacteria, as genetic deletion or chemical inhibition of PknG is sufficient to kill intracellularly residing bacteria (Walburger et al., 2004).

Important functional information could be extracted from the molecular structure of PknG. The N-terminal rubredoxin-motif, forming a complex with cadmium in the model, interacts with the kinase domain but does not restrict the binding of inhibitor and possibly ATP. By site-directed mutagenesis, the four cysteins of the rubredoxin motif were replaced by alanine residues which resulted in a catalytically inactive mutant suggesting that the rubredoxin motif controls the catalytic activity by limiting the interactions within the kinase domain. Rubredoxin motifs represent the simplest type of an iron-sulfur centre, consisting of an iron atom coordinated by the thiol groups of four cysteines. These motifs are known to confer stability to the protein (Henriques et al., 2006) and introducing mutations in this particular region might lead to severe conformational changes and instability. However, this was not true for PknG-C/S protein which did not display any detectable phenotype when analyzed by analytical gel filtration and C/D spectroscopy.
CXXC motif-containing proteins, regulated by oxidation and S-thiolation, have been shown to carry out protective and adaptive functions in the cell (Conway et al., 2008). The motif can have highly reductive or oxidative potential (Grauschopf et al., 1995; Moore et al., 1964). Mycobacteria encounter different oxygen conditions ranging from high oxygen levels outside their host to nearly oxygen depleted conditions as found in granulomas within the host. Therefore, it is likely that the N-terminus of PknG acts as a sensor which, upon certain redox stimuli, undergoes slight, but crucial conformational changes leading to interactions with the kinase domain which finally regulates the catalytic activity of the kinase.

The tetratricopeptide repeat (TPR), typically occurring in 3-16 copies per protein, is a degenerate 34-amino acid motif which mediates protein-protein interactions and the assembly of multiprotein complexes (Das, 1998; Sikorski et al., 1990). Proteins containing TPR repeats are localized in various subcellular compartments which include mitochondria,

cytoplasm and nucleus (Goebl M, 1991). TPR proteins are ubiquitously found in prokaryotes and eukaryotes. These proteins carry out functions in cell-cycle control, transcription repression, protein kinase inhibition, mitochondrial and peroxisomal protein transport, neurogenesis and stress response (D'Andrea, 2003; Lamb et al., 1995). A single TPR repeat contains two antiparallel α-helices with a turn-position in between (Das, 1998). The smallest functional unit was reported to be three tandem TPR motifs (Lamb et al., 1995). PknG, however, possesses only one classical tetratricopeptide repeat involved in dimerization of PknG. Whether this motif has an additional function possibly mediating one of these processes mentioned above, remains to be established.

Importantly, the crystal structure of PknG in complex with AX20017 provides insight into how high specificity for blocking a prominent kinase target can be achieved without compromising homologous kinases. Target selection and inhibitor selectivity is of utmost importance as chemical inhibition of a microbial kinase that is highly homologous to its eukaryotic counterparts poses potential risks since essential host signal transduction pathways may be affected as well (Noble et al., 2004).

The structural information presented here offers a basis for the rational design of new PknG drugs aimed at blocking the proliferation of *Mycobacterium tuberculosis*. One promising option to further improve the affinity, selectivity, and potency of AX20017 is to systematically explore modifications of the cyclopropyl ring as this part of the inhibitor does not appear to fully exploit its binding capacity to the unique N-terminal sequence of PknG. In this context, the finding that a small compound such as AX20017 targets an active conformation of PknG may have prospective rewards as the active conformation requires a high degree of structural conservation and the inhibitory mode of action is likely to be less tolerant for the development of resistant mutations (Noble et al., 2004).

One of the roadblocks in controlling tuberculosis relates to the ability of *Mycobacterium tuberculosis* to modulate the macrophage innate antimicrobial response, making its host permissive for mycobacterial survival and growth. Since blocking PknG reverts the macrophage into a degradative environment in which mycobacteria are efficiently cleared, the results described here open the possibility of developing a novel class of compounds that are desperately needed with respect to the global tuberculosis epidemic.

3.4 References

Anonymous (2006). Lancet 368, 964.

Av-Gay, Y., and Everett, M. (2000). The eukaryotic-like Ser/Thr protein kinases of Mycobacterium tuberculosis. Trends Microbiol *8*, 238 - 244.

Cole, S. T., Brosch, R., Parkhill, J., Garnier, T., Churcher, C., Harris, D., Gordon, S. V., Eiglmeier, K., Gas, S., Barry, C. E.*, et al.* (1998). Deciphering the biology of Mycobacterium tuberculosis from the complete genome sequence. Nature *393*, 537-544.

Cole, S. T., Eiglmeier, K., Parkhill, J., James, K. D., Thomson, N. R., Wheeler, P. R., Honore, N., Garnier, T., Churcher, C., Harris, D.*, et al.* (2001). Massive gene decay in the leprosy bacillus. Nature *409*, 1007-1011.

Conway, M. E., Coles, S. J., Islam, M. M., and Hutson, S. M. (2008). Regulatory control of human cytosolic branched-chain aminotransferase by oxidation and S-glutathionylation and its interactions with redox sensitive neuronal proteins. Biochemistry.

D'Andrea, L.D., Regan, L. (2003). TPR proteins: the versatile helix. Trends Biochem Sci *28*, 655-662.

Das, A., Cohen. P.W., Barford, D. (1998). The structure of the tetratricopeptide repeats of protein phosphatase 5: implications for TPR-mediated protein-protein interactions. EMBO J *17*, 1192-1199.

Goebl, M., Yanagida, M. (1991). The TPR snap helix: a novel protein repeat motif from mitosis to transcription. Trends Biochem Sci *16*, 173-177.

Goulding, C.W., Apostol, M., Anderson, D.H., Gill, H.S., Smith, C.V., Kuo, M.R., Yang, J.K., Waldo, G.S., Suh, S.W., Chauhan, R., Kale, A., Bachhawat, N., Mande, S.C., Johnston, J.M., Lott, J.S., Baker, E.N., Arcus, V.L., Leys, D., McLean, K.J., Munro, A.W., Berendzen, J., Sharma, V., Park, M.S., Eisenberg, D., Sacchettini, J., Alber, T., Rupp, B., Jacobs, W. Jr., Terwilliger, T.C. (2002). The TB structural genomics consortium: providing a structural foundation for drug discovery. Cur Drug Targets Infect Disod *2*, 121-141.

Grauschopf, U., Winther, J. R., Korber, P., Zander, T., Dallinger, P., and Bardwell, J. C. A. (1995). Why is DsbA such an oxidizing disulfide catalyst? Cell *83*, 947-955.

Henriques, B., Saraiva, L., and Gomes, C. (2006). Combined spectroscopic and calorimetric characterisation of rubredoxin reversible thermal transition. Journal of Biological Inorganic Chemistry *11*, 73-81.

Huse, M., and Kuriyan, J. (2002). The Conformational Plasticity of Protein Kinases. Cell *109*, 275-282.

John, A. H. (1997). CSF-1 and cell cycle control in macrophages. Molecular Reproduction and Development *46*, 19-23.

Johnson, L. N., Noble, M. E., and Owen, D. J. (1996). Active and inactive protein kinases: structural basis for regulation. Cell *85*, 149 - 158.

Knighton D.R., Zheng J., Ten Eyck L.F., Ashford V.A., Xuong N.H., Taylor S.S., Sowadski J.M. (1991). Crystal structure of the catalytic subunit of cyclic adenosine monophosphate-dependent protein kinase. Science *253*, 407-414.

Koul, A., Herget, T., Klebl, B., and Ullrich, A. (2004). Interplay between mycobacteria and host signalling pathways. Nat Rev Micro *2*, 189-202.

Lamb, J. R., Tugendreich, S., and Hieter, P. (1995). Tetratrico peptide repeat interactions: to TPR or not to TPR? Trends in Biochemical Sciences *20*, 257-259.

Leonard, C. J., Aravind, L., and Koonin, E. V. (1998). Novel families of putative protein kinases in bacteria and archaea: evolution of the "eukaryotic" protein kinase superfamily. Genome Res *8*, 1038 - 1047.

Manning, G., Whyte, D. B., Martinez, R., Hunter, T., and Sudarsanam, S. (2002). The protein kinase complement of the human genome. Science *298*, 1912 - 1934.

Masjedi, M., Farnia, P., Sorooch, S., Pooramiri, M., Mansoori, S., Zarifi, A., AkbarVelayati, A., and Hoffner, S. (2006). Extensively Drug Resistant Tuberculosis: 2 Years of Surveillance in Iran. Clinical Infectious Diseases *43*, 841-847.

Moore, E. C., Reichard, P., and Thelander, L. (1964). Enzymatic Synthesis of Deoxyribonucleotides. V. Purification and properties of thioredoxin reductase from Escherichia coli. J Biol Chem *239*, 3445-3452.

Nguyen, L., and Pieters, J. (2005). The Trojan horse: survival tactics of pathogenic mycobacteria in macrophages. Trends in Cell Biology *15*, 269-276.

Nguyen, L., Walburger, A., Houben, E., Koul, A., Muller, S., Morbitzer, M., Klebl, B., Ferrari, G., and Pieters, J. (2005). Role of protein kinase G in growth and glutamine metabolism of Mycobacterium bovis BCG. J Bacteriol *187*, 5852-5856.

Noble, M. E. M., Endicott, J. A., and Johnson, L. N. (2004). Protein kinase inhibitors: insights into drug design from structure. Science *303*, 1800-1805.

Nolen, B., Taylor, S., and Ghosh, G. (2004). Regulation of protein kinases: controlling activity through activation segment conformation. Molecular Cell *15*, 661-675.

Ortiz-Lombardia, M., Pompeo, F., Boitel, B., and Alzari, P. M. (2003). Crystal structure of the catalytic domain of the PknB serine/threonine kinase from Mycobacterium tuberculosis. J Biol Chem *278*, 13094-13100.

Russell, D. G. (2001). Mycobacterium tuberculosis: here today, and here tomorrow. Nat Rev Mol Cell Biol *2*, 569-586.

Sieker LC, S. R., LeGall J. (1994). Rubredoxin in crystalline state. Methods Enzymology *243*.

Sikorski, R. S., Boguski, M. S., Goebl, M., and Hieter, P. (1990). A repeating amino acid motif in CDC23 defines a family of proteins and a new relationship among genes required for mitosis and RNA synthesis. Cell *60*, 307-317.

Vieira, O. V., Botelho, R. J., and Grinstein, S. (2002). Phagosome maturation: aging gracefully. Biochem J *366*, 689-704.

Walburger, A., Koul, A., Ferrari, G., Nguyen, L., Prescianotto-Baschong, C., Huygen, K., Klebl, B., Thompson, C., Bacher, G., and Pieters, J. (2004). Protein kinase G from pathogenic mycobacteria promotes survival within macrophages. Science *304*, 1800-1804.

Xaus J, C. M., Valledor AF, Cardó M, Herrero C, Soler C, Lloberas J, Celada A. (2001). Molecular mechanisms involved in macrophage survival, proliferation, activation or apoptosis. immunobiology *204*, 543-550.

Young, T. A., Delagoutte, B., Endrizzi, J. A., Falick, A. M., and Alber, T. (2003). Structure of Mycobacterium tuberculosis PknB supports a universal activation mechanism for Ser/Thr protein kinases. Nat Struct Biol *10*, 168 - 174.

- CHAPTER 4 -

Analysis of PknG Autophosphorylation

manuscript in preparation

4.1 Introduction

PknG has been shown to promote intracellular survival of mycobacteria (Walburger et al., 2004). The question therefore arises which intrinsic property of PknG is responsible for the inhibition of phagosome-lysosome fusion. In this respect, gaining knowledge about PknG autophosphorylation and its relevance regarding regulation of kinase activity is important. Autophosphorylation can confer various attributes to a kinase; it may regulate the catalytic activity, influence the binding of allostoric effectors and has been shown to affect proteolysis and membrane association (Smith et al., 1993). Intramolecular phosphorylation occurs either within a specific region of the kinase domain (the activation segment) or outside the kinase domain at multiple other sites (Johnson et al., 1996).

Mass spectrometry (MS) analysis revealed that most mycobacterial kinases studied displayed several autophosphorylation sites which is in contrast to most eukaryotic kinases; and these sites identified were located mainly within the kinase domain or adjacent to this domain (Greenstein et al., 2005). In PknB, PknD, PknE, PknF, PknH, autophosphorylation occurs on two conserved threonine residues within the activation loop (Duran et al., 2005; Scheeff and Bourne, 2005). Introducing point mutations at these sites resulted in drastically decreased kinase activity towards myelin basic protein (MBP); treatments with mycobacterial phosphatase (PstP) resulted in inhibition of kinase activity (Boitel et al., 2003) strongly suggesting autophosphorylation as the predominant activation mechanism for MBP phosphorylation.
Alignments of the kinase domain demonstrated that none of these two specific residues are present in PknG or PknI, which are also characterized by shorter autophosphorylation loops (Boitel et al., 2003).

Kinases in general can be classified into so-called RD and non-RD kinases based on the presence of a conserved arginine (R) and aspartate (D) sequence in the catalytic loop of the kinase domain. The RD arginine interacts with the phosphorylated activation loop and controls its fold, finally resulting in the activation of kinase activity (Johnson et al., 1996; Nolen et al., 2004). Interestingly, PknG is unique among mycobacerial kinases in that the critical arginine residue in the kinase domain is lacking (figure 4.1). The fact that PknG is classified as a non-RD kinase therefore suggests absence of autophosphorylation in the activation loop (Scherr et al., 2007).

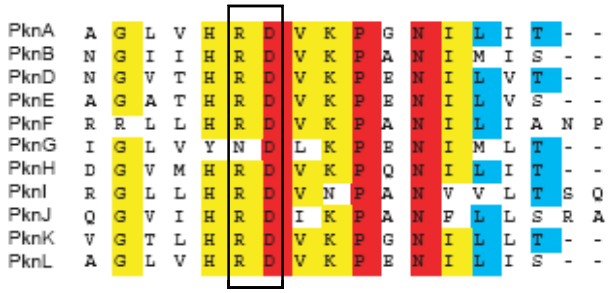

Figure 4.1. Sequence alignment of catalytic domains of the eleven mycobacterial kinases. PknG is the only kinase which does not possess the conserved arginine residue within the kinase domain.
Figure modified from Av-Gay (2000).

Previous experiments demonstrated that PknG undergoes autophosphorylation (Koul et al., 2001; Walburger et al., 2004), whereas a kinase-dead mutant of PknG (displaying a lysine-methionine point mutation at amino acid position 181 of the kinase domain) was not able to undergo autophosphorylation. In addition, the exact residues that become autophosphorylated have been mapped (P. Müller, master thesis).

In this chapter, studies are presented that further characterize autophosphorylation of PknG and preliminary work is described suggesting that autophosphorylation of PknG is important for its function during an infection.

4.2 Results

4.2.1 Autophosphorylation of PknG

PknG, overexpressed and purified from *E. coli*, undergoes autophosphorylation as analyzed by *in vitro* kinase assays (Walburger et al, 2004). Moreover, manganese was identified of being the cofactor for the catalysis. Magnesium, which often acts as cofactor, was found to inhibit the kinase reaction (figure 4.2).

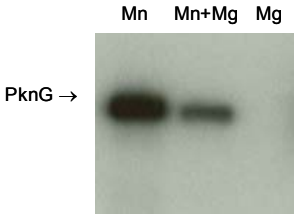

Figure 4.2.Autophosphorylation activity of PknG in presence of divalent ions. 0.5 µg PknG were incubated in a kinase buffer containing [γ-^{32}P]ATP for 30 min at 37°C, loaded on a SDS-gel and analyzed by autoradiography.

To analyze whether PknG is multiply phosphorylated, PknG was incubated with either ATP or shrimp alkaline phosphatase (SAP) and the resulting phosphorylated or dephosphorylated sample was analyzed by 7.5 % SDS-PAGE. The non-treated PknG sample was not running as one define band; instead, 3 diffuse bands were detected. In the case of phosphorylation by ATP, these bands were clearly shifted to the upper of these bands. In contrast, the SAP treatment led to a shift to the lower band suggesting that PknG is phosphorylated on multiple phosphorylation sites (figure 4.3).

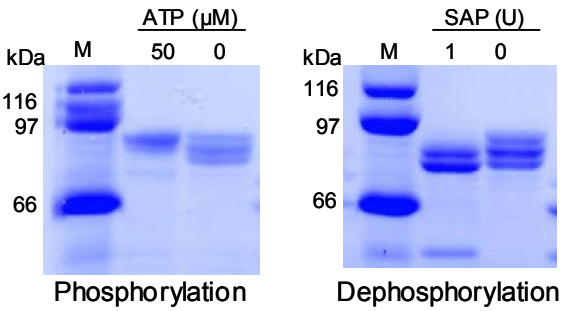

Figure 4.3. Multiple autophosphorylation of PknG. For phosphorylation, 2 µg PknG were incubated in kinase buffer containing 50 µM ATP. For dephosphorylation, PknG was treated with 1 U shrimp alkaline phosphatase. The samples were incubated for 30 min at 37°C. After addition of 5x sample buffer, PknG was boiled for 7 min at 95°C and loaded on a big 7.5% SDS-PAGE allowing a high resolution. The gel was stained in Coomassie.

Mapping of the autophosphorylation sites showed the presence of six phosphorylated threonine residues (T21, T23, T26, T32, T63, T64) in a short N-terminal region of PknG (P. Müller, master thesis).

4.2.2 Analysis of PknG kinase activity in the absence of autophosphorylation

To investigate whether autophosphorylation of PknG is required for its activity, two PknG mutant proteins - a mutant with mutated phosphorylation sites (P-mut) and the truncated PknG version missing 8 kDa of the N-terminus including all six phosphorylation sites (PknG-ΔN) were expressed and purified from *E. coli* (figure 4.4). To analyze autophosphorylation of these mutant proteins, PknG-P-mut and PknG-ΔN were tested in an *in vitro* kinase assay. As a control, PknG wildtype was included in the reaction.

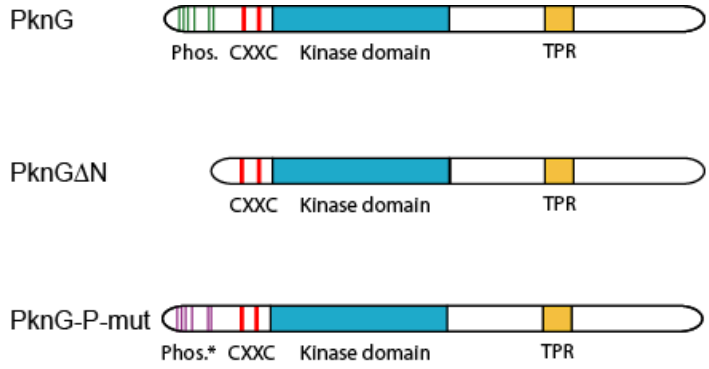

Figure 4.4. Expression of PknG mutant proteins. Truncated PknG-ΔN and PknG-P-mut carrying six threonine-to-alanine point mutations were cloned into pET15b, expressed and purified from *E. coli*.

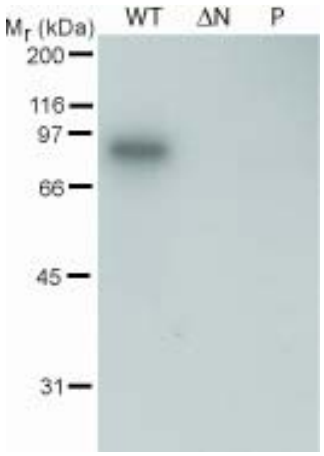

Figure 4.5. Analysis of autophosphorylation *in vitro*. A kinase assay was performed by incubating 0.5 µg PknG-WT, ΔN or PknG-P-mut in a kinase buffer containing [γ-^{32}P]ATP for 30 min at 37°C. The mixture was analyzed by 10% SDS-PAGE.

PknG was incubated for 30 min at 37°C in a kinase reaction buffer containing [^{32}γ]P-ATP. As expected, no autophosphorylation signal was detected for PknG-P-mut and PknG-ΔN (figure 4.5) in contrast to PknG wildtype displaying a strong signal. Thus, these two proteins are devoid of autophosphorylation and can be used to address the question whether autophosphorylation is involved in the regulation of kinase activity. PknG-P-mut and PknG-ΔN were incubated with an excess of PknG-N-term serving as a substrate for PknG (figure 4.6). The results of the kinase assay show that the amount of phosphorylated substrate is equal to wildtype PknG for both mutant proteins, implicating that PknG autophosphorylation is not needed to activate PknG kinase activity.

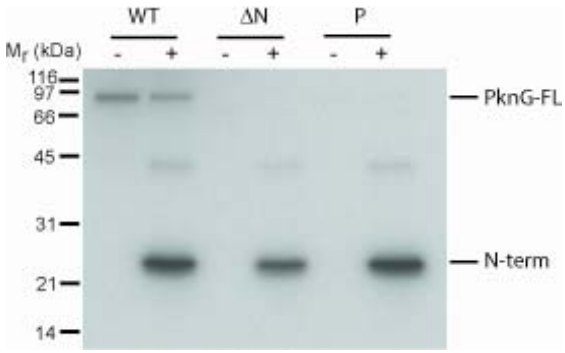

Figure 4.6. Analysis of substrate phosphorylation *in vitro*. A kinase assay was performed by incubating 0.5 µg PknG-WT, PknG-ΔN or PknG-P-mut in a kinase buffer containing [γ-^{32}P]ATP. As a substrate, 2 µg PknG-N-terminus (AA 1-140) were included. The reaction mix was incubated (30 min at 37°C) and analyzed by 12.5% SDS-PAGE and autoradiography.

4.2.3 Role of PknG autophosphorylation on intracellular trafficking and survival of pathogenic mycobacteria

To analyze a possible role of PknG autophosphorylation in intracellular trafficking or survival of mycobacteria, *Mycobacterium bovis* BCG-ΔPknG (Pasteur) expressing PknG-P-mut (D. Perisa) and PknG-ΔN (M. Bratschi) were generated. To test expression of the mutant proteins, mycobacterial lysates of the strains indicated in figure 4.7 were prepared using a mixer mill and equal amounts were loaded on a 10% SDS-PAGE and analyzed by Western blotting. Both mutant proteins, PknG-P-mut and PknG-ΔN, were expressed to the same level as wildtype PknG. As expected, no band was detected for the *M. bovis* BCGΔPknG strain (figure 4.7).

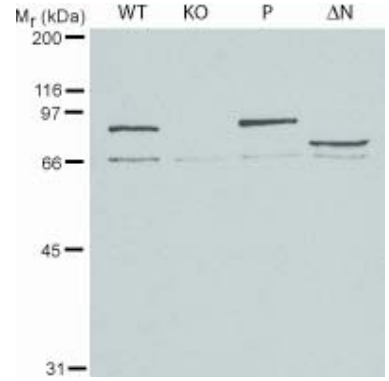

Figure 4.7. Expression of PknG mutant proteins. Cultures of *M. bovis* BCG wild type and PknG mutants (KO, ΔN, P-mut) were disrupted using the mixer mill. 5 µg lysate was run on a 10% SDS-PAGE gel. Western Blot analysis was performed using PknG specific polyclonal antibody FB18.

A growth curve was recorded to analyze whether autophosphorylation is needed for *in vitro* growth. Four cultures per strain were incubated for 6 days and the OD_{600} was measured regularly every 12 h. Overall, PknG-P-mut and PknG-ΔN strains grew with the same growth rate as PknG wildtype and KO strains (figure 4.8). These results show that the strains do not display growth defects.

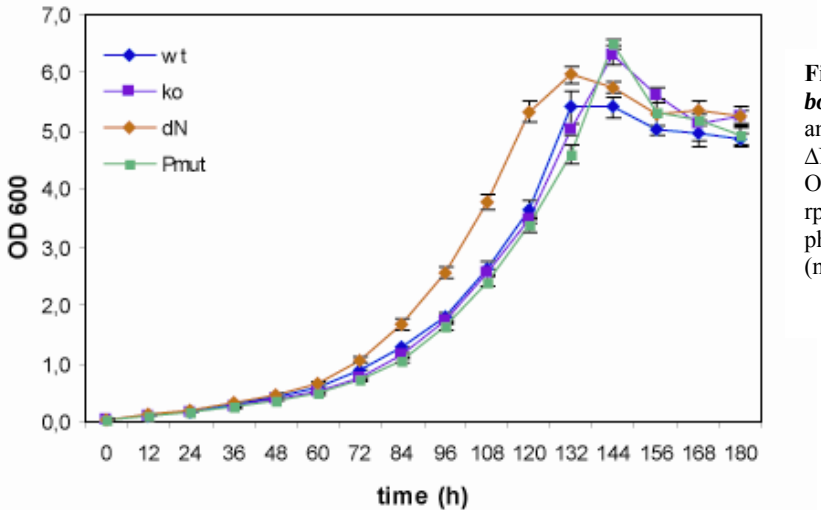

Figure 4.8. Growth curve of *M. bovis* BCG strains. Wildtype and mutant strains (WT, KO, ΔN, P-mut) were grown in 7H9-OADC medium for 6 days at 90 rpm and 37°C until stationary phase. The OD_{600} of the cultures (n=4) was measured every 12 h.

4.2.4 Analysis of intracellular survival of internalized mycobacteria

Three different experimental approaches were undertaken to study the *in vivo* role of PknG autophosphorylation. Bone marrow derived macrophages were infected for 1 h with *M. bovis* mutant strains PknG-P-mut and PknG-ΔN including *M. bovis* wildtype and ΔPknG strains as controls. After a chase time of 3 h, the cells were fixed and immunostained using α-LAMP1 and α-BCG antibody. Confocal microscopy was performed to analyze the intracellular localization of the bacteria within macrophages. It was found that wildtype *M. bovis* BCG was largely present in phagosomes, whereas a high percentage of *M. bovis* BCG-ΔPknG (~70%) resided in LAMP1-positive vacuoles. For mycobacteria expressing PknG-P-mut as well as PknG-ΔN, lysosomal delivery was also significantly increased (to about 60 %) suggesting that autophosphorylation of PknG regulates mycobacterial trafficking (personal communication D. Perisa).

The lysosomal localization of the mutant strains was independently confirmed by cell organelle electrophoresis, a method which allows the charge-based separation of lysosomes and phagosomes, followed by the detection of acid-fast stained mycobacteria in these subcellular compartments (personal communication B. Combaluzier, Hasan and Pieters, 1998; Hasan et al., 1997, Ferrari et al., 1999).

To investigate whether the mycobacteria are killed by bactericidal activities inside lysosomes, survival assays were carried out. To that end, bone marrow derived macrophages were infected for 1 h with *M. bovis* BCG wildtype, *M. bovis* BCG-ΔPknG, *M. bovis* BCG-ΔPknG overexpressing PknG-ΔN or PknG-P-mut, and the non-phagocytosed bacteria were removed. After different chase times the macrophages were lysed and medium containing

^{3}H-Uracil to be incorporated into mycobaterial RNA was added to the bacteria. After 24 h growth in labeling medium, the amount of incorporated ^{3}H-Uracil was measured by scintillation (figure 4.9).

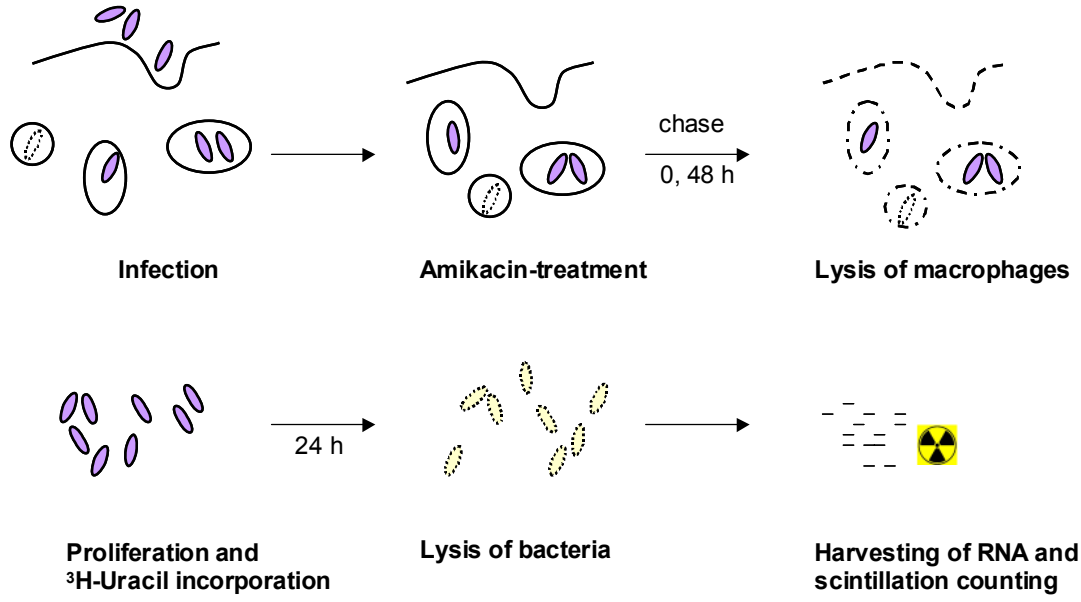

Figure 4.9. Survival assay (method). Bone marrow derived macrophages were infected for 1h with *M. bovis* BCG wild type and mutant strains. Extracellular bacteria were killed by amikacin and the macrophages were washed and lysed using 0.15 % saponin at indicated chase times. Mycobacterial survival was determined by bacterial incorporation of tritiated uracil for 24 h, followed by scintillation counting.

Preliminary results demonstrated that high cpm counts were obtained for wildtype bacteria, indicating bacterial proliferation, whereas PknG-KO bacteria displayed low counts pointing to killing inside lysosomes. The survival of the mutant strains overexpressing PknG-ΔN and PknG-P-mut was also drastically reduced, reaching a 6-7 x decreased level when compared to the wildtype (figure 4.10). These findings suggest that autophosphorylation of PknG is crucial for the capacity of the mycobacteria to escape lysosomal delivery.

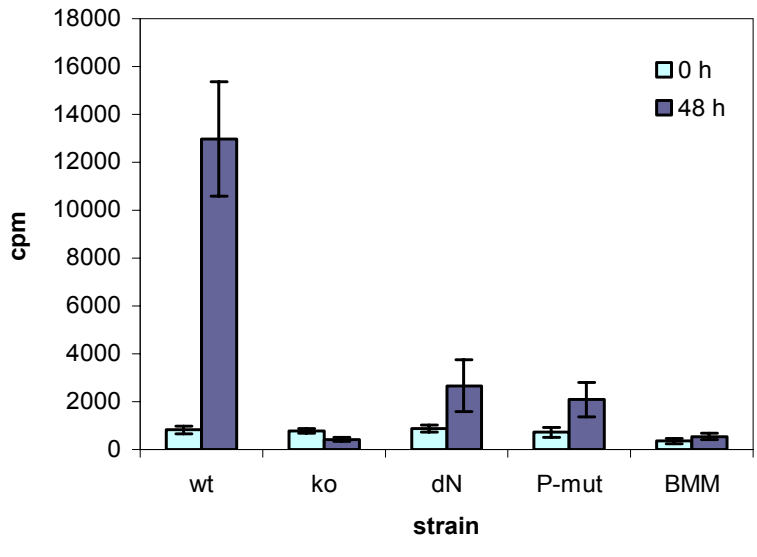

Figure 4.10. Survival assay. Survival of internalized *M. bovis* BCG wild type and mutant strains (KO, ΔN, P-mut). Mycobacterial survival was determined upon incorporation of tritiated uracil for 24 h, RNA harvesting and scintillation counting. Shown here is a one representative experiment performed in 10 wells.

4.3 Discussion

Previous studies revealed that PknG is phosphorylated on threonine residues located within a short stretch at the N-terminus of PknG. By performing kinase assays including PknG mutant proteins missing the potential phosphorylation sites, no signal could be detected, confirming the results obtained by mass spectrometry. Similarly, autophosphorylation of residues in the "activation" loop could be excluded experimentally.

The fact that PknG with mutated or depleted phosphorylation sites was still able to phosphorylate an "artificial" substrate to the same extent as the wildtype protein implies that PknG autophosphorylation is not necessary for kinase activity *per se*.

However, it needs to be stated that autophosphorylation of PknG seems to be relevant for its *in vivo* role, since mycobacteria expressing PknG defective of undergoing autophosphorylation were not able any more to prevent lysosomal delivery and killing within macrophages. More defined experiments are needed to specify the function of autophosphorylated PknG in mycobacterial trafficking.

In addition to the common function to activate kinases, autophosphorylation has been evidenced to be a prominent mechanism to create bindings sites for potential substrates which also could apply to PknG. Proteins containing forkhead-associated (FHA) domains for example recognize specific phosphothreonine-peptide motifs and states of the kinase (Durocher and Jackson, 2002; Pallen et al., 2002). Many of the so far identified *in vivo* and *in vitro* substrates of mycobacterial serine/threonine kinases have indeed been shown to possess FHA domains (Molle et al., 2004, Molle et al., 2003) At this point, however, is should be mentioned that the genome of *M. tuberculosis* comprises only six FHA containing proteins (Cole et al., 1998), a relatively small number in view of the whole phospho-proteome, which is supposed to encompass (roughly estimated) 500-1000 pSer/pThr containing proteins (Greenstein AE, 2005).

Taken together, it was demonstrated that autophosphorylation of PknG has a function different from the other mycobacterial kinases studied so far. Autophosphorylation was not linked to the catalytic activity of PknG, but was shown to be essential for the role of PknG in preventing lysosomal delivery and allowing survival of the bacteria.

4.4 References

Av-Gay, Y., and Everett, M. (2000). The eukaryotic-like Ser/Thr protein kinases of Mycobacterium tuberculosis. Trends Microbiol *8*, 238-244.

Boitel, B., Ortiz-Lombardia, M., Duran, R., Pompeo, F., Cole, S. T., Cervenansky, C., and Alzari, P. M. (2003). PknB kinase activity is regulated by phosphorylation in two Thr residues and dephosphorylation by PstP, the cognate phospho-Ser/Thr phosphatase, in Mycobacterium tuberculosis. Mol Microbiol *49*, 1493 - 1508.

Cole, S. T., Brosch, R., Parkhill, J., Garnier, T., Churcher, C., Harris, D., Gordon, S. V., Eiglmeier, K., Gas, S., Barry, C. E.*, et al.* (1998). Deciphering the biology of Mycobacterium tuberculosis from the complete genome sequence. Nature *393*, 537-544.

Duran, R., Villarino, A., Bellinzoni, M., Wehenkel, A., Fernandez, P., Boitel, B., Cole, S. T., Alzari, P. M., and Cervenansky, C. (2005). Conserved autophosphorylation pattern in activation loops and juxtamembrane regions of Mycobacterium tuberculosis Ser/Thr protein kinases. BBRC *333*, 858-867.

Durocher, D., and Jackson, S. P. (2002). The FHA domain. FEBS Letters *513*, 58-66.
Ferrari, G., Langen, H., Naito, M., and Pieters, J. (1999). A coat protein on phagosomes involved in the intracellular survival of mycobacteria. Cell *97*, 435-447.

Greenstein, A.E., Grundner, C., Echols, N., Gay, L.M., Lombana, T.N., Miecskowski, C.A., Pullen, K.E., Sung, P.Y., Alber, T. (2005). Structure/function studies of Ser/Thr and Tyr protein phosphorylation in Mycobacterium tuberculosis. J Mol Microbiol Biotechnol *9*, 167-181.

Hasan, Z., and Pieters, J. (1998). Subcellular fractionation by organelle electrophoresis: separation of phagosomes containing heat-killed yeast particles. Electrophoresis *19*, 1179-1184.
Hasan, Z., Schlax, C., Kuhn, L., Lefkovits, I., Young, D., Thole, J., and Pieters, J. (1997). Isolation and characterization of the mycobacterial phagosome: segregation from the endosomal/lysosomal pathway. Mol Microbiol *2*, 427.

Johnson, L. N., Noble, M. E., and Owen, D. J. (1996). Active and inactive protein kinases: structural basis for regulation. Cell *85*, 149 - 158.

Koul, A., Choidas, A., Tyagi, A. K., Drlica, K., Singh, Y., and Ullrich, A. (2001). Serine/threonine protein kinases PknF and PknG of M. tuberculosis: characterization and localization. Microbiology *147*, 2307-2314.

Molle, V., Soulat, D., Jault, J.-M., Grangeasse, C., Cozzone, A. J., and Prost, J.-F. (2004). Two FHA domains on an ABC transporter, Rv1747, mediate its phosphorylation by PknF, a Ser/Thr protein kinase from Mycobacterium tuberculosis. FEMS Microbiology Letters *234*, 215-223.

Nolen, B., Taylor, S., and Ghosh, G. (2004). Regulation of Protein Kinases: controlling activity through activation segment conformation. Molecular Cell *15*, 661-675.

Pallen, M., Chaudhuri, R., and Khan, A. (2002). Bacterial FHA domains: neglected players in the phospho-threonine signalling game? Trends in Microbiology *10*, 556-563.

Scheeff, E., and Bourne, P. (2005). Structural evolution of the protein kinase-like superfamily. PloS Comput Biol *5*.

Scherr, N., Honnappa, S., Kunz, G., Mueller, P., Jayachandran, R., Winkler, F., Pieters, J., and Steinmetz, M. O. (2007). From the Cover: Structural basis for the specific inhibition of protein kinase G, a virulence factor of Mycobacterium tuberculosis. Proceedings of the National Academy of Sciences *104*, 12151-12156.

Smith, J., Francis, S., and Corbin, J. (1993). Autophosphorylation: a salient feature of protein kinases. Mol Cell Biochem *127*, 51-70.

Walburger, A., Koul, A., Ferrari, G., Nguyen, L., Prescianotto-Baschong, C., Huygen, K., Klebl, B., Thompson, C., Bacher, G., and Pieters, J. (2004). Protein kinase G from pathogenic mycobacteria promotes survival within macrophages. Science *304*, 1800-1804.

- CHAPTER 5 -

Localization of PknG within Eukaryotic Cells

preliminary studies

5.1 Introduction

PknG, a eukaryotic-type serine/threonine protein kinase expressed by pathogenic mycobacteria is secreted into the cytosol of macrophages, where it interferes with the maturation of the phagosome, thereby ensuring intracellular survival of the bacilli. Moreover, it was demonstrated that the kinase activity of PknG was required to block the fusion of phagosomes with lysosomes (Walburger, 2004). How, precisely, PknG achieves blocking of phagosome-lysosome fusion, has not been defined.

Knowledge on the localization of PknG within the host cell might help to delineate its function. Therefore, in this chapter, two different approaches were used to study the localization of PknG. Firstly, by localizing PknG in established cell lines (HeLa, HEK293 and Mel JuSo) transfected with *pknG* expression vectors and secondly, PknG localization was analyzed within macrophages upon infection.

The results of this work may contribute to elucidate in which subcellular compartment PknG is localized and the findings obtained might be helpful with regard to the identification of potential substrates or interacting partners present in the same subcellular environment.

5.2 Results

5.2.1. Localization of PknG in eukaryotic cells

In order to analyze the role of PknG in eukaryotic cells, localization studies were carried out. To that end, different human cell lines, namely HeLa, HEK293 and Mel JuSo cells, were transfected with the eukaryotic *pEGFP-N1::pknG* vector in which the *gfp* gene was replaced by *pknG*. After 24 h, the cells seeded on slides were fixed by 3% PFA and immunostained using protein A purified polyclonal α-PknG antibody or, alternatively, with affinity purified polyclonal α-PknG antibody and crude anti-serum FB18. Fluorescence microscopy revealed that PknG was largely localized in the nucleus in all three cell lines (figure 5.1). No differences were observed for the different primary antibodies used.

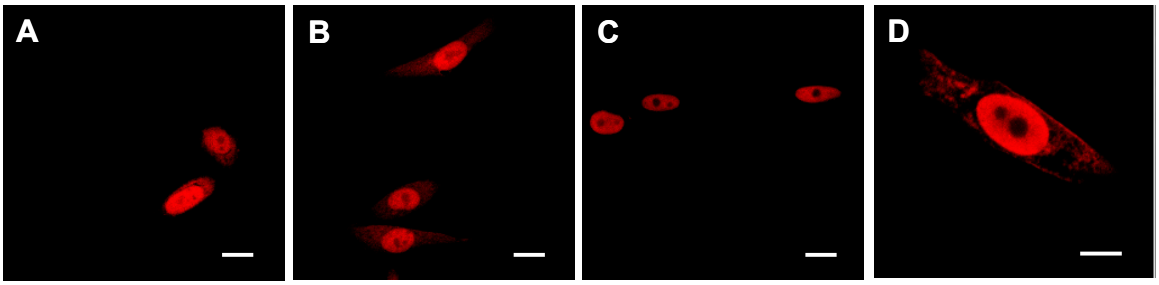

Figure 5.1. Nuclear localization of PknG. HeLa (A) and Mel JuSo (B) cells transfected with *pEGFP-N1::pknG* were incubated for 24 h at 37°C. In addition, Mel JuSo cells (C, D) transfected with *pIRES::pknG.* The cells were fixed by 3% PFA and immunostained using Protein A purified α-PknG and Alexa-568 antibodies and analyzed by fluorescence microscopy. Bar: (A-C) 20 µm, (D) 10 µm.

To further confirm these findings, *pknG* was cloned into a different eukaryotic vector, pIRES, for expression of full length PknG. The experiment was performed as described above using Mel JuSo cells (figure 5.1). Again, PknG was detected in the nucleus of the cells.

To determine the domain or sequence responsible for translocating PknG to the nucleus, different truncated versions of *pknG* were cloned and ligated into the pIRES vector (figure 5.2). The following experiments were carried out using HeLa cells. Cells were transfected, fixed using 100% MeOH and stained with protein A purified α-PknG and Alexa-568 antibodies prior to analysis by fluorescence microscopy. The analysis of the mutant proteins (figure 5.3) revealed that PknG-ΔN1 and PknG-ΔC1 localized to the nucleus, similar to the localization of PknG full length. Nuclear localization was also observed for PknG-ΔN2 and PknG-kin, but here the protein formed distinct clusters. This finding might be explained by improper folding of these two proteins both missing the N-terminal rubredoxin motif.

However, the sequence for nuclear translocation must still be present. In cells expressing PknG-ΔC2 and PknG-ΔC3, most of the signal was found in the cytoplasm; in some cases even excluding the nucleus. For the K/M mutant, the localization was not clear, since the protein was found in the area of the nucleus as well as in the cytoplasm.

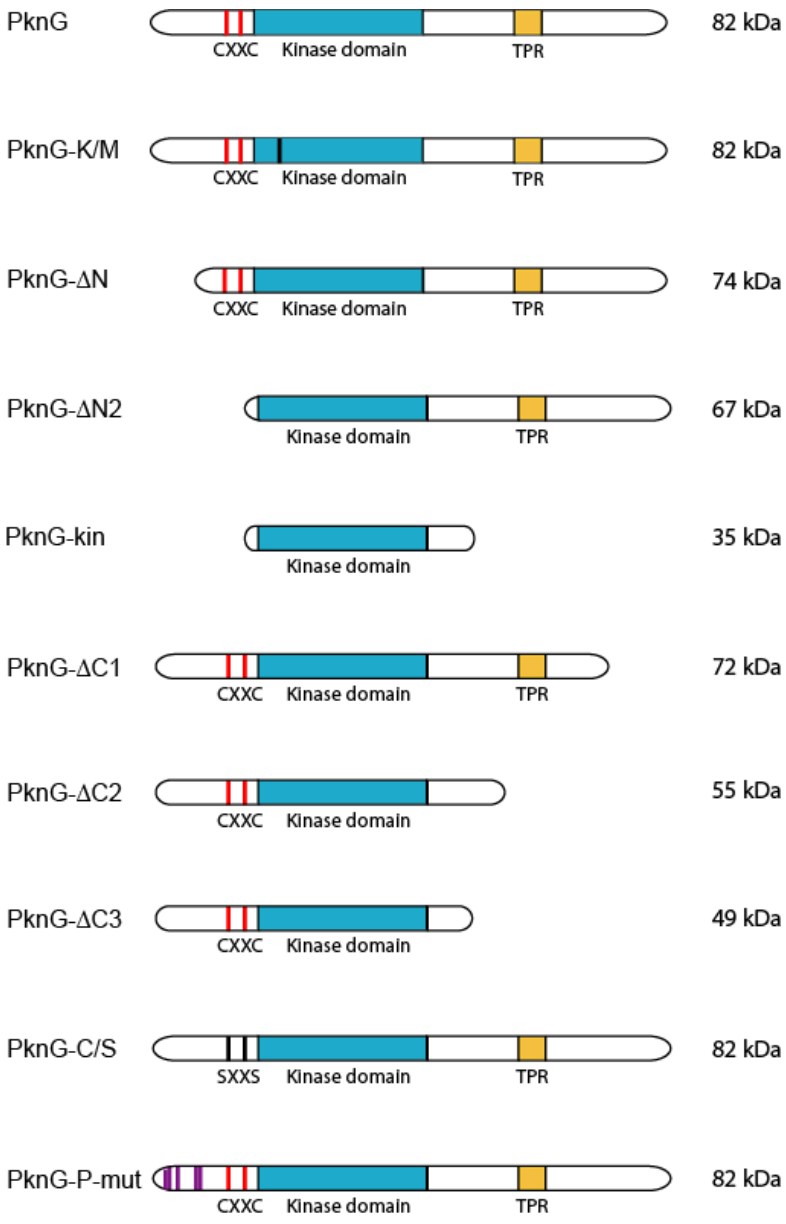

Figure 5.2. Overview of the PknG mutant proteins expressed in eukaryotic cells. Using the jetPEI transfection reagent, HeLa cells were transfected with different pIRES vectors for expression of wildtype PknG and mutant proteins. After 24 h, the cells seeded on slides were fixed, immunostained and prepared for microscopy analysis.

Due to the cytoplasmic localization of the mutants displaying a C-terminal deletion, this domain including the TPR motif might be responsible for the nuclear localization. However, even the isolated PknG kinase domain located in the nucleus making thed result difficult to interpret. Vectors for expression of PknG P-mutant and C/S mutant were constructed, but not included at this stage of the analysis.

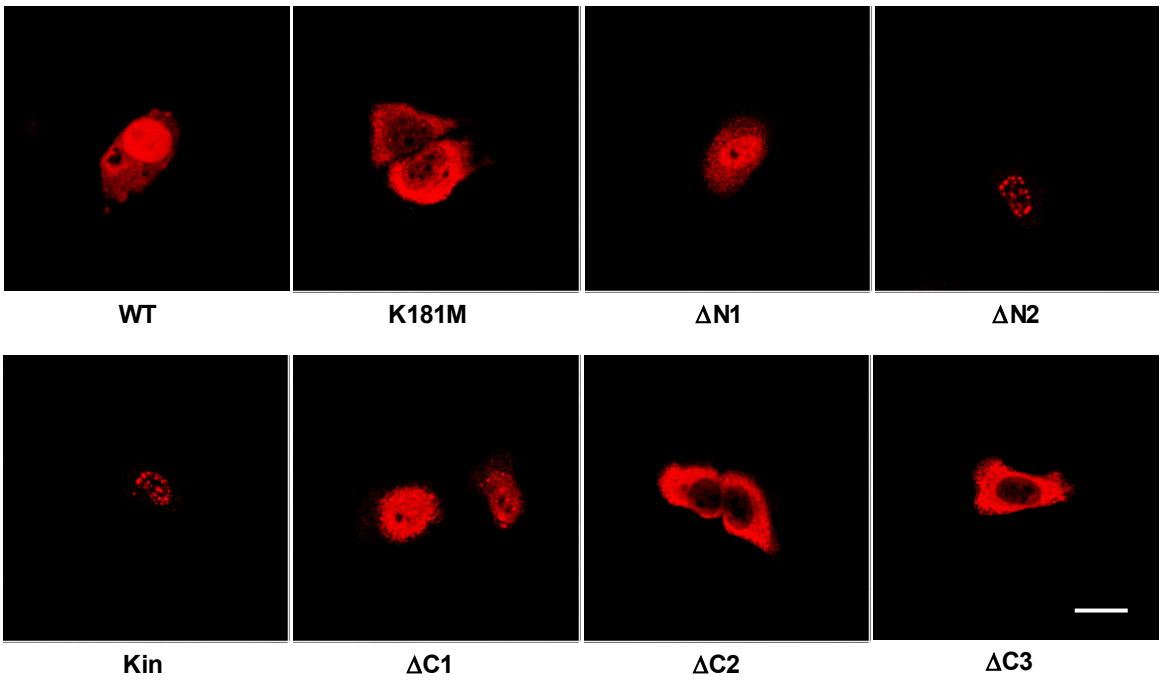

Figure 5.3. HeLa cells expressing PknG and mutant proteins. HeLa cells were transfected with pIRES constructs for the expression of PknG wildtype and mutant proteins K/M, ΔN1, ΔN2, Kin, ΔC1, ΔC2 and ΔC3. The cells were fixed by 3% PFA, immunostained using α-PknG and Alexa-568 antibodies and analyzed by immunofluorescence microscopy. Bar: 20 µm.

In parallel, expression of PknG and mutant proteins was analyzed. HeLa cells were lysed 24 hours after transfection and the lysates were analyzed by Western Blot analysis. The results (figure 5.4) demonstrated that the proteins were expressed to different levels. For PknG-ΔN2 and PknG-kin, no band was detectable suggesting absence of expression. However, the microscopy data clearly showed that PknG-ΔN2 and PknG-kin were expressed, but to a smaller extend. In addition, the localization pattern of

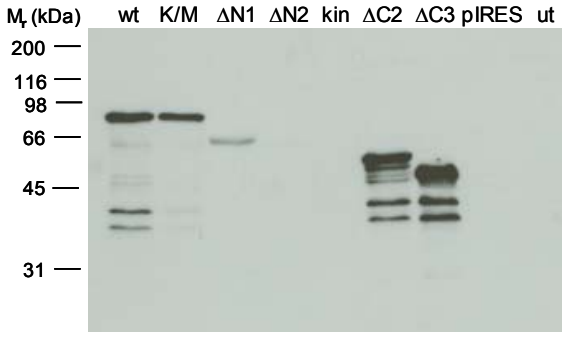

Figure 5.4. Western Blot analysis of PknG expression. Lysates of HeLa cells were prepared by using Triton X-100. Per sample, 15 µg lysate were loaded on a 10% SDS-PAGE. PknG was detected using the same antibody (protein A purified FB18) as for the microscopy analysis.

protein clusters differed from the diffused localization observed for PknG full length. These findings might support the idea of improper PknG folding. Another kinase domain construct, expressed and purified from *E. coli* was shown to be unstable in previous studies.

In order to confirm the localization patterns of PknG by using a different expression vector, *pknG* and truncated fragments (figure 5.2) were additionally cloned into a vector which allowed the expression of 3xFLAG-tagged proteins (figure 5.5). In case the nuclear localization for PknG wildtype is reproduced experimentally, 3xFLAG-*pknG* can be transferred into a mycobacterial vector in order study the localization under more realistic conditions upon infection of host cells.

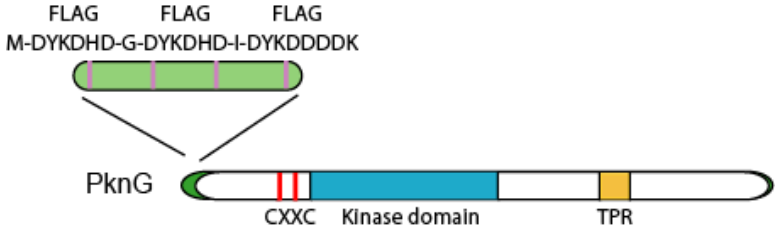

Figure 5.5. FLAG-PknG (wildtype). The FLAG-tag is a small polypeptide which is repeated 3x (with slight modifications) and fused N-terminally to PknG wt or mutant protein.

Preliminary analysis of the localization of FLAG-PknG in Mel JuSo and HeLa cells showed that PknG wildtype localized in both cell types to the nucleus as observed before (figure 5.6). The nuclear localization was more even more distinct when using the FLAG vector and monoclonal α-FLAG antibody (as opposed to the α-PknG antibody).

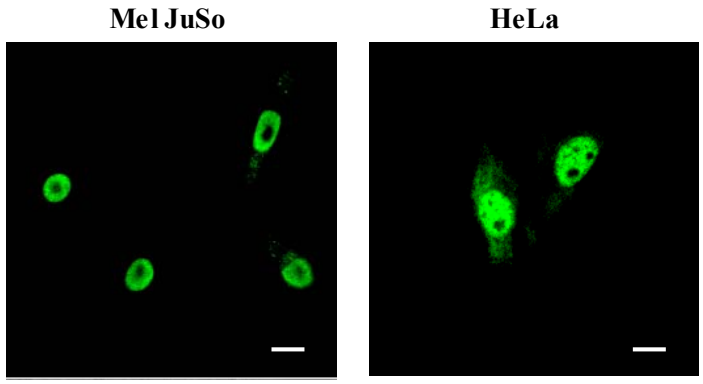

Figure 5.6. Expression of FLAG-PknG (wt) by Mel JuSo and HeLa cells. Mel JuSo and HeLa cells were transfected on-slide with the *3xFLAG::pknG* vector. After 24 h, cells were fixed by 100% MeOH, stained by monoclonal α-FLAG and Alexa-488 antibodies and analyzed by immunofluorescence microscopy.
Bar: 10 µm.

In addition, transfections were performed with different vectors to express FLAG-tagged PknG wildtype as well as the FLAG-tagged mutant proteins PknG-K181M, PknG-ΔN1, PknG-ΔN2, PknG-kin, PknG-ΔC1, PknG-ΔC2 and PknG-ΔC3 (figure 5.2).

It was found that PknG-ΔN1, PknG-ΔN2, PknG-ΔC1 localized, like PknG-wt, to the nucleus (figure 5.7). The kinase domain showed a different localization by forming distinct spots in the nucleus. Coronin 1, used as a control for cytoplasmic localization (Gatfield and Pieters, 2000), was exclusively detected in the cytoplasm excluding the nucleus. For unknown reasons, no FLAG signal was detectable for PknG-ΔC2, PknGΔ-C3 and PknG-K/M.

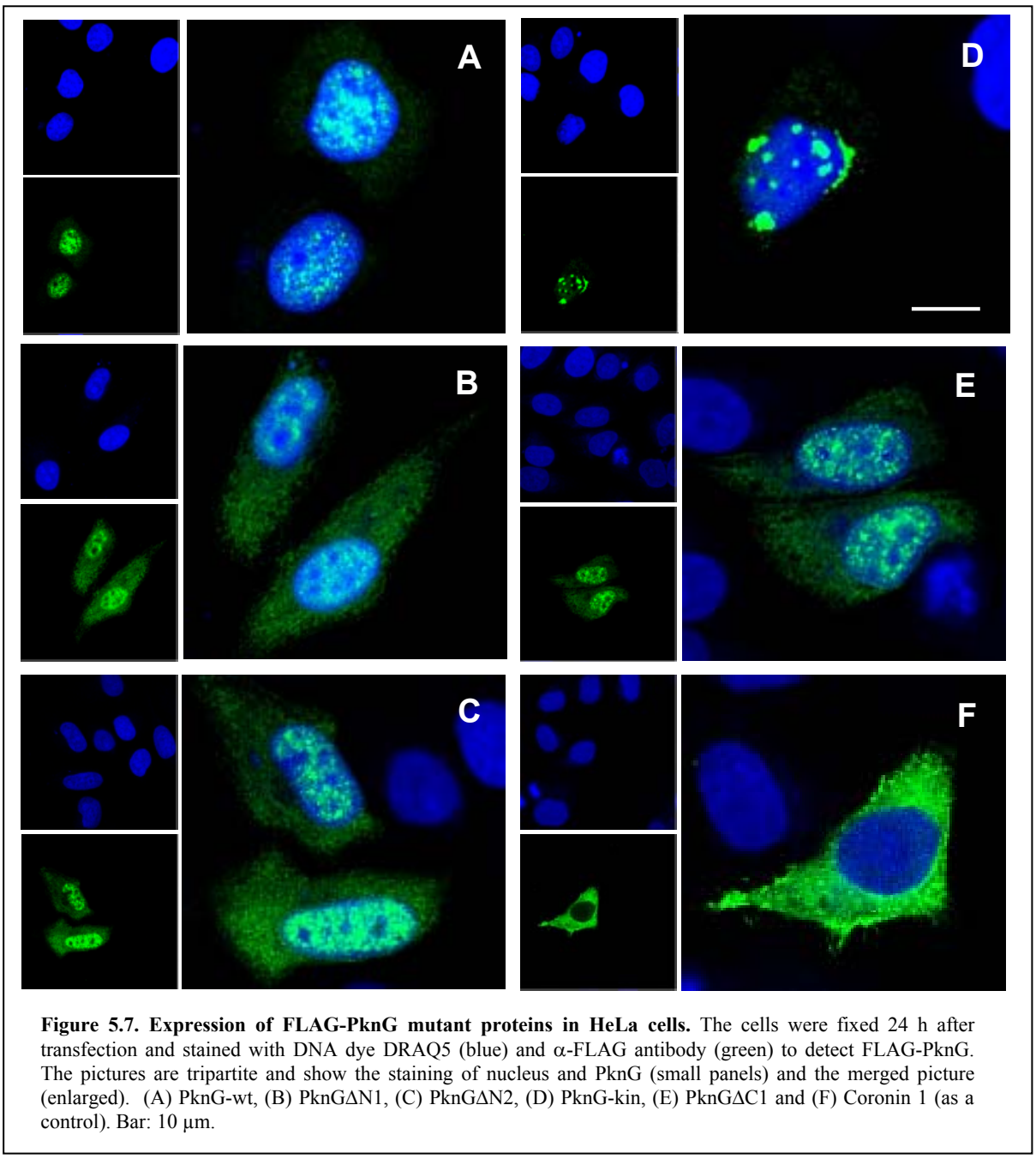

Figure 5.7. Expression of FLAG-PknG mutant proteins in HeLa cells. The cells were fixed 24 h after transfection and stained with DNA dye DRAQ5 (blue) and α-FLAG antibody (green) to detect FLAG-PknG. The pictures are tripartite and show the staining of nucleus and PknG (small panels) and the merged picture (enlarged). (A) PknG-wt, (B) PknGΔN1, (C) PknGΔN2, (D) PknG-kin, (E) PknGΔC1 and (F) Coronin 1 (as a control). Bar: 10 µm.

However, by using the protein A purified α-PknG antibody, a signal for all constructs was obtained. The mutant proteins with a C-terminal deletion were localized in the cytoplasm and nucleus whereas the kinase-dead mutant formed distinct dots in the cytoplasm (figure 5.8).

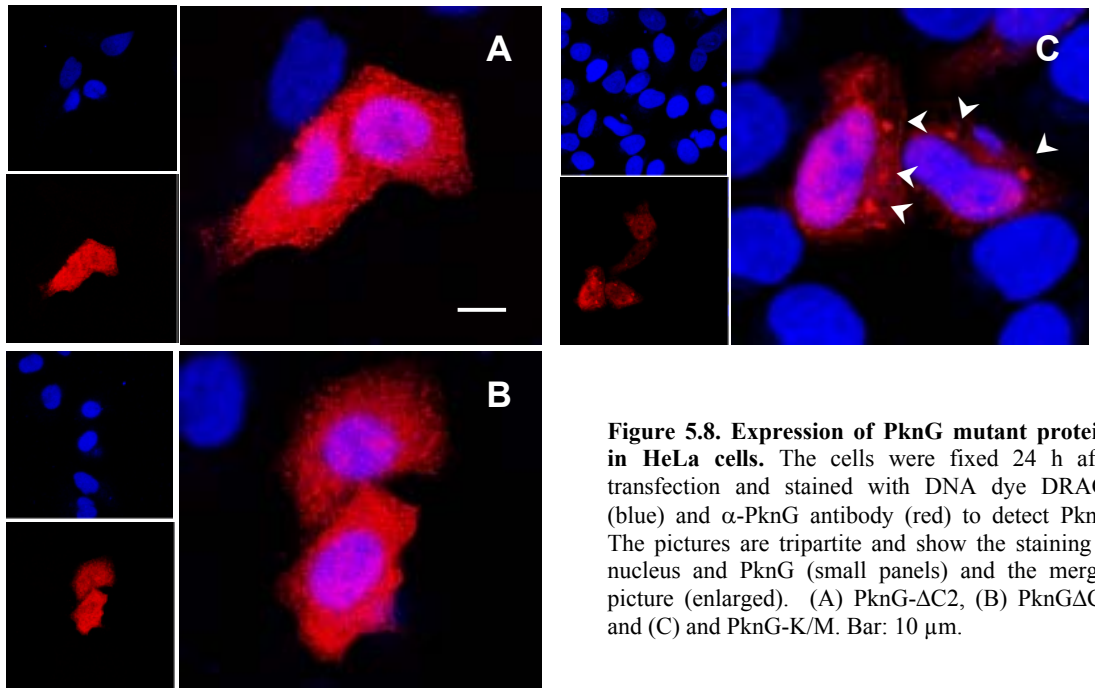

Figure 5.8. Expression of PknG mutant proteins in HeLa cells. The cells were fixed 24 h after transfection and stained with DNA dye DRAQ5 (blue) and α-PknG antibody (red) to detect PknG. The pictures are tripartite and show the staining of nucleus and PknG (small panels) and the merged picture (enlarged). (A) PknG-ΔC2, (B) PknGΔC3, and (C) and PknG-K/M. Bar: 10 µm.

Taken together, the results obtained before with the α-PknG antibody were reproduced by using the N-terminal FLAG-tag as an epitope for the antibody.

In an additional study, the same *3xFLAG::pknG* constructs were used for the transfection of J774 macrophages. The localization patterns were identical to the ones of HeLa cells, with the exception that PknG-K/M was predominantly found in the cytoplasm (personal communication V. Sundara-murthy). The fact that PknG localizes also in macrophages to the nucleus (figure 5.9) justifies the construction of a mycobacterial vector for the expression of PknG upon infection of macrophages.

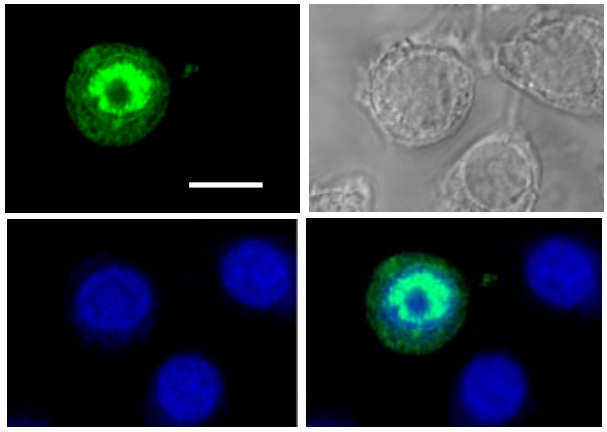

Figure 5.9. Expression of PknG wildtype in J774 macrophages. The cells were seeded on slides, incubated for 2 h and transfected using the jetPEI reagent. After 24 h transfection, the cells were fixed by MeOH and stained with DRAQ5 (blue) to label the nucleus (DNA) and α-FLAG antibody (green) to detect 3xFLAG-PknG.
Bar: 10 µm

5.2.2. Construction of a mycobacterial FLAG-PknG vector to be used for infections

To be able to investigate the role of PknG upon infection of macrophages, a mycobacterial vector was constructed allowing the expression of FLAG-tagged PknG. To do so, *3xFLAG::pknG* was used as a template for the construction of the subcloning vector *pGEM::3xFLAG::pknG.* Sequence analysis of the FLAG region was performed to screen for mutants containing the three N-terminal FLAG repeats. The plasmid DNA from a positive clone was prepared and the insert was ligated into the target vector pSD5.

Both, *Mycobacterium smegmatis* which does not express PknG and *Mycobacterium bovis* BCG pasteur depleted of *pknG* were transformed with a *pSD5::3xFLAG::pknG* and plated on 7H10-Kanamycin agar. The colonies obtained 2-3 days (*M. smegmatis*) or 3-4 weeks (*M. bovis* BCG Pasteur) later were analyzed for the presence of *3xFLAG-PknG*.

Western Blot analysis was performed using a monoclonal α-FLAG antibody. All clones tested were found to express 3x-FLAG-PknG (figure 5.10).

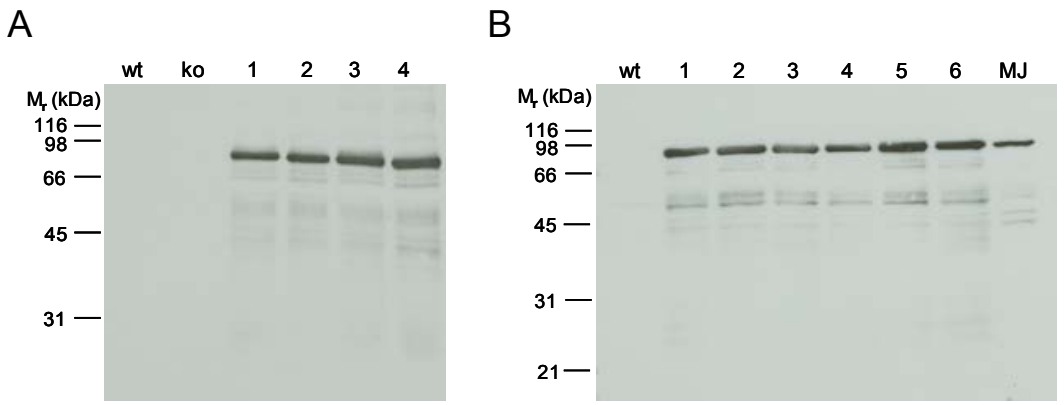

Figure 5.10. Expression of 3x FLAG-PknG by mycobacteria. Using the mixer mill, lysates of *M. bovis* BCG Pasteur ΔPknG (left panel) and *M. smegmatis* (right panel) transformed with *3xFLAG::pknG* were prepared and the protein concentration was determined. Ten µg were loadad on a 10% SDS-PAGE and analyzed using the α-FLAG antibody. As controls, *M. bovis* wildtype (wt) and ΔPknG (ko) as well as *M. smegmatis* (wt) and a lysate of PknG transfected Mel JuSo cells (MJ) were used.

Thus, both mycobacterial strains can be used for the infection of J774 macrophages to analyze the localization of secreted PknG within its host cell, the macrophage.

5.3 Discussion

PknG was shown to localize in the nucleus of HeLa, Mel JuSo and J774 macrophages. However, PknG does not possess a classical nuclear localization sequence (NLS) (Boulikas, 1993); thus it remains unclear how PknG is translocated into the nucleus. Nevertheless, the nuclear localization observed by microscopy as described here should be further verified by performing biochemical experiments, for example by cell fractionation and subsequent analysis of PknG in the nuclear fraction.

The analysis revealed that PknG displayed a diffuse distribution within the nucleus; however, certain nuclear structures were clearly excluded (see figure 5.1-D). Therefore it is worth to investigate in detail to which nuclear compartments PknG localizes. A motif scan (Dellaire et al., 2003) predicted that PknG might localize to the nuclear lamina, however the nucleoplasm seems more likely to be the site of localization with regard to the PknG pattern observed in the nucleus.

Proteins with a diffused nuclear localization are detected throughout the nucleoplasm but are generally excluded from nucleoli (Sutherland et al., 2001). Many transcription factors display a nuclear diffused localization pattern; among them are C2H2 zinc finger proteins which represent the largest class of these nuclear diffused proteins, accounting for more than 12% of all DNA binding proteins (Sutherland et al., 2001).

A motif scan using the PROSITE database predicted a FtsK-like domain at the C-terminus of PknG (amino acid position 687-750). FtsK is known to translocate DNA in order to transport chromosomes within the bacterial cell (Massey et al., 2006; Ptacin, 2006). The degree of structural similarity between the FtsK and PknG remains to be established. However, the PknG-ΔC1 mutant lacking this region still localized to the nucleus, therefore, DNA binding mediated by this motif seems unlikely. Potential PknG-DNA interactions can be tested for example by performing band-shift experiments.

In conclusion, it was found that PknG localizes to the nucleus in mammalian cells, independent from the cell line, vector or antibody used in the different studies. Experiments involving infected macrophages will be required to analyze the localization of mycobacterial PknG released within host cells.

Definitive conclusions regarding the exact subnuclear localization or the domain responsible for nuclear import cannot be drawn at this stage of analysis; however, preliminary data show that the C-terminal domain might contain a sequence which determines the subcellular localization. In addition, the finding that PknG is located in the nucleus might stimulate the substrate search within the nucleus.

5.4 References

Boulikas, T. (1993). Nuclear localization signals (NLS). Crit Rev Eukaryot Gene Expr *3*, 193-227.

Dellaire, G., Farrall, R., and Bickmore, W. A. (2003). The Nuclear Protein Database (NPD): sub-nuclear localisation and functional annotation of the nuclear proteome. Nucl Acids Res *31*, 328-330.

Gatfield, J., and Pieters, J. (2000). Essential role for cholesterol in entry of mycobacteria into macrophages. Science *288*, 1647-1651.

Massey, T. H., Mercogliano, C. P., Yates, J., Sherratt, D. J., and Löwe, J. (2006). Double-stranded DNA translocation: structure and mechanism of hexameric FtsK. Molecular Cell *23*, 457-469.

Ptacin, J. L. N., M.; Bustamante, C; Cozzarelli, N.R. (2006). Identification of the FtsK sequence-recognition domain. Nat Struct Mol Biol *13*, 948-950.

Sutherland, H. G. E., Mumford, G. K., Newton, K., Ford, L. V., Farrall, R., Dellaire, G., Caceres, J. F., and Bickmore, W. A. (2001). Large-scale identification of mammalian proteins localized to nuclear sub-compartments. Hum Mol Genet *10*, 1995-2011.

Walburger, A., Koul, A., Ferrari, G., Nguyen, L., Prescianotto-Baschong, C., Huygen, K., Klebl, B., Thompson, C., Bacher, G., and Pieters, J. (2004). Protein kinase G from pathogenic mycobacteria promotes survival within macrophages. Science *304*, 1800-1804.

- CHAPTER 6 -

Antigen 84, an Effector of Pleiomorphism in *Mycobacterium smegmatis*

Based on

Journal of Bacteriology (2007), Vol. 189

Liem Nguyen, Nicole Scherr, John Gatfield, Anne Walburger,

Jean Pieters and Charles Thompson

6.1 Abstract

In most rod-shaped bacteria, maintenance of the cell shape is accomplished by MreB-like proteins forming an actin-like cytoskeletal scaffold for cell wall synthesis; however, components that determine the more flexible rod-like shape in actinobacteria are unknown. *Mycobacterium smegmatis* expresses an essential protein, termed Ag84, which is homologous to eubacterial DivIVA proteins that function in cell division.
To elucidate the function of Ag84, the protein was overexpressed in *M. smegmatis*. Upon overexpression, the cells became elongated and wider; Ag84 was distributed asymmetrically to one pole, causing an aberrant cell shape presumably through uncontrolled cell wall expansion. In addition, Ag84 was found to form oligomers *in vitro*, consistent with more complex structures observed *in vivo*. The results obtained for Ag84 point to a role in cell divison and cell shape control.

6.2 Introduction

One reason for the success of mycobacteria as pathogens is their ability to remain dormant within the host for decades, without being recognized by the human immune system. During latency, mycobacteria persist while undergoing minimal replication (Manabe and Bishai, 2000). In the case of reactivated disease, *M. tuberculosis* actively replicates *in vivo*. The factors responsible for alternating between these two states have not yet been determined. However, one critical component of this process might be the regulation of cell division and cell wall synthesis in response to certain signals sensed in the hostile environment of the host (Kang et al., 2005). Two component-systems and serine/threonine protein kinases such as PknA and PknB are likely to transmit signals by reversible phosphor-transfer reactions to effector proteins involved in the control of cell division and cell shape.

In rod-shaped bacteria, cell division usually results in the formation of hemispherical cell poles, which then remain inert (De Pedro et al., 1997). Elongation of the bacterial cell requires extension of the lateral cell wall through incorporation of new peptidoglycan into the wall, a process in which MreB, a homologue of actin, is involved (Carballido-Lopez, 2006). Rod-like bacteria express MreB and MreB-like (Mbl) proteins which, when assembled, form cytoskeletal structures defining the site of cell wall synthesis (Daniel and Errington, 2003;

Egelman, 2003; Jones et al., 2001). In addition, by binding proteins such as MreC, MreD or RodA, the Mre-based cytoskeleton recruits enzymes, for example penicillin-binding proteins (PBPs), which are part of the cell wall synthesis machinery (Cabeen and Jacobs-Wagner, 2005; Divakaruni et al., 2005; Kruse et al., 2005; Leaver and Errington, 2005). MreB depletion in *E. coli* was reported to result in the formation of coccoid cells, supporting the role of MreB in the control of cell shape (Kruse et al., 2005). The function of MreB is control of cell width, whereas Mbl proteins are responsible for control of the cell length; thus, both proteins help maintaining the rod-like cell shape (Stewart, 2005).

Interestingly, Actinobacteria, gram-positive bacteria having a high G+C content, display a different and mreB-independent mode of cell elongation. Here, the presence of MreB does not correlate with a rod-like shape. Mycobacterial genomes lack *mreB* homologs, but have primarily a rod-like shape. However, it should be noted that mycobacteria are as well pleiomorphic under certain conditions. It has been demonstrated that *M. tuberculosis* cells are shortened in older cultures (Nyka, 1974), can become filamentous within macrophages (Chauhan et al., 2006), ovoid under carbon starvation (Ojha et al., 2000) and have different cell shapes also in the stationary phase of growth (Dahl, 2005). Thus far, no cell shape determinants have been identified in mycobacteria.

Not only the control of the cell shape, but also cell division seems to be different in mycobacteria. Septum formation, a critical step of cell division, is initiated by the assembly of FtsZ proteins into a ring structure at the midcell of rod-shaped bacteria. Two mechanisms have been described which determine the site of septum formation: First, nucleoid occlusion which excludes septum formation along the central part of the rod and second, proteins of the MinCD system (Edwards and Errington, 1997; Mulder and Woldringh, 1989), which in *B. subtilis* localize to the poles and inhibit FtsZ formation in this region, thereby targeting the midcell as a site of cell division (Marston and Errington, 1999; Marston et al., 1998). In *B. subtilis*, the protein responsible for retaining MinC and MinD at the poles, is DivIVA (Edwards and Errington, 1997).
However, in mycobacteria, such a MinCD system does not exist and factors defining the site of septum formation have not yet been found.

By sequence analysis, Ag84 has been identified to be the mycobacterial orthologue of the *B. subtilis* cell division protein DivIVA. This protein, encoded by the *wag31* gene, is a highly

conserved mycobacterial antigen recognized by sera from people infected with *M. tuberculosis* and *M. leprae* (Hermans et al., 1995). In gram-positive species, functional studies of DivIVA demonstrated that the protein is involved in regulation of septum formation and nucleoid segregation (*B. subtilis*). In addition, a role in morphology has been proposed as shown in *Streptomyces coelicolor* (Flardh, 2003). *B. subtilis wag31* is not essential, but inactivation or overexpression of DivIVA resulted in a strong morphological phenotype such as production of mini-cells or generation of filamentous cells (Cha and Stewart, 1997). Depletion of *wag31* led to non-viable cells in several gram-positive bacterial species, e.g. *Brevibacterium lactofermentum*, *Enterococcus faecalis* as well as *S. coelicolor*, (Flardh, 2003; Ramirez-Arcos et al., 2005; Ramos et al., 2003). Overexpression of DivIVA in other actinobacteria such as *S. coelicolor*, led to enlarged ovoid cells and ghost cells indicating lysis. Interestingly, in *Staphylococcus aureus*, neither cell morphology nor growth or chromosome segregation was affected in a *divIVA* null mutant (Pinho and Errington, 2004).

Ag84 is composed of 260 AA corresponding to a molecular weight of 28.3 kDa. The C-terminal part of Ag84 is predicted to comprise a coil-coiled domain of 54 amino acids (source: Swissprot).

Given the fact that certain proteins involved in cell shape control (MreB or Mbl proteins) or cell division (MinC, MinD) are missing in mycobacteria, the question arises how these processes are regulated and coordinated in this species which is characterized by a complex life-style. Studying the effect of Ag84 overexpression and investigating the structural organization of Ag84 (molecules) might therefore help to define a role for Ag84 in mycobacteria. Moreover, the outcome of the experiments might contribute to a better understanding of mycobacterial cell biology.

6.3 Results

6.3.1 Effects of Ag84 overexpression on cell morphology

To investigate the role of Ag84 in mycobacteria, transduction experiments were carried out to delete the *wag3* locus. However, it was found that *wag31* is essential for mycobacterial survival. Viable cells were only obtained when a vector containing *wag31* under control of an acetamid-inducible promoter was provided *in trans* (Nguyen et al, 2007).

Therefore, to shed light on the function of Ag84, the protein was overexpressed in *M. smegmatis*, a non-pathogenic representant of fast-growing mycobacteria. To that end, *M. smegmatis* electrocompetent cells were transformed with *pMV361::ag84$_{MS}$* (pNDL4) and *pMV361::ag84$_{TB}$* (pNDL8) for expression of Ag84 from *M. smegmatis* (MS) and *M. tuberculosis* (TB); as a control, the bacteria were transformed with vector *pMV361*. On day 2 after transformation, colonies became visible and live cells resuspended in medium were analyzed by phase-contrast microscopy. It was found that Ag84 overexpressing cells displayed a strong phenotype reflected in altered cell morphology and increased cell size. The bacteria showed a wide diversity of different cell shapes ranging from bulbous and bulky cell morphology to bowling-pin, or oversized rod-like shaped cells (figure 6.1), the two latter ones being the most commonly found aberrant cell shapes. No phenotypical differences could be detected when comparing the mutant strains expressing Ag84$_{MS}$ or Ag84$_{TB}$, respectively.

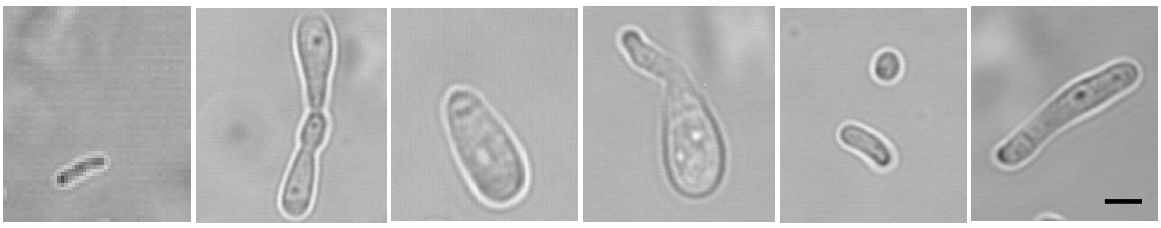

Figure 6.1. Morphology of *M. smegmatis* cells overexpressing Ag84. The bacteria were transformed with either pNDL4 (*pMV361::ag84*$_{MS}$) or pNDL8 (*pMV361::ag84*$_{TB}$), grown on 7H10-10% OADC agar (25 µg/ml Kan), resuspended and observed in an early growth stage by phase-contrast microscopy. The first panel shows *M. smegmatis* transformed with *pMV361* vector as a control. Scale bar: 2 µm.

An additional phenotype found among these cells was branch formation. Individual stages of bud initiation, bud emergence and branch formation were detected; these observations were confirmed by electron microscopy (Nguyen et al., 2007).

Electron microscopy studies also revealed that cell division was affected in Ag84 overexpressing cells. Septum formation, normally taking place in the midcell, occurred adjacent to one pole, in nearly all cases close to the narrow pole. In some cases, this asymmetric cell division gave rise to the formation of minicells (Nguyen et al., 2007).

6.3.2 Effects of Ag84 overexpression on cell size

To analyze the result of Ag84 overexpression regarding cell size, *M. smegmatis* was transformed with *pMV361::ag84*$_{MS}$ and analyzed on day 2 after transformation. In this initial growth phase, the cell size, comprising cell length and width, was drastically altered (figure 6.2). Microscopical analysis revealed that 95-100 % of the cells displayed a strong increase in cell length and width when compared to wildtype bacteria typically being 2-2.5 µm long and 0.4-0.6 µm wide. In several cases, cells of 20 µm and more were observed, which is about 10x the normal size of mycobacteria.

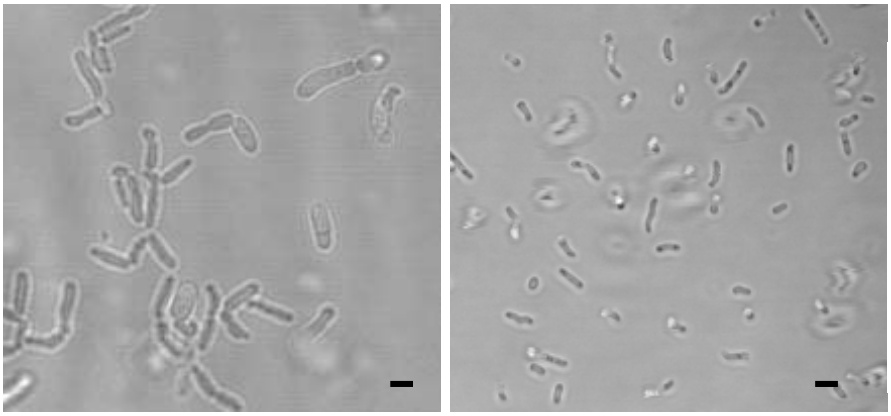

Figure 6.2. Effect of Ag84 overexpression in mycobacteria. Cells transformed with *pMV361::ag84*$_{MS}$ (left panel) or with pMV361 vector control, (right panel), incubated for 2 days and analyzed by phase-contrast. Bar in the lower right corner: 2 µm.

To analyze whether this phenotype is still detectable at later time points of growth, the morphology of mycobacteria with special focus on the cell size was observed for a period of 8 days. *M. smegmatis* was transformed with pNDL1 (*pMV361::ag84*$_{MS}$*::gfp)*, pNDL4 (*pMV361::ag84*$_{MS}$*)* and pNDL8 (*pMV361::ag84*$_{TB}$*)* and vector *pMV361* as a control. Starting on day 2 after transformation, the cells were resuspended in medium and analyzed by phase-contrast and fluorescence microscopy. To quantify the changes in cell size, width and length of ~ 100 cells were measured for one week. The analysis revealed, that the average size decreased from around 1.5 x 6 µm to 0.6 x 2.5 µm similar to wildtype dimensions (see figure 6.3).

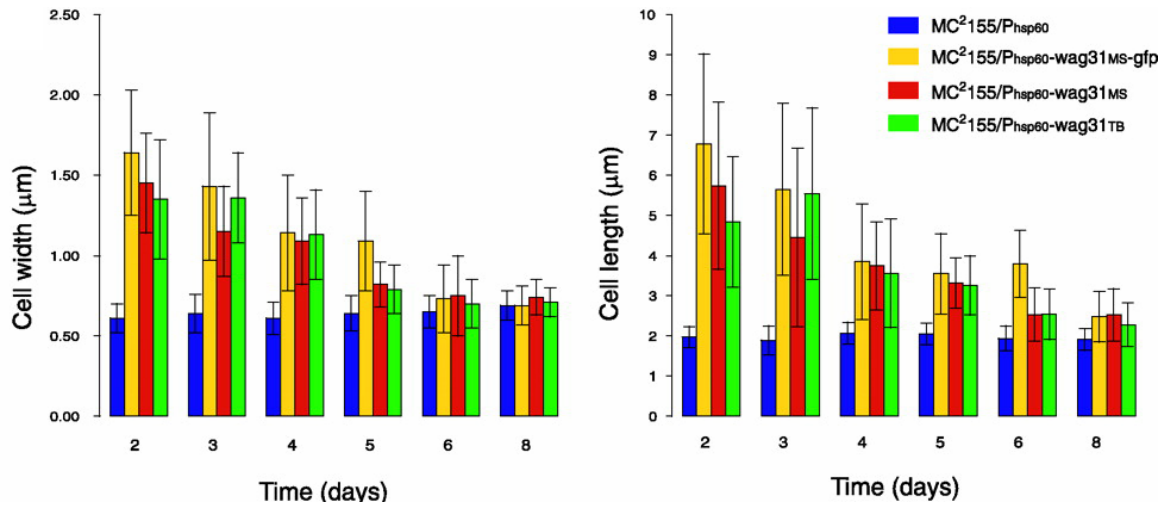

Figure 6.3. Quantification of the cell size over time. Mean values of cell length and width of *M. smegmatis* MC^{2}155 cell measured at interval time points (days) after transformation with pMV361 (blue), pNDL1 (yellow), pNDL4 (red) and pNDL8 (green). Cell size was measured as described in the text. Error bars represent standard deviation of the mean (n~100 cells per strain).

To investigate whether the increased cell size and the aberrant cell morphology observed in the initial growth phase are reflected in the protein expression levels, western blot analysis was carried out. Lysates of *M. smegmatis* expressing Ag84$_{MS}$-GFP were prepared at the times indicated (figure 6.4) and analyzed using Ag84 specific antibody. Two bands per sample were detected; the lower band corresponding to Ag84 expressed from its native promoter and the upper band representing Ag84$_{MS}$-GFP overexpressed from the hsp$_{60}$ promoter. Comparison of the expression levels revealed that Ag84$_{MS}$-GFP overexpression is 2-3 x higher than expression of native Ag84 in the early growth phase (see figure 6.4). However, the amount of Ag84$_{MS}$-GFP decreased over time to about 50% on day 8. In accordance with the loss of phenotype on day 6, levels of Ag84-GFP were considerably reduced at these time points.

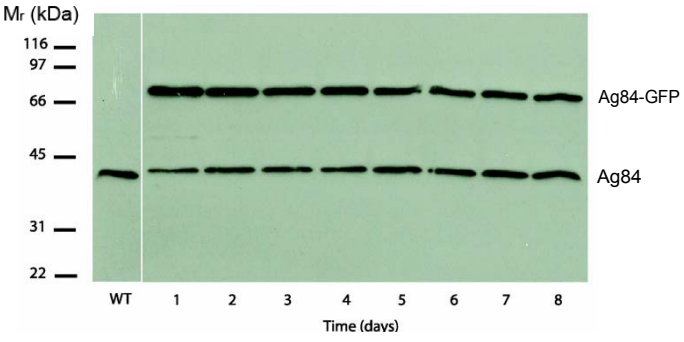

Figure 6.4. Kinetics of Ag84 overexpression associated with induced changes in cell morphology. *M. smegmatis* lysates were prepared daily from cells grown on agar plate and analyzed by western blots using Ag84 specific F126-2 antibody.

6.3.3 Intracellular localization of Ag84

Since $Ag84_{MS}$ contained a C-terminal GFP-tag, the localization of Ag84 within bacteria could be adressed. Initial experiments with *M. smegmatis* cells transformed with a vector containing *wag31::gfp* for integration at the chromosomal locus showed that Ag84 is equally distributed at both cell poles (data not shown). However, in oversized bowling pin-shaped cells, $Ag84_{MS}$-GFP was asymmetrically distributed, localizing mainly to the enlarged pole, which suggests that Ag84 influenced polar cell wall extension resulting in increased cell length and width (figure 6.5).

In addition, studies including the membrane marker FM4-64 revealed that septum formation did not occur adjacent to high accumulations of Ag84, but at the opposite site at the narrow pole containing less Ag84 (data not shown).

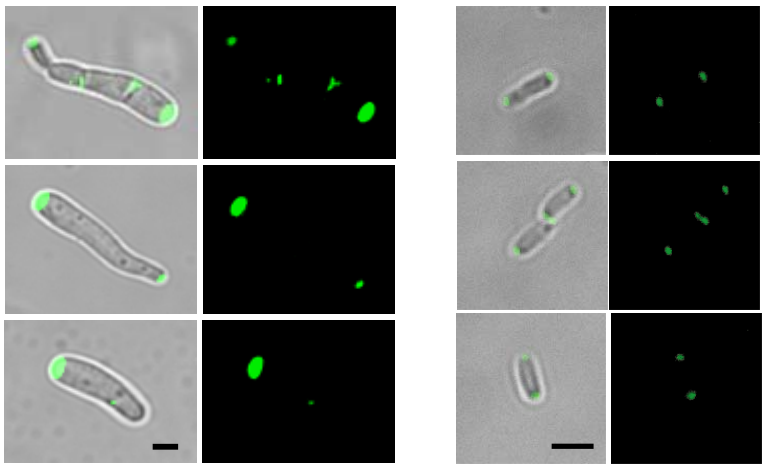

Figure 6.5. Intracellular localization of Ag84. *M. smegmatis* cells overexpressing Ag84-GFP were analyzed by phase-contrast microscopy for 8 days. Depicted here are cells analyzed on day 2 (A) and day 10 (B) after transformation. Bar: 2 µm

A quantitative analysis over a 8 days period showed that along with the decrease in cell size and the progressively normalized cell shape, the intensity of $Ag84_{MS}$-GFP per cell declined and became more equally distributed between the cell poles (figures 6.5, 6.6). It was demonstrated that 2% of the cells displayed an asymmetric Ag84 distribution in the early growth phase, whereas at later time points, around 95% of the cells exhibited a symmetric distribution similar to the wildtype (figure 6.6). Furthermore, in some cells, Ag84 was found to localize to structures within the cylindrical part of the cell; these structure are believed to represent an early stage of bud initiation (data not shown).

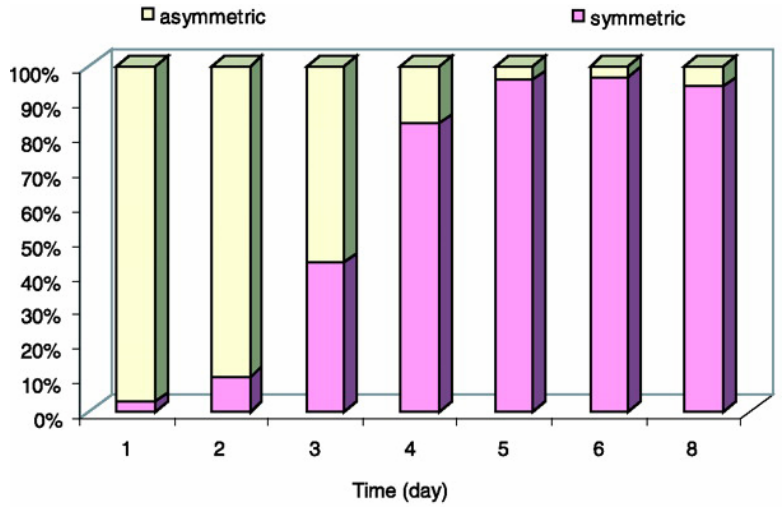

Figure 6.6. Time-dependent symmetric versus asymmetric localization of Ag84 in *M. smegmatis* overexpressing Ag84-GFP. Bacteria from colonies grown on plates at 37°C were resuspended in liquid medium and diluted to a density of 10 to 20 cells per focal plane. Around 100 cells were analyzed at interval time points after transformation.

6.3.4 Oligomerization of Ag84

In order to investigate whether Ag84, observed at the cell poles, is an integral protein of the cell wall, the subcellular localization of Ag84 was analyzed. Cell fractionation with *M. smegmatis* lysates, followed by Western blot analysis using monoclonal antibodies was performed. Ag84 was only found in the supernatant indicating that Ag84 is a cytosolic protein (figure 6.7). The fact that Ag84 is not present in the membrane fraction suggests that the polar localization observed by microscopy is not explained by strong hydrophobic interactions with the cell wall.

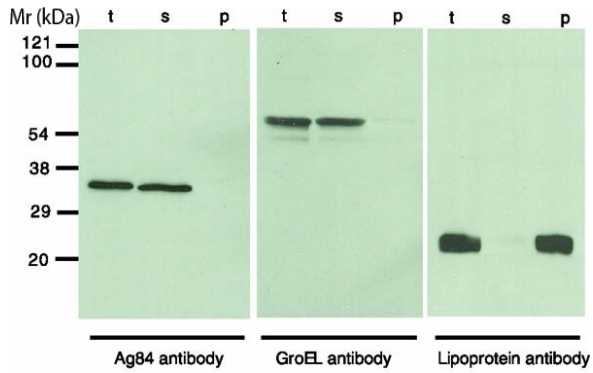

Figure 6.7. Subcellular localization of Ag84 in *M. smegmatis* lysates. Bacterial cultures were grown at 37° C in 7H9-OADC medium and cellular fractionation was carried out as described in Material and Methods. Ag84 was detected in subcellular fractions by Western Blot using F126-2 antibody. GroEL and lipoprotein specific antibodies were used as controls for cytosolic and membrane proteins, respectively (t: total cell extract, s: supernatant, p: pellet).

Another possibility would be that polar localization is a consequence of the three-dimensional shape of Ag84 multimers that fit into the curvature of the pole. To test this, a series of experiments was carried out. Initial *in silico* analysis (MultiCoil program; 67)

predicted two coil-coiled domains which are commonly known for catalyzing polymerization (data not shown).

To analyze whether Ag84 oligomerizes *in vivo*, *M. bovis* BCG lysates were prepared and treated with increasing concentrations of the cross-linking agent formaldehyde. Western blot analysis revealed the presence of Ag84 oligomers, which, according to their molecular weight, could be assigned as dimers, tetramers and hexamers (figure 6.8). A 19 kDa lipoprotein unable to polymerize was used as a control. The presence of oligomers was also analyzed with purified Ag84 by incubating the sample with different concentrations of formaldehyde, and bands corresponding to dimers, tetramers and hexamers were identified. However, the existence of higher-order multimers could not be excluded due to the limited resolution of the SDS-PAGE.

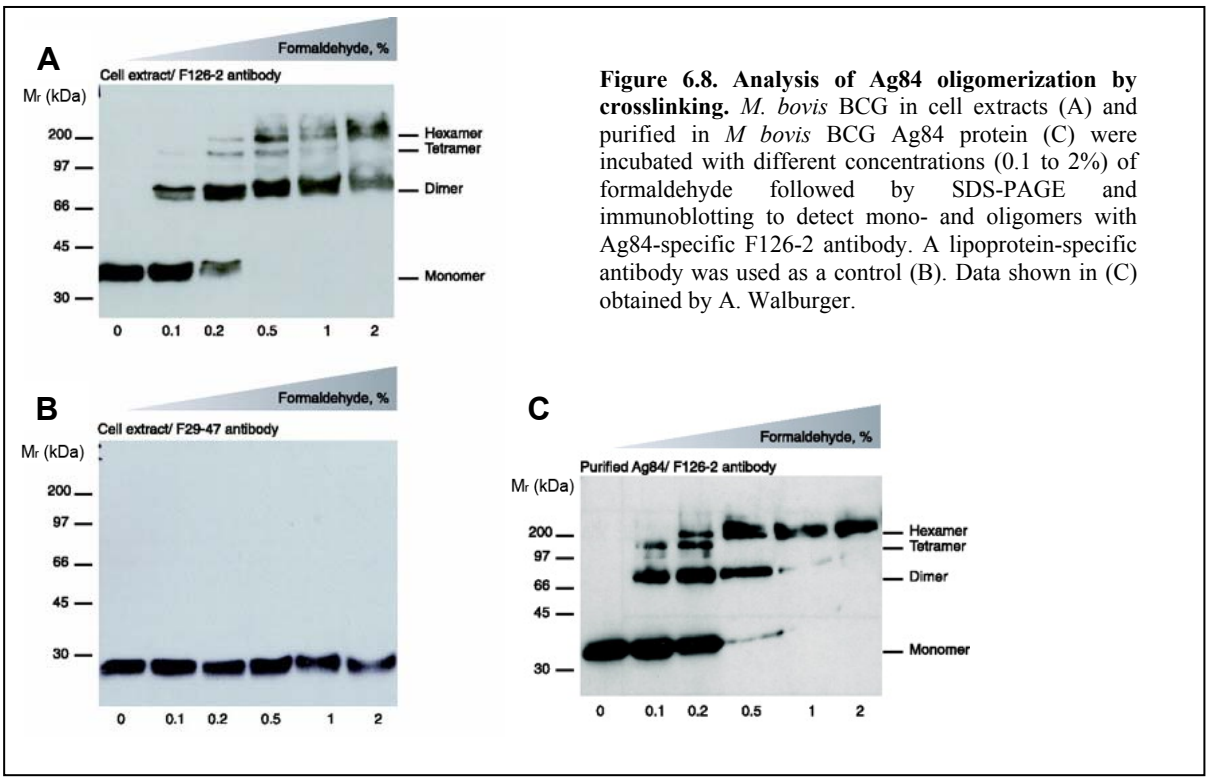

Figure 6.8. Analysis of Ag84 oligomerization by crosslinking. *M. bovis* BCG in cell extracts (A) and purified in *M bovis* BCG Ag84 protein (C) were incubated with different concentrations (0.1 to 2%) of formaldehyde followed by SDS-PAGE and immunoblotting to detect mono- and oligomers with Ag84-specific F126-2 antibody. A lipoprotein-specific antibody was used as a control (B). Data shown in (C) obtained by A. Walburger.

Finally, Ag84 oligomerization was analyzed by size-exclusion chromatography. To that end, *M. bovis* BCG was lysed and the lysate was applied to a gel filtration column. The eluted, protein-containing fractions were collected and tested for presence of Ag84 by Western blotting (figure 6.9). Ag84 was detected in a single fraction with an approximate molecular weight of 670 kDa confirming the presence of oligomers.

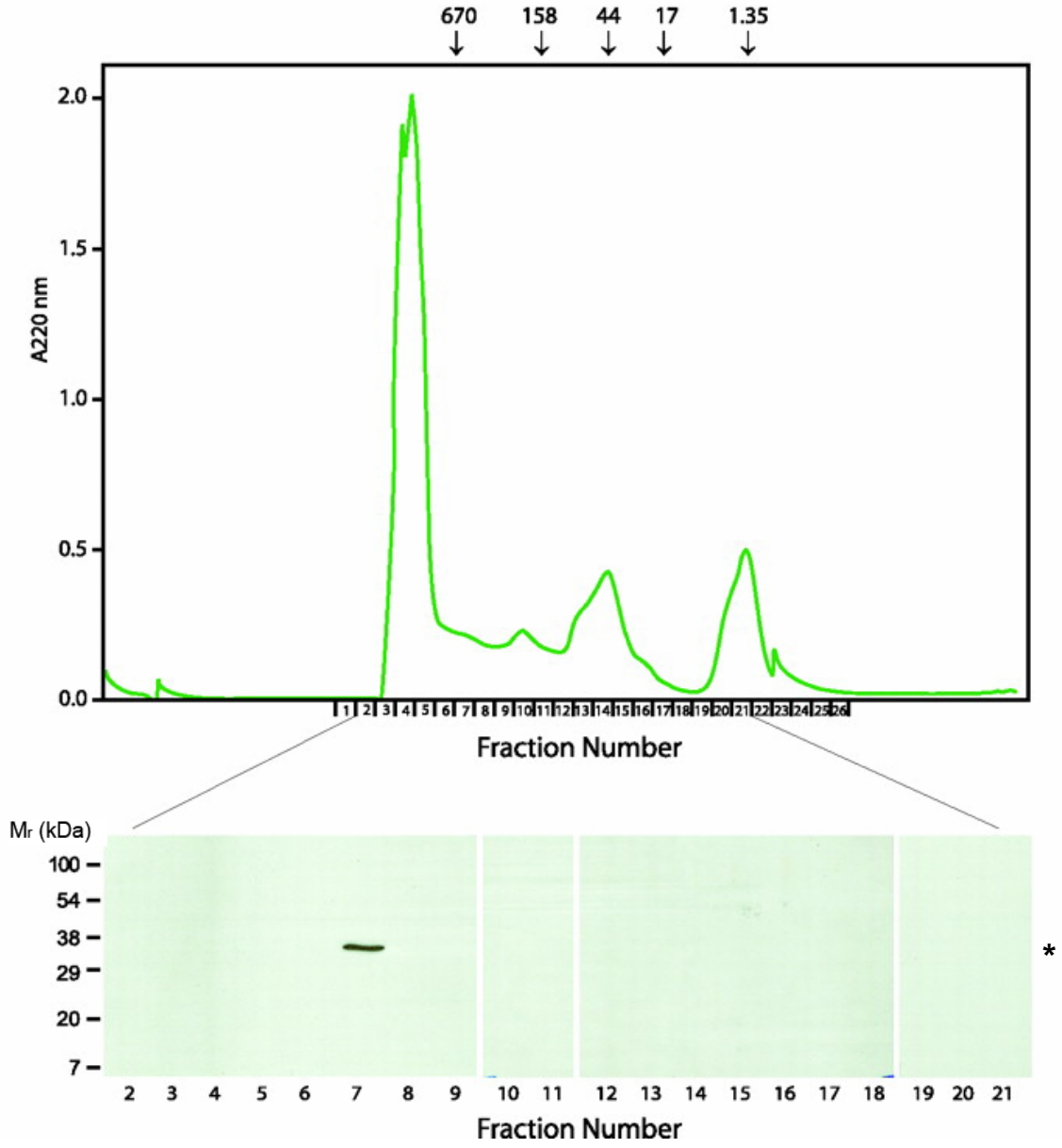

Figure 6.9. Size-exclusion chromatography to analyze the molecular weight of Ag84 oligomers. Cell lysates of *M. bovis* BCG were applied to a gel filtration column equilibrated in PBS and fractions were collected. Values representing the molecular weights of standards eluting at different fractions are indicated above the chromatogram. (*) Ag84.

6.4 Discussion

The fact that the *wag*31 gene is essential for survival, as well as the effects of Ag84 overexpression suggest that Ag84 plays a crucial role in cell growth and division. In wildtype bacteria having an average rod-like cell shape of 2 µm x 0.6 µm, Ag84 is distributed equally at the cell poles. This equal distribution inhibits septum formation near the poles during elongation and ensures balanced cell wall extension. Upon overexpression, Ag84 accumulates at one pole which is accompanied by various morphological effects like bulbous and bowling pin-like cell shapes. Such an increase in volume and cell mass can only be accomplished by a highly active cell wall synthesis machinery pointing to a possible role of Ag84 in cell growth. In addition, mutant mycobacteria exhibit defects in septum formation accompanied by the generation of mini cells. Septum formation only occurred in regions adjacent to the smaller cell pole implying that Ag84 might carry out a function in regulation (inhibition) of septum formation. The model proposed summarizes and illustrates the effects of Ag84 (figure 6.10).

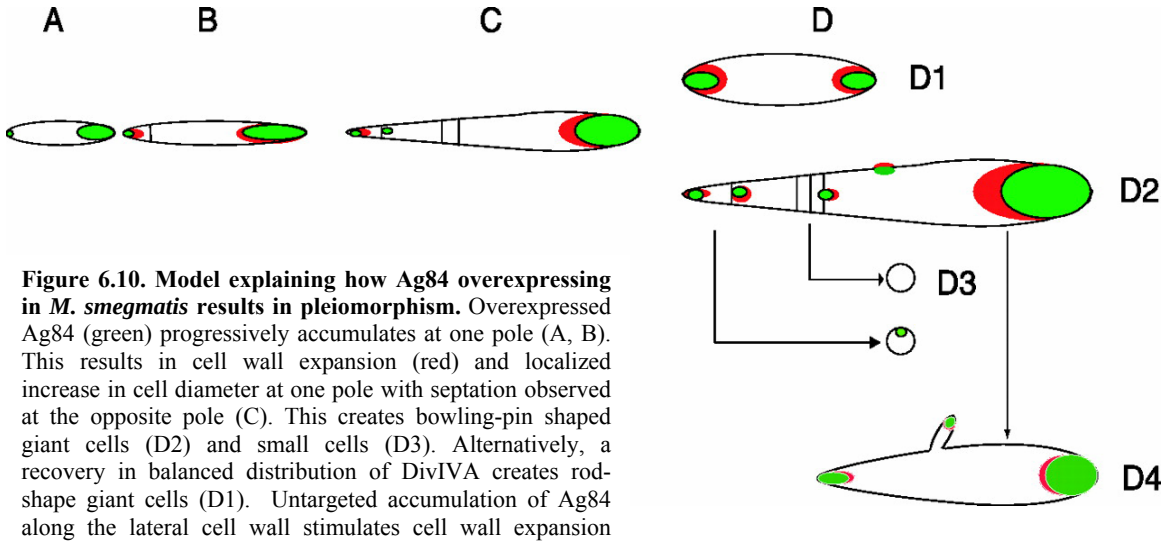

Figure 6.10. Model explaining how Ag84 overexpressing in *M. smegmatis* results in pleiomorphism. Overexpressed Ag84 (green) progressively accumulates at one pole (A, B). This results in cell wall expansion (red) and localized increase in cell diameter at one pole with septation observed at the opposite pole (C). This creates bowling-pin shaped giant cells (D2) and small cells (D3). Alternatively, a recovery in balanced distribution of DivIVA creates rod-shape giant cells (D1). Untargeted accumulation of Ag84 along the lateral cell wall stimulates cell wall expansion leading to the formation of branches (D4).

Oligomerization of DivIVA has been studied in-depth in *B. subtilis*. Using analytical ultracentrifugation and blue native gel electrophoresis, oligomers of 10-12 molecules have been detected (Muchova et al., 2002). Individual mutants carrying single point mutations within the predicted catalytical core displayed partly altered multimerization and had a morphological phenotype reflected in an increased cell length indicating that oligomerization of DivIVA seems to be important for its biological function (Muchova et al., 2002). Coiled-coil structures, composed of two or more alpha-helices wound around one another, are

known to stabilize higher-order structures, often at membrane interfaces (Rose et al., 2005). By cryonegative stain transmission electron microscopy, *B. subtilis* DivIVA was shown to exist as doggy-bone shaped oligomers, which further polymerize end-to-end to form pairs (Stahlberg et al., 2004). These assemble to strings and continued lateral oligomerization results in wires which then form a two-dimensional network. The lattice-forming properties might have a biological function similar to FtsZ, the tubulin homologue which polymerizes in a GTP-dependent manner to form filaments and sheets. DivIVA, as a homologue of tropomyosin which is known to bind actin, might oligomerize in order to anchor different proteins allowing the control of complex processes (Stahlberg et al., 2004).

Interestingly, Ag84 was identified of being the substrate of protein kinase A (PknA) *in vitro* and *in vivo*. The kinase specifically phosphorylates Ag84 on a single threonine residue (threonine 73) within the intercoiled region. Moreover, it has been demonstrated that the phosphorylation state of Ag84 is important for its functionality. Therefore it is likely that Ag84 activity is regulated by phosphorylation through PknA which, in principle, could trigger Ag84 oligomerization and activity. PknA, an essential serine/protein kinase, has been shown to be involved in chromosome segregation and maintenance of cell morphology supporting a role of Ag84 in a pathway controlling cell shape and division.

In conclusion, it has been demonstrated that *M. smegmatis* Ag84 is an essential protein responsible for maintaining the cell shape presumably by ensuring balanced cell wall extension in mycobacteria, which is likely to occur upon oligomerization of Ag84. By forming more complex/organized structures, Ag84 may provide a rigid scaffold stabilizing the cell shape and thereby possibly creating a binding surface for interacting proteins. The observation that Ag84 prevents septum formation in adjacent regions suggests that Ag84 in mycobacteria has an additional role in cell division. Thus, *M. smegmatis* Ag84 is a multifunctional protein which may compensate for the lack of cell shape (Mre, Mbl) and cell division (MinC, MinD) proteins in this genus of rod-shaped bacteria.

6.5 References

Cabeen, M. T., and Jacobs-Wagner, C. (2005). Bacterial cell shape. Nat Rev Microbiol *3*, 601-610.

Carballido-Lopez, R. (2006). The bacterial actin-like cytoskeleton. Microbiol Mol Biol Rev *70*, 888-909.

Cha, J. H., and Stewart, G. C. (1997). The divIVA minicell locus of Bacillus subtilis. J Bacteriol *179*, 1671-1683.

Chauhan, A., Madiraju, M. V., Fol, M., Lofton, H., Maloney, E., Reynolds, R., and Rajagopalan, M. (2006). Mycobacterium tuberculosis cells growing in macrophages are filamentous and deficient in FtsZ rings. J Bacteriol *188*, 1856-1865.

Dahl, J. L. (2005). Scanning electron microscopy analysis of aged Mycobacterium tuberculosis cells. Can J Microbiol *51*, 277-281.

Daniel, R. A., and Errington, J. (2003). Control of cell morphogenesis in bacteria: two distinct ways to make a rod-shaped cell. Cell *113*, 767-776.

De Pedro, M. A., Quintela, J. C., Holtje, J. V., and Schwarz, H. (1997). Murein segregation in Escherichia coli. J Bacteriol *179*, 2823-2834.

Divakaruni, A. V., Loo, R. R., Xie, Y., Loo, J. A., and Gober, J. W. (2005). The cell-shape protein MreC interacts with extracytoplasmic proteins including cell wall assembly complexes in Caulobacter crescentus. Proceedings of the National Academy of Sciences *102*, 18602-18607.

Edwards, D. H., and Errington, J. (1997). The Bacillus subtilis DivIVA protein targets to the division septum and controls the site specificity of cell division. Molecular Microbiology *24*, 905-915.

Egelman, E. H. (2003). Actin's prokaryotic homologs. Current Opinion in Structural Biology *13*, 244-248.

Flardh, K. (2003). Essential role of DivIVA in polar growth and morphogenesis in Streptomyces coelicolor A3(2). Molecular Microbiology *49*, 1523-1536.

Hermans, P. W., Abebe, F., Kuteyi, V. I., Kolk, A. H., Thole, J. E., and Harboe, M. (1995). Molecular and immunological characterization of the highly conserved antigen 84 from Mycobacterium tuberculosis and Mycobacterium leprae. Infect Immun *63*, 954-960.

Kang, C.-M., Abbott, D. W., Park, S. T., Dascher, C. C., Cantley, L. C., and Husson, R. N. (2005). The Mycobacterium tuberculosis serine/threonine kinases PknA and PknB: substrate identification and regulation of cell shape. Genes Dev *19*, 1692-1704.

Kruse, T., Bork-Jensen, J., and Gerdes, K. (2005). The morphogenetic MreBCD proteins of Escherichia coli form an essential membrane-bound complex. Molecular Microbiology *55*, 78-89.

Leaver, M., and Errington, J. (2005). Roles for MreC and MreD proteins in helical growth of the cylindrical cell wall in Bacillus subtilis. Molecular Microbiology *57*, 1196-1209.

Manabe, Y. C., and Bishai, W. R. (2000). Latent Mycobacterium tuberculosis-persistence, patience, and winning by waiting. Nature Medicine, 1327-1329.

Marston, A. L., and Errington, J. (1999). Selection of the midcell division site in Bacillus subtilis through MinD-dependent polar localization and activation of MinC. Molecular Microbiology *33*, 84-96.

Marston, A. L., Thomaides, H. B., Edwards, D. H., Sharpe, M. E., and Errington, J. (1998). Polar localization of the MinD protein of Bacillus subtilis and its role in selection of the mid-cell division site. Genes Dev *12*, 3419-3430.

Muchova, K., Kutejova, E., Scott, D. J., Brannigan, J. A., Lewis, R. J., Wilkinson, A. J., and Barak, I. (2002). Oligomerization of the Bacillus subtilis division protein DivIVA. Microbiology *148*, 807-813.

Mulder, E., and Woldringh, C. L. (1989). Actively replicating nucleoids influence positioning of division sites in Escherichia coli filaments forming cells lacking DNA. J Bacteriol *171*, 4303-4314.

Nguyen, L., Scherr, N., Gatfield, J., Walburger, A., Pieters, J., and Thompson, C. J. (2007). Antigen 84, an effector of pleiomorphism in Mycobacterium smegmatis. J Bacteriol *189*, 7896-7910.

Nyka, W. (1974). Studies on the Effect of Starvation on Mycobacteria. Infect Immun *9*, 843-850.

Ojha, A. K., Mukherjee, T. K., and Chatterji, D. (2000). High intracellular level of guanosine tetraphosphate in Mycobacterium smegmatis changes the morphology of the Bacterium. Infect Immun *68*, 4084-4091.

Pinho, M. G., and Errington, J. (2004). A divIVA null mutant of Staphylococcus aureus undergoes normal cell division. FEMS Microbiology Letters *240*, 145-149.

Ramirez-Arcos, S., Liao, M., Marthaler, S., Rigden, M., and Dillon, J.-A. R. (2005). Enterococcus faecalis divIVA: an essential gene involved in cell division, cell growth and chromosome segregation. Microbiology *151*, 1381-1393.

Ramos, A., Honrubia, M. P., Valbuena, N., Vaquera, J., Mateos, L. M., and Gil, J. A. (2003). Involvement of DivIVA in the morphology of the rod-shaped actinomycete Brevibacterium lactofermentum. Microbiology *149*, 3531-3542.

Rose, A., Schraegle, S., Stahlberg, E., and Meier, I. (2005). Coiled-coil protein composition of 22 proteomes - differences and common themes in subcellular infrastructure and traffic control. BMC Evolutionary Biology *5*, 66.

Stahlberg, H., Kutejova, E., Muchova, K., Gregorini, M., Lustig, A., Muller, S. A., Olivieri, V., Engel, A., Wilkinson, A. J., and Barak, I. (2004). Oligomeric structure of the Bacillus subtilis cell division protein DivIVA determined by transmission electron microscopy. Molecular Microbiology *52*, 1281-1290.

Stewart, G. C. (2005). Taking shape: control of bacterial cell wall biosynthesis. Molecular Microbiology *57*, 1177-1181.

7. Summary and conclusions

The genome of *M. tuberculosis* comprises eleven serine/threonine protein kinases which carry out various functions, e.g. in cell division, metabolism and pathogenicity. Nine of these eleven kinases are membrane-bound and have a C-terminal extracellular domain and an intracellular Hanks-type kinase domain located at the N-terminus. Protein kinase G (PknG) differs from these kinases, because it is predicted to be a cytosolic protein since it lacks a transmembrane domain. The kinase domain is preceded by a long N-terminal stretch containing two CXXC motifs. Moreover, PknG possesses a tetratricopeptide repeat within its C-terminal domain. PknG, expressed by pathogenic mycobacteria upon infection, has been shown to be secreted into the macrophage cytosol where it modulates and prevents phagosome-lysosome fusion, finally resulting in survival of the bacilli.

A potent inhibitor, termed AX20017, was identified which specifically inhibited the catalytic activity of PknG *in vitro*. Infection of J774 macrophages with mycobacteria treated with AX20017 led to an increase rate of lysosomol delivery events. The same effect was observed when macrophages were infected with mycobacteria expressing a kinase-dead-version of PknG which strongly supports the idea that PknG activity is required for mycobacterial survival. A broad-ranged kinase assay screen including 25 kinases representatively chosen from the six major kinase families showed that the inhibitor was highly selective by inhibiting only PknG with high efficiency. Normal cellular processes within host cells were not affected.

To elucidate the structural basis of inhibition of PknG and to learn more about the function of the kinase, the structure of PknG in complex with its inhibitor was solved. Since PknG full length was shown to be unstable, limited analysis was performed and a truncated version of PknG missing 8 kDa of the N-terminus was constructed. A purification protocol was established that allowed the purification of pure and stable protein. Crystallization assays were performed to screen for optimal conditions. The structure of dimeric PknG in complex with its specific inhibitor AX20017 was solved at a resolution of 2.4 Å using SIRAS. Three domains of PknG were defined:

a) The N-terminal region encompassing the two CXXC motifs, which were shown to complex iron, thus forming a rubredoxin domain

b) The kinase domain displaying a closed configuration, with the inhibitor occupying the nucleotide-binding pocket
c) and the C-terminal domain with the tetratricopeptide repeat mediating dimerization of the two PknG molecules.

The structure explained the high specificity of inhibition by AX20017. In total, 15 polar and non-polar interactions between the inhibitor and the kinase- or N-terminal domain were determined. Sequence alignments with all 518 human kinases derived from six major kinase families revealed that 6 of these interactions were not detected in any other kinase underlining the high specificity of inhibition. By expressing proteins with mutated inhibitor binding sites, these sites of interaction were further confirmed.

Moreover, the molecular model of the kinase allowed insights into the regulation of PknG. Site-directed mutagenesis on the four cysteines forming the rubredoxin motif completely abolished PknG activity. This, in combination with the observed interactions between the rubredoxin domain and the lobes of the kinase domain, suggested that PknG activity might be regulated by the N-terminal globular domain.

PknG undergoes autophosphorylation, similar to most mycobacterial kinases studied thus far. However, in-depth analysis of PknG autophosphorylation revealed significant differences. Whereas most mycobacterial kinases display a conserved autophosphorylation pattern on the activation loop, phosphorylated residues in PknG were exclusively identified at the N-terminus. For PknG, classified as the unique mycobacterial non-RD kinase due to a missing arginine residue in the catalytic loop, absence of autophosphorylation in the activation loop was suggested. By performing kinase assays using constructs lacking the potential N-terminal phosphorylation sites, this assumption was confirmed. Moreover, by analyzing these mutants on an endogenous substrate, it was demonstrated that autophosphorylation is not a prerequisite for activating the catalytic activity of PknG.
Infection experiments with mycobacteria expressing mutated unphosphorylated PknG protein indicated that autophosphorylation is crucial for the role of PknG in preventing lysosomal delivery. Preliminary results of survival assays showed that mycobacteria which express PknG devoid of autophosphorylation sites were rapidly transferred to lysosomes and degraded.

To further understand the activity of PknG within host macrophages, PknG was localized in eukaryotic cells. Upon transfection, PknG was detected in the nucleus of HeLa, Mel JuSo and HEK cells. Transfection assays with different truncated PknG constructs point to the C-terminal TPR containing domain of PknG for being responsible for nuclear translocation.

In addition, Ag84, a downstream target of PknA, was studied. To address its function, Ag84 was overproduced in mycobacteria. Overexpression resulted in drastic changes in cell morphology, particularly in cell size and shape. Localization studies revealed that wildtype Ag84 localized equally to the cell poles, whereas overexpressed Ag84 was asymmetrically distributed at the poles leading to unbalanced cell wall extension. Furthermore, overexpressed Ag84 was found to affect cell division by preventing septum formation adjacent to the cell pole with higher Ag84 concentrations. Biochemical analysis revealed that Ag84 is a cytosolic protein. As an alternative explanation for the polar localization, oligomerization of Ag84 was analyzed. Chemical crosslinking and size-exclusion chromatography analysis showed that Ag84 is able to form oligomers of >6 molecules which might act as a complex scaffold fitting to the curvature of the cell poles. This complex structure then might allow recruiting other proteins involved in processes such as cell wall synthesis.
Ag84 is the first effector protein, for which a role in mycobacterial cell shape control has been described. In addition, Ag84 was found to be involved in septum formation and therefore has a similar role as *B. subtilis* DivIVA, which in *Bacillus* however interacts with the MinCD system that is absent in mycobacteria.

To conclude, the results presented in this thesis contribute to a better understanding of mycobacterial virulence. The knowledge of the structure of PknG might be particular useful with regard to the design of more potent drugs and the biochemistry data obtained for PknG allowed important insights into function and regulation of this eukaryotic-like serine/threonine protein kinase. Taken together, the results add more information to the complex network of mycobacteria-host interactions.

I. Abbreviations

aa	Amino acid
Ab	Antibody
Ag84	Antigen 84
Amp	Ampicillin
AP	Alkaline phosphatase
APS	Ammonium persulfate
ATP	Adenosine triphosphate
BCA	Bicinchoninic acid
BCG	Bacille Calmette Guérin
BMM	Bone marrow-derived macrophages
BSA	Bovine serum albumin
CAPS	*N*-cyclohexyl-3-aminopropanesulfonic acid
CLAAP	Chymostatin, leupeptin, aprotinin, antipain, pepstatin
conc.	Concentration
CPM	Counts per minute
DMEM	Dulbeccos's modified Eagle's medium
DMSO	Dimethylsulfoxide
DLS	Dynamic light scattering
dNTP	Deoxynucleoside triphosphate
DTT	Dithiothreitol
ECL	Enhanced chemiluminescence
EDTA	Ethylendiamine tetraacetate
EtBr	Ethidium bromide
EtOH	Ethanol
FBS	Fetal bovine serum
FCS	Fetal calf serum
FF	Fast flow
FHA	Forkhead-associated (domain)
FPLC	Fast performance liquid chromatography
G418	Geneticin
GFP	Green fluorescent protein
HEK	Human embryonic kidney
HiLoad	High load (column)
HRP	Horseradish peroxidase
IC	Inhibitory concentration
Ig	Immunglobulin
Kan	Kanamycin
KD	Kinase domain
KO	Knock-out
LAM	Lipoarabinomannan
LAMP-1	Lysosome-associated membrane protein 1
LB	Lysogeny Broth (Luria-Bertani Broth)
LM	Lipomannan
MDR	Multi drug-resistant (strains)
MeOH	Methanol
MHC	Major Histocompatibility Complex
MM	Master mix
Mr	Molecular weight

MS	Mass spectrometry
NLS	Nuclear Localization Signal
NMR	Nuclear magnetic resonance
OADC	Oleic acid, albumin, dextrose and catalase supplement
OD	Optical density
O/N	Over night
PAGE	Polyacrylamide gel electrophoresis
PBS	Phosphate buffered saline
PCR	Polymerase chain reaction
PFA	Paraformaldehyde
PEG	Poly ethylene glycol
PFA	Paraformaldehyde
pH	Potential hydrogenii
PknX	Protein kinase x
PMSF	Phenylmethylsulfonylfluoride
rpm	Round per minute
RT	Room temperature
SAP	Shrimp alkaline phosphatase
SB	Sample buffer
SD	Sensor domain
SDS	Sodium dodecylsulfate
SIRAS	Single isomorphous replacement anomalous scattering
SLS	Static light scattering
TB	Tuberculosis
TBE	Tris-borate-EDTA
TCA	Trichloracetic acid
TE	Tris-EDTA
TEMED	N, N, N', N'-tetraethylmethlylendiamide
TEN	Tris-EDTA-NaCl
TLC	Thin-layer chromatography
TPR	Tetratricopeptide repeat
Tris	Tris(hydroxyethyl)aminomethane
TX-100	Triton X-100
U	Unit
UV	Ultraviolett
WT	Wild type
XDR	Extremely drug-resistant (strains)

II. Acknowledgements

First of all, I would like to thank Jean Pieters for supervising my PhD thesis, and for letting me work on this exciting and challenging project. Jean was never at a loss for ideas or pragmatic suggestions and also fully supported my scientific "extracurricular" activities.

I'm also very grateful to Michel Steinmetz who gave me the opportunity to work at the PSI and who invested lots of time and money in the crystallization project. I especially appreciated the motivating discussions we had on PknG.

Furthermore, I want to express my gratitude to Peter Philippsen for listening to my worries, for his understanding and for his scientific advices.

My thanks also go to Martin Spiess who evaluated my work as a member of my thesis committee.

I would like to thank Srinivas Honnappa who guided me through the crystallization work. Without his help, the structure of PknG would still be unknown!

In addition, I thank Gabriele Kunz for her dedicated assistance in the PknG project.

Moreover, thanks to Liem Nguyen and Charles Thompson for a good collaboration on Ag84.

Special thanks go to:

- ✪ Benoit Combaluzier for the fun-time we had together :-)
- ✪ Rajesh Jayachandran for bringing sunshine to our lab and for sharing some lab weekends and night shifts with me
- ✪ Edith Houben for advice in PknG issues
- ✪ Lotte Kuhn for her helpfulness and for countless critical discussions we had either in the lab or on her terrace and for co-organizing our lab outings
- ✪ Ingrid Ziekau (Medical Microbiology) for great assistance and for being a good friend

Thanks as well to:

✪ Anna Melone and Varadha Sundaramurthy for their expertise in microscopy
✪ Philipp Müller for his preparatory work on PknG
✪ Yong Cheng and Thomas Fiedler for keeping up the spirit in our lab
✪ Sonja Dames for introducing me into C/D spectroscopy and for scientific input
✪ Christian Kambach (PSI) for guiding us through the optimal solubility screen
✪ Sivaraman Padavattan for suggesting the Wizard kits for crystallization
✪ Wolfgang Oppliger for advice when encountering technical problems
✪ Jürg Widmer for instant help in technical questions
✪ Verena Zellweger for her outstanding organizational skills
✪ Daniel Michel and Maja Heckel for technical and administrative support
✪ the former labmembers Imke Albrecht, Anne Walburger, Giorgio Ferrari, Jan Massner, Bettina Zanolari, Cristina Baschong, Damir Perisa and Martin Bratschi for help and suggestions
✪ Joe and Pierre for distraction :-)

and finally to:

☆ my friends
☆ my dear family for all their love and support.